INTERACTIONS OF ANTI-CANCER Ru(III)-COMPLEXES WITH SERUM PROTEINS

by

Naniye Cetinbas
B.Sc., Yildiz Technical University, 2003

THESIS SUBMITTED IN PARTIAL FULFILLMENT OF
THE REQUIREMENTS FOR THE DEGREE OF

MASTER OF SCIENCE

In the
Department of Chemistry

SIMON FRASER UNIVERSITY

Spring 2009

APPROVAL

Name:	**Naniye Cetinbas**
Degree:	**Master of Science**
Title of Thesis:	**Interactions of Anti-cancer Ru(III)-complexes with Serum Proteins**

Examining Committee:

Chair:	Dr. Paul C.H. Li Professor
	Dr. Charles J. Walsby Senior Supervisor Assistant professor
	Dr. George R. Agnes Supervisor Professor
	Dr. David J. Vocadlo Supervisor Associate professor
	Dr. Margo M. Moore Internal Examiner Professor

Date Defended/Approved: January 16, 2009

ABSTRACT

Interactions of anti-cancer Ru(III)-complexes, KP1019, KP418, and NAMI-A, with human serum transferrin (hsTf) and albumin (hsA), and their speciation in serum were characterized. NAMI-A was distinguished from KP1019 and KP418 by the instability of its Ru(III) oxidation state. EPR studies suggested a ligand-exchange mediated binding of KP1019 and KP418 to hsTf and hsA. With hsA a hydrophobic interaction was also detected. KP1019 exhibited a different speciation profile in serum from that of KP418. UV-visible studies demonstrated a faster hsTf-binding ability of KP1019 over KP418. It was proposed that these differences might partially explain the disparate anti-cancer activities of KP1019 and KP418. EPR analysis of KP1019-binding to the His249Ala mutant of hsTf and to diferric-hsTf revealed a Ru(III)-state stabilizing role of the iron-binding site of hsTf in KP1019 binding. In addition, a procedure for expression and purification of full-length recombinant hsTf in *P. pastoris* was devised.

Keywords: Anti-cancer Ru(III)-complexes; EPR; transferrin; albumin; protein expression; *P. pastoris*;

To my Ece Naz…

ACKNOWLEDGEMENTS

I am grateful to my senior supervisor Dr. Charles Walsby for allowing me to work on this project, and for his expertise and support in this work. I am indebted to my committee members, Dr. George Agnes and Dr. David Vocadlo, and the internal examiner Dr. Margo Moore for their valuable suggestions.

I cannot express the depth of my gratitude enough to my former supervisor and current committee member, Dr. David Vocadlo, who gave me a chance in his lab and taught me everything I know about the molecular biology techniques. He also taught me how to plan research, work independently, and think critically. Without his guidance I would not be able to reach my academic goals. Thank you for being an excellent teacher and role model.

I would like to thank the Vocadlo and O'Neill groups for access to their instruments, without which this thesis would not be possible. I am thankful to the undergraduate students Joshua Dubland, Allan Wang, Jonathan Jiang, and Roberto Trousollini, who helped me with different aspects of my research. I am also thankful to my past and current fellow group members Stephanie Taylor, Tommy He, and Mike Webb for their help in the lab.

Lastly, I wish to thank my family and my husband for their endless support and encouragement. My special thanks go to my little daughter, Ece Naz, who despite her young age was incredibly patient and understanding during the research and writing of this project. To her I dedicate this thesis.

TABLE OF CONTENTS

LIST OF FIGURES

LIST OF TABLES

LIST OF ABBREVIATIONS

BSA	Bovine serum albumin
DMSO	Dimethyl sulfoxide
EDTA	Ethylene diamine tetraacetic acid
EPR	Electron paramagnetic resonance
ENDOR	Electron-nuclear double resonance
hsTf	Human serum transferrin
hsA	Human serum albumin
IBB	Iron-binding buffer
IDA	Iminodiacetic acid
KP418	Imidazolium-*trans*-[tetrachlorobis(1*H*-imidazole)ruthenate(III)]
KP1019	Indazolium-*trans*-[tetrachlorobis(1*H*-indazole)ruthenate(III)]
NAMI-A	Imidazolium-*trans*-[DMSO-imidazole-tetrachlororuthenate(III)]
NTA	Nitrilotriacetic acid
SDS-PAGE	Sodium dodecyl sulfate polyacrylamide gel electrophoresis

CHAPTER 1: INTRODUCTION

1.1 Anti-cancer Ru(III)-complexes

The discovery of the anti-tumor activity of cisplatin (*cis*-[$Pt(NH_3)_2Cl_2$]) about 40 years ago has stimulated research into development of new metallo-pharmaceuticals for the treatment of cancer.[1] Among thousands of synthesized and studied platinum complexes, only cisplatin, carboplatin, and oxaliplatin have been approved for use in the clinics, and are the most commonly prescribed anti-cancer drugs world-wide.[2] Cytotoxic chemotherapy of cancer with these conventional anti-cancer drugs is often limited by serious, sometimes life-threatening side effects because these drugs target all dividing cells including the normal healthy ones. In addition, intrinsic or acquired resistance of tumor cells also limits their successful use.[3-5] Therefore, new platinum- and non-platinum-based anti-cancer compounds are continuously being developed with the aim of targeted therapies against a broad spectrum of malignancies.[1, 6] Among several transition metal compounds tested, Ru(III)-complexes are emerging as effective anti-cancer agents alternative to platinum-complexes.

A plethora of studies have focused on three Ru(III)-complexes KP1019 (figure 1.A, $[HInd]^+$ *trans*- $[RuCl_4(HInd)_2]^-$, Hind = Indazole), KP418 (figure 1.B, $[HIm]^+$ *trans*- $[RuCl_4(HIm)_2]^-$ (HIm = Imidazole), and NAMI-A (figure 1.C, $[HIm]^+$ [trans-$RuCl_4$(DMSO)(Im)]$^-$, Im = Imidazole), all of which possess remarkable anti-

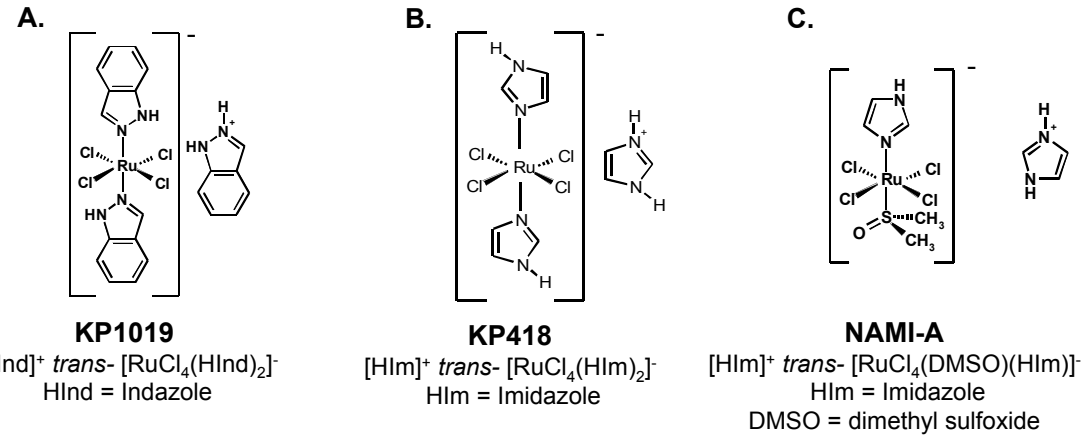

Figure 1-1 Structure of anti-cancer Ru(III)-complexes.

tumor activity against various tumor types in animal models.[6] Of these three Ru(III)-complexes, NAMI-A and KP1019 were the first Ru(III)-based anti-cancer compounds to enter clinical trials in 1999 and 2003 respectively.[1] KP418 was not qualified for phase 1 clinical trials due to its lower anti-cancer activity and more significant side-effects compared to KP1019. Both KP1019 and NAMI-A have recently completed clinical phase I trials with marked success.[2, 7] These complexes have been shown to differ in their biological targets and their mechanism of action. Both KP1019 and its imidazole analog KP418 exhibit cisplatin-like cytotoxicity through DNA binding, inducing apoptosis in colon carcinomas and various types of explanted human tumors.[8, 9] By contrast, NAMI-A has no significant effect on primary tumors but it is strikingly effective in reducing the formation and growth of lung metastases of solid tumors.[10]

1.2 Mechanism of Ru(III)-mediated tumor inhibition

The remarkable anti-tumor activity but lower side-effects of KP1019 and NAMI-A compared to cisplatin has stimulated intensive efforts to understand their mechanism of action as well as the active species that are responsible for their tumor inhibition. These studies centred on: 1) hydrolysis reactions in physiological media, and identification of the species formed;[11-16] 2) the link between structure and reduction potential in terms of anti-cancer activity;[14, 17-20] 3) interactions with the serum proteins, hsTf and hsA;[21-29] 4) interactions with the intracellular molecules, such as nucleotides and glutathione.[15, 30-36] The findings of these studies have helped in understanding some aspects of Ru(III)-complex-mediated tumor inhibition, and are briefly described below.

1.2.1 Chemical properties and structure-activity relationships

Aquation of metal complexes following their administration *in vivo* is an important activation mechanism for reactions with biomolecules. Faster aquation rates of metal complexes usually correlate to their increased anti-tumor activities, while inert complexes are typically weakly active or completely inactive.[37] For instance, aqua-products of cisplatin, *cis*-$[Pt(NH_3)_2Cl(H_2O)]$ or *cis*-$[Pt(NH_3)_2(H_2O)_2]$, where one or both of the chloro-groups are replaced by a molecule of water, are the active species that react with DNA.[38] Consequently, the lability of chloro-groups on the Ru(III)-centre of the complexes studied in this work, is a factor in their cytotoxic properties. On the other hand, the mode of action of Ru(III)-complexes has been suggested to be different from that of cisplatin,[2] primarily due to the octahedral geometry of Ru(III)-complexes versus

the square planar geometry of cisplatin, which may also be a factor in activity of KP1019 against cisplatin-resistant tumors. Ru(III)-complexes also exhibit differential anti-cancer activities within their own class. A number of structure-activity relationship studies have revealed that, aquation rate, protein binding properties, and anti-cancer activities of Ru(III)-complexes can be tuned by changing the ligands on the Ru(III)-centre.[14, 17-19, 37]

1.2.2 Activation by reduction theory

According to the 'activation by reduction' theory, Ru(III)-complexes act as prodrugs that are activated in hypoxic tumor tissues by reduction of the Ru(III)-centre to Ru(II). This theory is based on the fact that the electrochemical potential inside tumors is generally lower than in normal tissue.[39] This is caused by the failure of new blood vessels to form fast enough in tumors to overcome the rapid consumption of oxygen and other nutrients, resulting in lower oxygen content in tumors as compared to normal tissues (hypoxia).[39] Hence, tumor cells depend more on glycolysis for energy and produce excess lactic acid leading to lower pH.[39] Therefore the environment inside tumors is more reductive as compared to normal tissues. These differences between the tumor tissue and normal tissue are believed to facilitate the reduction of Ru(III) to the active Ru(II)-species selectively in tumors, which may be a factor in the comparatively limited side-effects of Ru(III)-complexes.[33, 39]

1.2.3 Biomolecular targets

Although KP1019 and KP418 share common structural features with NAMI-A, such as octahedral geometry and the position and number of chloro-ligands, the identity of the axial ligands on the Ru(III)-centre appears to affect the anti-cancer activity of these complexes substantially, as well as their biological targets.[14, 17, 18] These findings suggest that the mode of action of these complexes may be quite different.

KP1019 and KP418

Both KP1019 and KP418 exhibit anti-cancer activity against a number of primary tumors, particularly against colorectal tumors by inducing cytotoxicity.[40, 41] *In vitro* studies have demonstrated a preferential accumulation of ruthenium in the nuclei of tumor cells treated with KP1019.[42] In addition, other studies have shown that KP1019 and KP418 both form coordination complexes with purines in DNA.[30, 43] Therefore it was suggested that both KP1019 and KP418 bind to DNA, causing cytotoxic DNA lesions, and eventually apoptosis.[2] While KP1019, KP418, and cisplatin all target the purines in DNA, DNA lesions caused by Ru(III)-complexes are likely to be different from those caused by cisplatin because of the differences in their geometry/coordination number.

NAMI-A

In vitro studies have shown that the anti-metastatic activity of NAMI-A does not involve cisplatin-like cytotoxicity and DNA binding.[10, 44, 45] For example, when mice, transplanted with Lewis lung carcinoma cells, were treated with

NAMI-A, no change in primary tumor growth was observed. However, formation of spontaneous lung metastases was significantly reduced.[46] Several studies have aimed to elucidate the mechanism of action and biological targets of NAMI-A, and these results indicate that NAMI-A inhibits the proteins involved in metastasis; such as matrix metalloproteinases.[47] NAMI-A also inhibits angiogenesis[48, 49] and induces actin-dependent tumor cell adhesion.[50] In addition, NAMI-A induces endothelial cell apoptosis and inhibits cell proliferation by down-regulating the mitogen-activated protein kinase/extracellular signal-regulated kinase signaling pathway.[51] Nevertheless, recent studies demonstrated some activity of NAMI-A also against different human tumor cell lines via DNA binding and cytotoxicity, however, a much lower reactivity with DNA as compared to cisplatin was reported.[36, 52]

1.2.4 Interactions with serum proteins

It is now well established that following their intravenous administration Ru(III)-complexes interact with serum proteins, primarily with human serum transferrin (hsTf) and human serum albumin (hsA).[21, 22, 25, 26, 53-57] Ru(III)-complexes exhibit higher affinity towards hsTf and hsA than cisplatin[23] and it is hypothesized that Ru(III)-complex/serum protein interaction is an important step in the Ru(III)-complex-mediated targeted tumor inhibition. In the following subsections, the structure and functions of hsTf and hsA are briefly described in conjunction with their proposed role in the anti-cancer activity of Ru(III)-complexes.

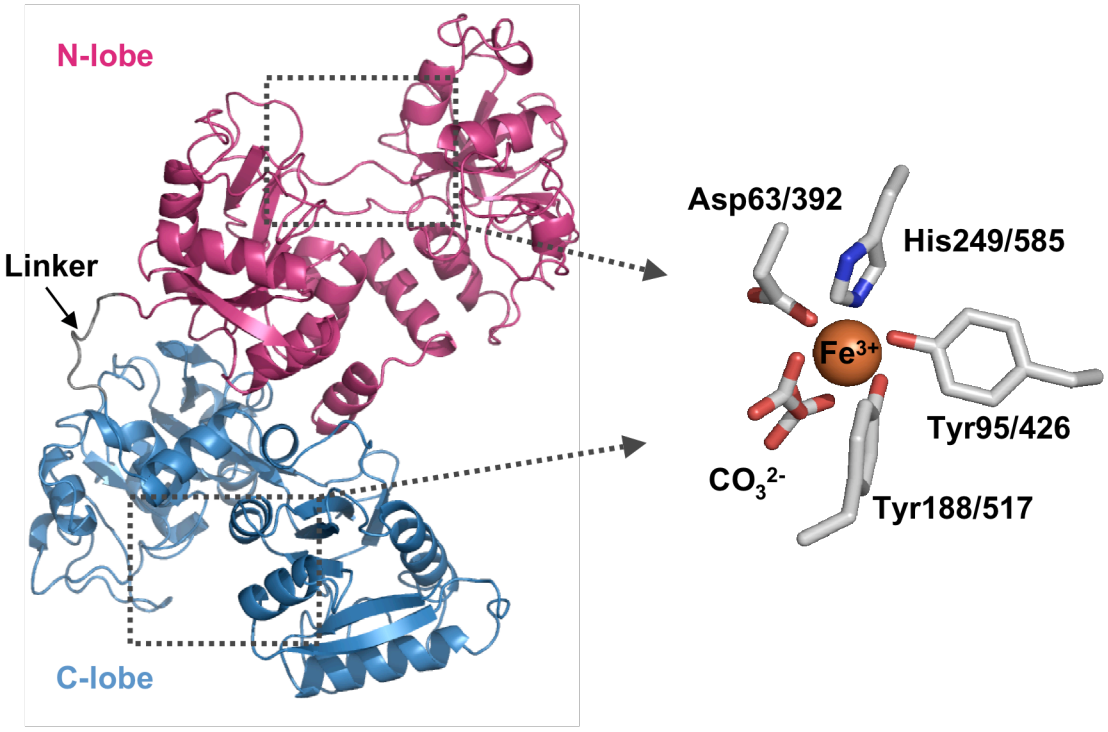

Figure 1-2 Structure of human serum transferrin (hsTf). hsTf is arranged into two homologous lobes representing the N-terminal and C-terminal halves of hsTf which are joined by a short 'linker' peptide. Each lobe has an identical iron-binding site in its deep binding cleft comprising the liganding residues (Asp63, His249, Tyr95, and Tyr188 in the N-lobe; Asp392, His585, Tyr426, and Tyr517 in the C-lobe). A synergistic CO_3^{2-} completes the octahedral geometry of Fe^{3+}. Figures were generated using PyMOL.[58] The structural data was obtained from the Protein Data Base, Research Collaboratory for Structural Bioinformatics (RCSB, PDB) under the identifiers 2HAV[59] (for overall structure of apo-hsTf) and 1A8E[60] (for iron-binding site).

Human serum Transferrin (hsTf)

hsTf is a ~77 kDa monomeric, glycosylated iron-binding and transport protein composed of two similar lobes (N-lobe, and C-lobe) corresponding to its N-terminal and C-terminal halves, each containing an iron binding site in a deep cleft.[61, 62] The iron binding site is formed of four iron-coordinating residues; an aspartate, a histidine, and two tyrosines. In addition, two oxygen ligands from a

synergistically bound carbonate anion (CO_3^{2-}) are required to complete the octahedral geometry of a coordinated Fe^{3+}. Although the two iron binding sites of hsTf contain identical ligands, the C-lobe exhibits a higher affinity for Fe^{3+} than the N-lobe.[63] *In vitro* studies have demonstrated that the N-lobe releases iron at pH ~5.7, while a lower pH (~4.7) is needed for iron-release from the C-lobe.[64, 65] In addition to Fe^{3+}-delivery to iron-requiring cells, hsTf plays crucial roles in sequestering iron and preventing iron-catalyzed free radical formation in serum, and in limiting growth of invading microorganisms.[66, 67]

Transferrin cycle

A hsTf molecule binds two Fe^{3+} ions in serum (diferric-hsTf) and transports them into cells via receptor mediated endocytosis in a strictly pH-dependent manner.[68-70] Upon iron-binding at the extracellular pH 7.4, hsTf adopts a closed conformation and two diferric-hsTf molecules dock onto a transferrin receptor (TfR) on the cell surface. The diferric-hsTf/TfR complex is internalized into an endosome. In the acidic environment of the endosome (pH~5.5), hsTf assumes an open conformation and releases both Fe^{3+} ions to a chelating anion. Apo-hsTf remains bound to TfR and the whole complex is recycled back to the cell surface where apo-hsTf is released from TfR to serum to start the 'transferrin cycle' once again (figure 1.3).

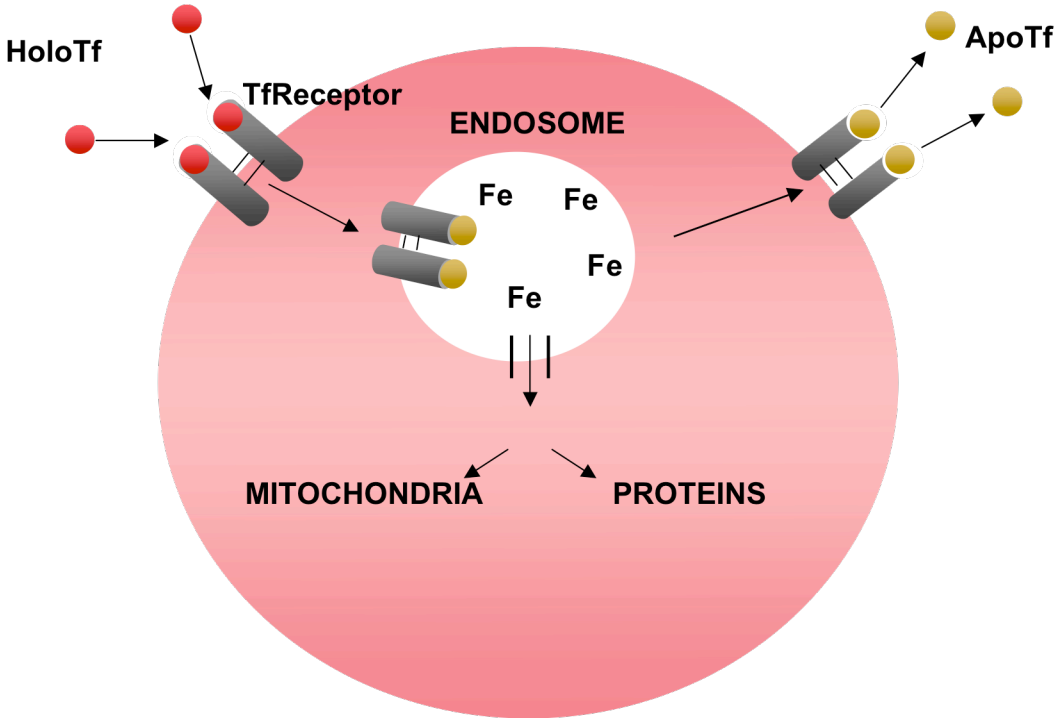

Figure 1-3 A schematic representation of natural transferrin cycle. Two molecules of diferric-hsTf bind to a TfR and the whole complex is internalized into an endosome. In the endosomic pH (~5.5) iron is released from both lobes of hsTf. Apo-hsTf/TfR complex is recycled back to the cell surface, where apo-hsTf is released into the extracellular fluid.

hsTf mediated Ru(III)-complex delivery to cancer cells

In blood, hsTf is only about 30% saturated with Fe^{3+}, which allows hsTf to bind other metal ions and transport them into cells.[65] Because of the ability of hsTf to carry metal species into cells, there have been several studies focused on the development of novel drug design strategies exploiting the natural function of hsTf. In several cancers, expression of TfR on the cell surface is upregulated partly due to an increased requirement for iron in rapidly growing cells.[68] This property allows the use of hsTf as an effective metal-based drug delivery system

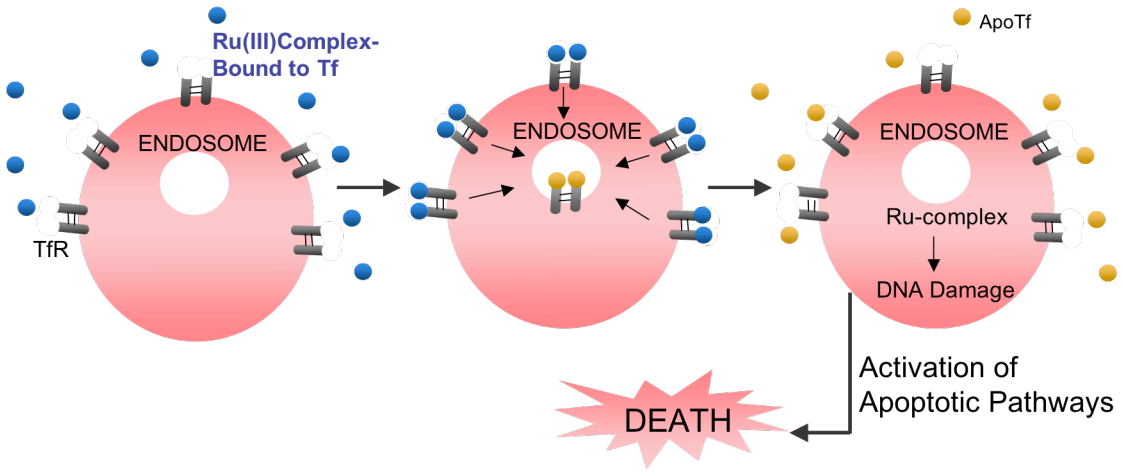

Figure 1-4 An Illustration of hsTf mediated Ru(III)-complex delivery to cancer cells. The unusually large number of TfRs on the surface of cancer cells enables their specific targeting through natural transferrin cycle. Ru(III)-complexes bound to hsTf taken up by cancer cells where they cause oxidative stress and DNA damage eventually leading to cell death by activation of apoptotic pathways.[2]

into cancer cells while leaving normal cell relatively unaffected and consequently minimizing side-effects.[2, 6, 39, 71] Although only less than 1% of the Ru(III)-complexes (e.g. KP1019) bind to hsTf in blood,[2, 24] the success of Ru(III)-complexes as anti-cancer agents with lower side-effects compared to cisplatin has been atributed to their relatively selective accumulation in cancer cells through the transferrin cycle (figure 1.4).[2, 6]

Human serum albumin (hsA)

hsA is a 66 kDa nonglycosylated single-chain protein comprising three homologous domains (I - III) that are arranged to form a heart-shaped molecule.[72-74] Each domain in turn consists of two subdomains designated as A and B (figure 1.5). The amino acid sequence of hsA contains a total of 17

disulfide bridges, one free thiol (Cys34, located in subdomain IA) and a single tryptophan (Trp214, located in subdomain IIA).[74] hsA is the most abundant protein in the circulatory system with a concentration of ~40 mg/mL, which makes it an important factor in the binding and delivery of many pharmaceuticals to sites of disease.[75] Its flexible structure and a variety of ligand binding sites allows hsA to bind a wide range of chemically diverse endogenous and exogenous ligands. The main ligand binding sites are Sudlow's sites 1 and 2, which are located within the hydrophobic cavity of the subdomains IIA and IIIA respectively.[76] Bulky heterocyclic anions such as the anticoagulant drug Warfarin bind to Sudlow's site 1, whereas the aromatic carboxylates such as ibuprofen bind to the Sudlow's site 2.[77] In addition, a long chain fatty acid binding site in domain III[78, 79] and a heme binding site in domain I[80, 81] have been reported. The Cys34 in subdomain I forms the binding site for cysteine and glutathione.[82] hsA has also been shown to form complexes with some mercury and gold compounds.[83] The N-terminal His3 residue of hsA constitutes a strong binding site for metal ions such as Cu(II) and Ni(II).[84]

A previous study demonstrated that hsA binds four molecules of KP1019 *in vitro* and the possible complex binding sites were proposed to be at the histidine residues located in the domain IIA binding pocket of hsA or at the other histidines near this region.[26] Binding of the Ru(III)-complexes to the most abundant serum protein, hsA, may partially contribute to the selective accumulation of the complexes in tumor cells due to the enhanced permeability and retention effect.[2]

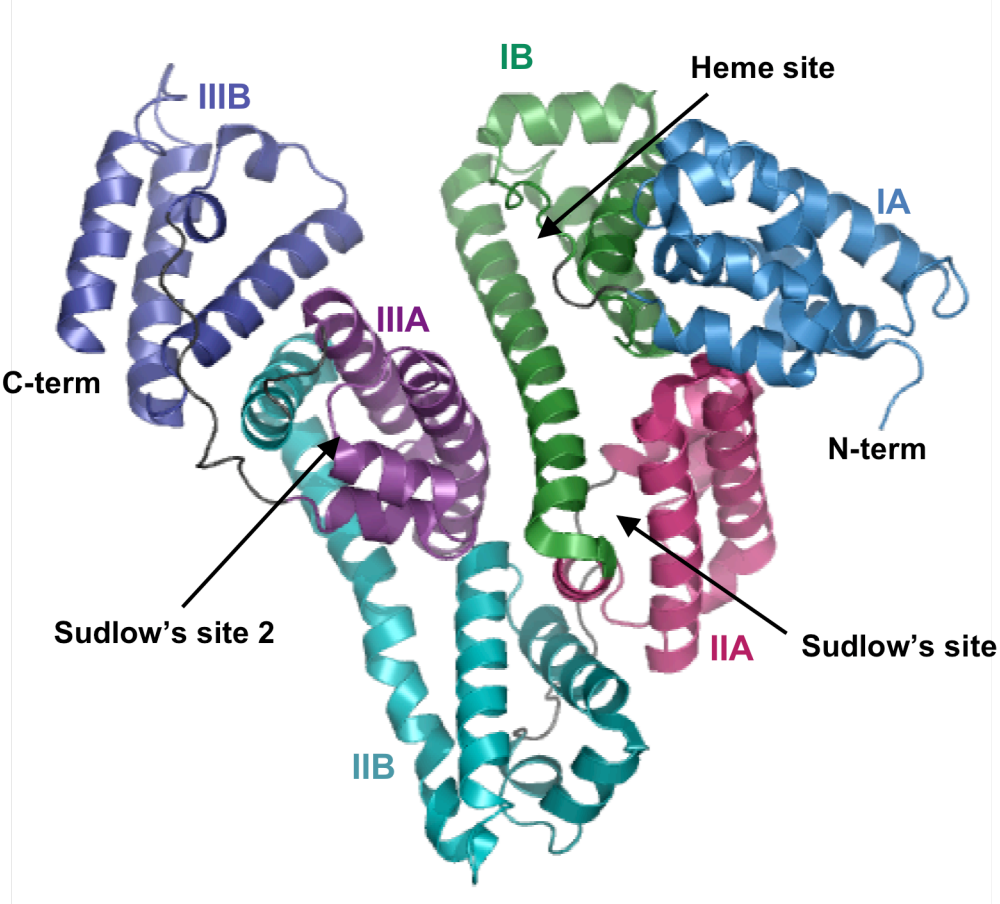

Figure 1-5 Structure of human serum albumin (hsA). hsA is arranged into three homologous domains forming a heart-shaped molecule. Each domain is made up of two subdomains designated as A and B. The two primary drug binding sites, Sudlow's site 1 and Sudlow's site 2 are located within the hydrophobic cavities of subdomain IIA and IIIA respectively. The principal heme binding site is found in the domain I. Figure was generated using PyMOL.[58] The structural coordinates were obtained from the RCSB, PDB under the identifier 1N5U.[81]

1.2.5 Clinical studies

In a clinical phase I dose escalation study, KP1019 was intravenously administered to eight patients with solid tumors in doses ranging from 25 mg to 600 mg twice weekly over three weeks. A disease stabilization for 8 to 10 weeks and only mild toxicities arising from KP1019 treatment was observed in five of the

six evaluable patients included into the study.[2] The pharmacokinetic studies on KP1019 revealed a long terminal half-life ($t_{1/2}$ = 69 – 284 hours) of the complex in blood which was mainly in the protein-bound form.[2]

In the phase I clinical studies, NAMI-A was tested in 24 patients and it was found that NAMI-A can be administered safely at a dose of 300 mg/m^2/day for five days, every 3 weeks.[7] In the same study the terminal half-life of NAMI-A was found to be approximately 50 hours.

1.3 Introduction to the research

Despite a plethora of studies on anti-cancer Ru(III)-complexes, the precise mechanisms by which they exert their tumor-specific effects as anti-cancer agents remain elusive. Careful evaluation of the interactions of Ru(III)-complexes with serum proteins and the species formed following their intravenous administration is crucial in understanding their precise mode of action.

This thesis aims to characterize the interactions of three Ru(III)-complexes: KP1019, KP418, and NAMI-A, with the main serum protein targets hsTf and hsA as well as the species they form in serum. This knowledge will help categorize the Ru(III)-complexes with respect to their anti-cancer activities and the processes they undergo before they enter tumor cells, which will ultimately guide development of novel metal-based anti-cancer drugs with improved clinical efficacy.

1.4 Experimental objectives

Chapter 2:

Characterization of the interactions of the Ru(III)-complexes with hsTf and hsA

The first objective of this research was to characterize the Ru(III)-complexes with respect to their interactions with hsTf and hsA using electron paramagnetic resonance (EPR) spectroscopy. The motivation for this study was to identify differences or similarities in the interactions of the Ru(III)-complexes with the serum proteins in terms of the oxidation state and environment of the ruthenium-centre in the complex/protein adducts. These studies were performed both with isolated proteins and in serum.

Determination of the role of iron-binding site of hsTf in KP1019-binding

The success of KP1019 as an anti-cancer agent has been correlated to its ability to bind hsTf at the iron-binding sites.[27] KP1019 bound to diferric-hsTf is approximately 80-fold more effective at inhibiting growth of human colon cancer cells in culture compared to the complex alone, yet KP1019 bound to apo-hsTf exhibits less toxicity than the free complex.[85] Therefore the significance of KP1019-binding to hsTf at the iron-binding sites were investigated by EPR spectroscopy.

Determination of the role of His249 in the iron-binding site of hsTf in KP1019-binding

Binding of Ru(III)-complexes to hsTf at the iron-binding site has been suggested to be via coordination of the ruthenium-centre to the imidazole group of His249.[27, 86] However, direct evidence for this interaction has been lacking.

Therefore, this research also addressed this issue by EPR analysis of the ability of His249Ala mutant of hsTf to bind KP1019.

Chapter 3 and Chapter 4:

Development of a procedure for expression and purification of recombinant full-length hsTf in *Pichia pastoris*

Due to the large number of disulfide bonds in hsTf, use of a eukaryotic expression system for production of the iron-binding site mutants of hsTf was necessary. Because of its economic and timesaving nature, the *Pichia pastoris* (*P. pastoris*) expression system was chosen for the production of wild-type and mutant proteins. However, a literature procedure for expression of full-length hsTf in *P. pastoris* has not been reported. In this thesis such a procedure was developed. In addition, a protocol for easy purification of the recombinant protein from *P. pastoris* expression medium using immobilized metal-ion affinity chromatography was devised.

CHAPTER 2: SPECTROSCOPIC ANALYSIS OF THE INTERACTIONS BETWEEN THE ANTI-CANCER Ru(III)-COMPLEXES AND SERUM PROTEINS

2.1 Abstract

The aim of this study was to characterize the interactions of the anti-cancer Ru(III)-complexes KP1019, KP418, and NAMI-A with serum proteins, and the species they form in serum, which is important in understanding Ru(III)-complex mediated tumor inhibition. To achieve this, electron paramagnetic resonance (EPR) spectroscopy, a powerful technique sensitive to the changes in the electronic and structural environment of paramagnetic samples, was utilized as the main analytical technique. The Ru(III)-state of NAMI-A was found to be unstable in buffer (pH 7.4), and reduction to Ru(II) was not prevented in the presence of hsTf. In contrast, KP1019 and KP418 were stable in the +3-oxidation state both in buffer and in the presence of hsTf and hsA. These complexes were found to bind to both serum proteins via ligand-exchange. The EPR data suggested that the complexes initially bind to hsA via hydrophobic interactions. EPR studies of KP1019 and KP418 in serum indicated that Ru(III)/Ru(II) reduction is insignificant when incubated in serum at 37 °C over a period of 24 hours. The structural transformation of KP1019 in serum at 37 °C took place in three steps. In the first step, KP1019 binds to serum protein(s) via hydrophobic interactions as soon as it is introduced into serum. In the following steps, ligand-exchange by side chain(s) of protein residue(s) occurs. On the other hand,

KP418 followed a different path, in which its structural transformation was almost complete as soon as it was introduced into serum and did not change significantly over 24 hours. Another difference between KP1019 and KP418 was observed from the UV-visible studies of the complexes with apo-hsTf, that binding of KP1019 to apo-hsTf was much faster than that of KP418. Despite the similar structures of KP1019 and KP418, the disparate behavior of KP1019 in serum and its faster binding ability to hsTf may partially account for the differential anti-cancer activities of these complexes.

EPR studies with iron-binding site His249 mutant of N-terminal half molecule of hsTf and diferric-hsTf (iron binding sites are saturated with Fe^{3+}) suggested that the interaction of KP1019 at the iron binding sites of hsTf is necessary for stabilization of its +3 oxidation state. This finding has important implications for the mechanism of action of KP1019 in which the Ru(III) / Ru(II) reduction/activation in serum is prevented when it is bound to the iron-binding sites of hsTf (and possibly to the certain ligand binding pockets of hsA) prior to delivery to cancer cells. This study represents the first EPR analyses of the anti-cancer Ru(III)-complexes in physiological buffer and in serum, as well as of their interactions with serum proteins hsTf and hsA.

2.2 Introduction

KP1019, KP418, and NAMI-A are promising anti-cancer agents with lower side-effects than platinum based anti-cancer drugs. Serum protein interactions are important components of their tumor-specific activities.[2, 33] Hence, several studies have examined the interactions of these complexes with the serum

proteins hsTf and hsA.[21-29] In the case of KP1019 and KP418 particular attention has been given to the interactions with hsTf since it provides the most effective route for delivery of these complexes to tumor cells.[6] Intriguingly, in the animal studies with an autochthonous colon cancer model, KP1019 exhibited far less toxicity but slightly higher anti-cancer activity than the structurally very similar complex KP418.[40] This was correlated to the differences in their hsTf-binding behavior, KP1019 binding being much faster and specific at the iron-binding sites.[85, 86]

In earlier studies, accumulation of KP1019 specifically in tumor cells was proposed to be mediated by hsTf.[27, 86] However, considering the ~20-fold greater concentration of hsA than hsTf in blood, the effect of binding to hsA cannot be disregarded. This issue was addressed in recent studies and it was shown that binding of KP1019 to hsA in the bloodstream is thermodynamically more favorable compared to hsTf with overall binding constants of 1.06×10^3 M^{-1} (hsA) and 5.6×10^3 M^{-1} (hsTf),[23] whereas binding to hsTf is more kinetically favourable ($k = 28.7 \times 10^4$ for hsTf and $k = 10.6 \times 10^4$ for hsA)[57] suggesting that hsA may act as a KP1019 repository as well as a natural drug carrier to tumor cells. Another study analyzed plasma samples from cancer patients treated with KP1019 in clinical phase I trials using modern chromatography/mass spectrometry techniques and demonstrated exclusive binding of the drug to a 60-80 kDa protein fraction.[24] Analysis of this fraction confirmed the presence of hsA and hsTf, however only less than 1% of the total KP1019 was found to be associated

with hsTf. Nevertheless, the authors surmised that this amount was adequate for efficient uptake into tumor cells via transferrin pathway.[2]

Although these studies revealed the identity of the serum proteins and their strength in binding to the complexes, the exact role and nature of the Ru(III)-complex-protein interactions and biological consequences of these interactions with respect to their differential anti-cancer activities remain unclear. In particular, information on the electronic and structural properties of these complexes after their intravenous administration is needed for identification of the species formed outside the cells, which in turn will contribute to understanding the mechanism of KP1019, KP418, and NAMI-A mediated tumor inhibition and the factors involved in their differential anti-cancer activities. EPR spectroscopy has the power to determine such properties, including the oxidation state of the complexes and structural changes around the Ru(III)-centre. Herein, the interactions of Ru(III)-complexes with serum proteins hsTf and hsA were characterized by EPR spectroscopy. KP1019 and KP418 were further studied using UV-visible spectroscopy. In hopes of explaining the differential anti-cancer activities of these structurally similar complexes, the electronic and structural properties of their species formed in serum were examined to assess whether the speciation of these complexes distinctive in serum. Furthermore different opinions on the importance of KP1019 binding to iron-binding sites of hsTf with respect to its anti-cancer activity exist in the literature.[27, 85-87] Therefore this issue was investigated by EPR studies on the interactions of KP1019 with iron-binding site His249Ala mutant of N-terminal half molecule of hsTf and with differric-hsTf.

2.2.1 Electron Paramagnetic Resonance (EPR) Spectroscopy

EPR spectroscopy detects species that contain unpaired electrons. An isolated electron, without any outside forces, has an intrinsic angular momentum called "spin" with an associated magnetic moment μ. When an external magnetic field, B_0 is applied, the Zeeman effect causes the magnetic moments of the unpaired electrons to align with (lowest energy state) or against (highest energy state) the magnetic field. These orientations correspond to values of the spin magnetic quantum numbers; m_s = -1/2 (when aligned parallel with the external magnetic field), or m_s = +1/2 (when aligned antiparallel with the external magnetic field). The Zeeman energy is given by;

$$\mathbf{E_{Zeeman} = g_e \beta_e B m_s}$$

where g_e = free electron g-value, β_e = Bohr magneton, B = applied magnetic field. Therefore an unpaired electron has two energy levels in an applied magnetic field. EPR spectroscopy measures the difference (Zeeman splitting) between these to energy states. In an EPR experiment, a sample containing unpaired electron(s) is placed in a large uniform magnetic field to split the two distinct energy levels. Usually the microwave frequency is kept constant and the magnetic field is swept. An EPR spectrum is generated when the energy of the microwave frequency exactly matches with the energy difference between the two energy states of the unpaired electron (figure 2.1). This is called the "resonance condition" and given by:

$$\mathbf{h\nu = g_e \beta_e B_0}$$

where h = Planck's constant, ν = microwave frequency.

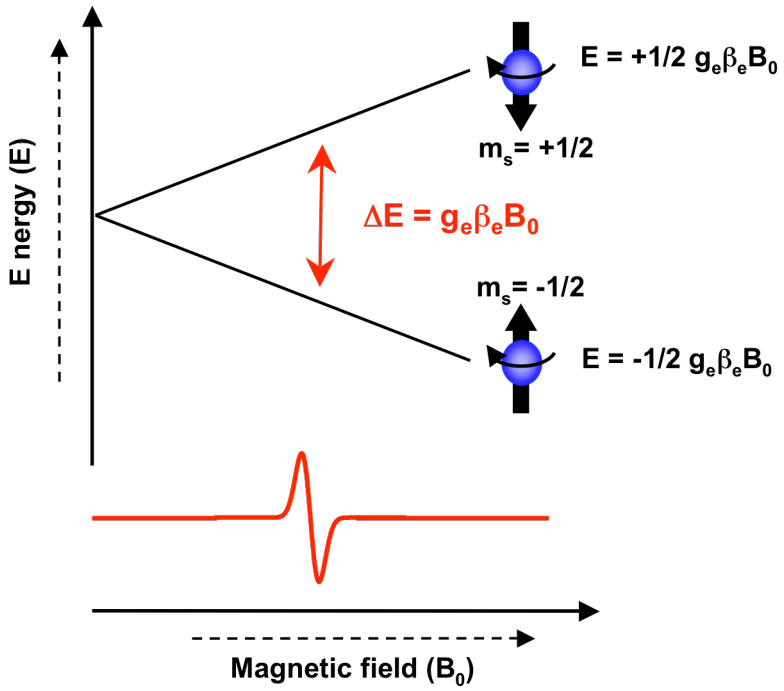

Figure 2-1 Spin state energy levels of an unpaired electron as a function of external magnetic field. When an external magnetic field is applied the unpaired electron orients parallel or antiparallel with the magnetic field creating two distinct energy levels for the electron. The unpaired electron at the ground energy level (m_s = - 1/2) is excited to the upper energy level (m_s = + 1/2) by microwave irradiation. An EPR transition is obtained when the energy difference between the upper and lower energy levels ($\Delta E = g_e\beta_eB_0$) is exactly matched by the energy of microwave irradiation ($E = h\nu$). This is called the "resonance condition" and is given by $h\nu = g_e\beta_eB_0$

There are several different microwave frequencies (band) commonly used in EPR spectrometers. Among these, X-band (ν = 9.4 GHz) and Q-band (ν = 35 GHz) frequencies are the most common.

Different paramagnetic species can be characterized by their unique resonant fields. These differences are quantified in terms of the "g-value", which is calculated by:

$$g = \frac{h\nu}{\beta_e B_0}$$

In paramagnetic transition metal ions, magnetic moment of unpaired electrons is modified due to the coupling of orbital angular momentum and spin angular momentum (spin-orbit coupling). For transition metal ion complexes containing an unpaired electron the ligand field may also change the magnetic moment of the electron spin by affecting the spin-orbit coupling. Therefore, the g-value differs from the free electron g-value, g_e, by an amount that depends on the magnitude of spin-orbit coupling which in turn depends on the size of the nucleus containing the unpaired electron as well as the nature of the ligands and their symmetry.

Due to the orientation of the orbitals at paramagnetic centres, the magnitude of spin-orbit coupling is direction dependent, which causes anisotropy in the g-value. Thus, in a paramagnetic molecule the g-values, when measured along x, y, and z molecular directions define a principle axis system (g_x, g_y, g_z). In a low viscosity solution, molecular tumbling causes the anisotropy to be averaged out giving an EPR spectrum with a single g-value (isotropic, $g_x = g_y = g_z = g$). In powder samples or frozen solutions, individual molecules are fixed in place, and the resulting EPR spectra are statistically weighted averages of all possible orientations. The corresponding “powder pattern” EPR spectra (figure 2.2) are classified according to the local symmetry of each paramagnetic molecule: isotropic ($g_x=g_y=g_z=g$), uniaxial ($g_x=g_y\neq g_z$), and rhombic ($g_x\neq g_y\neq g_z$).

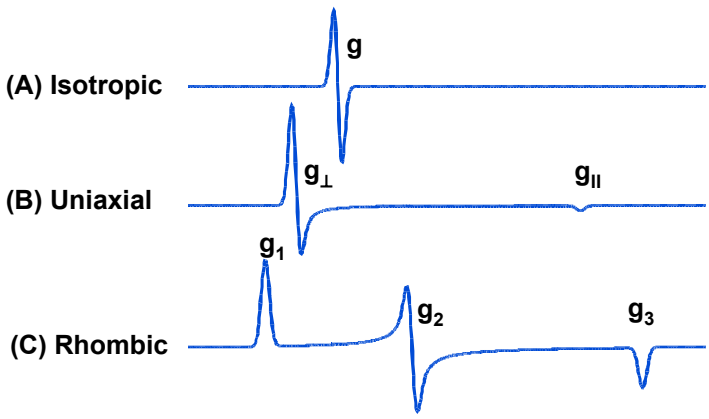

Figure 2-2 Typical EPR spectra for paramagnetic systems with (A) isotropic symmetry ($g_x=g_y=g_z=g$), (B) uniaxial symmetry ($g_x=g_y\neq g_z$, where $g_\perp$ corresponds to $g_x=g_y$ and g_{II} corresponds to g_z) (C) rhombic symmetry ($g_x\neq g_y\neq g_z$, which are generally represented by g_1, g_2, and g_3).

EPR spectroscopy is an excellent technique to study the electronic and structural changes in Ru(III)-complexes under biologically relevant conditions. Specifically, the change in the oxidation state can be easily followed by this technique. When in the +3-oxidation state, the ruthenium-centre of the complexes investigated in this research has single unpaired electron that can be detected by EPR (figure 2.4. A). On the other hand the reduced +2 state, Ru(II), has no unpaired electrons, and therefore has no EPR signal. In addition to the oxidation state, EPR can also detect the changes in the ligand field. Since the g-values are measured along the principal axes of the complex (x, y, and z, figure 2.4. B), changes in the ligand field of the paramagnetic Ru(III)-centre (increased or decreased symmetry around the Ru(III)-centre) can cause shifts in the g-values, leading to distinct changes in the EPR spectrum.

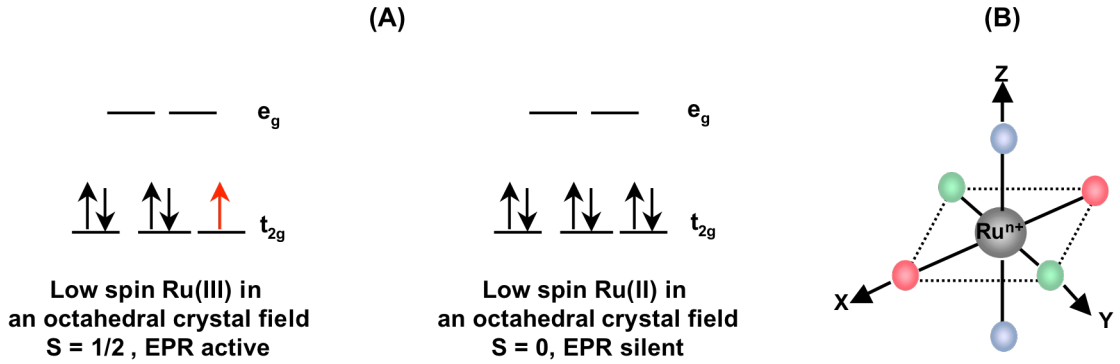

Figure 2-3 **(A)** d-orbital splitting for Ru(III) and Ru(II) in an octahedral crystal field. Almost all ruthenium complexes are low spin and have octahedral geometry. When the ruthenium centre is in the +3 oxidation state, (Ru(III), paramagnetic) the complex has an unpaired electron which can be detected by EPR spectroscopy. On the other hand, the +2 oxidation state has no unpaired electrons (Ru(II), diamagnetic) and hence has no EPR signal. **(B)** Schematic representation of an octahedral ruthenium complex. The g-values are measured in the x, y, and z directions, therefore they are very sensitive to the changes in the nature of the ligands.

2.3 Materials and Methods

2.3.1 Materials

All reagents and lyophilized proteins were purchased from Sigma-Aldrich. The buffer components were from Bioshops Canada. Whole rabbit blood was obtained from the animal facilities of University of British Columbia – Animal care centre. Amicon®Ultra-4 (or Ultra-15) Centrifugal Filter Units were from Millipore. Quartz EPR sample tubes were from Wilmad (Buena, NJ).

2.3.2 Synthesis of Anticancer Ru(III)-complexes

The anti-cancer Ru(III)-complexes, KP1019, KP418, and NAMI-A, were synthesized and characterized by an undergraduate student in our laboratory (Joshua Dubland) as described in the literature.[88-90]

2.3.3 Preparation of apo- and Fe_2-hsTf

Apo-hsTf

The commercial apo-hsTf was not completely free of iron and required further iron removal for Ru(III)-complex binding studies. The desired amount of lyophilized protein was dissolved in iron-removal buffer (500 mM sodium acetate buffer containing 1 mM EDTA and 1 mM NTA -nitrilotriacetic acid- pH 4.5), concentrated down to minimum volume using an Amicon centrifugal filter unit. The protein concentrate was resuspended in the iron-removal buffer and this process was repeated until a clear coloured protein concentrate was obtained. A sequential dilution and concentration in 100 mM KCl, 100 mM $NaClO_4$, and finally in 100 mM KCl was performed to ensure the removal of any residual chelating agents EDTA and NTA from the protein.[91] After final concentration, the concentrated protein was exchanged into the iron-binding buffer (IBB; 50 mM HEPES, 150 mM NaCl, 20 mM $NaHCO_3$, pH 7.4) by a two times repeated dilution and concentration in IBB.

Fe_2-hsTf (diferric hsTf)

Apo-hsTf in IBB was mixed with $Fe(NTA)_2$ at a 1 : 2.5 molar ratio and incubated at 37 °C for 1 hour. The excess $Fe(NTA)_2$ was removed by the repeated concentration and dilution of the protein solution in IBB. $Fe(NTA)_2$ was prepared by dissolving $FeCl_3$ in NTA at a molar ratio of 1:2. The pH was increased to 4 by drop-wise addition of 1 M NaOH.

2.3.4 Preparation of hsA

Lyophilized commercial hsA was dissolved in IBB and used without purification or metal-removal.

2.3.5 Preparation of rabbit serum

Serum was prepared from whole rabbit blood according to the literature methods.[92] Briefly, the blood was clotted at 37 °C for 60 min and the clot was carefully separated from the sides of the 50 mL falcon tube by using a long Pasteur pipette. The tube was left at 4 °C overnight to allow the clot to contract. Serum was separated from the clot by carefully decanting the fluid into a centrifuge tube and centrifuged at 3,000 RPM for 10 min in order to remove the remaining clots and red blood cells as well as other insoluble material in the blood. The supernatant was divided into 2 mL aliquots and stored at -20 °C.

2.3.6 Expression of the iron-binding site mutants of hsTf

The N-terminal half molecule of hsTf with and without the native signal sequence of hsTf was generated by PCR amplification using the template DNAs pPICZα-A/Tf-Kex2 and pPICZα-A/TfNS-Kex2 respectively (see 3.3.2 of this thesis for details). The forward and reverse primers were:

TF-Xho1F: (5′-GCTC**CTCGAG**ATGAGGCTCGCCGTGG -3′)

NTf-Xba1R: (5′- GTG**TCTAGA*TTA***TACTCATAGCCCAGGTAC -3′)

and

NTfNS-Kex2-Xho1F: (5′- GCTC**CTCGAG**AAAAGAGAGAGGTCCCTG -3′)

NTf-Xba1R: (5′- GTG**TCTAGA*TTA***TACTCATAGCCCAGGTAC -3′)

These primers amplified the codons for the Kex2 site, codons for 1-318 residues of mature hsTf, and introduced a stop codon at the end. The forward primer Tf-Xho1F also amplified the hsTf signal sequence (between the *Xho I* site and the Kex2 site). The resulting ~1 kb PCR products were cut with *Xho I* and *Xba I* restriction endonucleases and purified from 1% agarose gel using the gel extraction kit from Qiagen. These fragments, flanking the *Xho I* and *Xba I* sticky ends, were inserted into the *Xho I* and *Xba I* sites of the expression vector pPICZα-A, which was also digested with the same restriction enzymes and purified from 1% agarose gel. The resulting ~4.7 kb plasmid DNAs contained the N-lobe of hsTf with (pPICZα-A/NTf-Kex2) and without the native signal sequence of hsTf (pPICZα-A/NTfNS-Kex2). The correct insertion of the fragments into the vector was confirmed by DNA sequencing.

The iron binding residues of the N-lobe of hsTf, Asp63, Tyr95, Tyr188, and His249, were replaced by Ala residue by site-directed mutagenesis one at a time. pPICZα-A/NTf-Kex2 and pPICZα-A/NTfNS-Kex2 plasmids were used as templates and the site-directed mutagenesis was carried out by PCR as described in section 3.3.3. The mutagenic primer sets are given below.

D63A-F: (5'- GATGCTGTGACACTG**GCT**GCAGGTTTGGTGTATG -3')

D63A-R: (5'-CATACACCAAACCTGC**AGC**CAGTGTCACAGCATC -3')

Y95A-F: (5'- GGATCCACAGACTTTC**GCT**TATGCTGTTGCTGTGG -3')

Y95A-R: (5'- CCACAGCAACAGCATA**AGC**GAAAGTCTGTGGATCC -3')

Y188A-F: (5'- CTTAACCAATACTTCGGC**GCT**TCGGGAGCCTTCAAGTGTC -3')

Y188A-R: (5'-GACACTTGAAGGCTCCCGA**AGC**GCCGAAGTATTGGTTAAG -3')

H249A-F: (5'- CCAGGTCCCTTCT**GCT**ACCGTCGTGGC -3')

H249A-R: (5'- GCCACGACGGT**AGC**AGAAGGGACCTGG -3')

In order to verify the correct mutation, the sequencing primers 5' AOX1 (for D63A and Y95A) and 3' AOX1 (for Y188A and H249A) primers (section 3.3.2) were used in the DNA sequencing. Transformation of the *P. pastoris* GS115 cells and expression of the site-directed mutants of the N-lobe/hsTf were performed as described in detail in section 3.3.

2.3.7 EPR spectroscopy

EPR Instrument

X-band EPR spectra were collected at 77 K or 20 K using a Bruker EMX plus X-band (~9.5 GHz) spectrometer. Samples measured at 77 K were prepared in 3 mm outer diameter quartz EPR tubes immersed in liquid nitrogen in a finger dewar, which was placed directly into the cavity of the instrument. Helium gas was bubbled into the finger dewar to reduce bubbling of liquid nitrogen and the spectral noise associated with it. Measurements at 20 K were performed using a Bruker ER4112HU helium temperature control system and a continuous flow liquid helium cryostat. 4 mm outer diameter quartz EPR tubes were used in the experiments.

Q-band EPR spectra were collected at 20 K using the same Bruker EMX plus spectrometer, but operating with a Q-band (34 GHz bridge) and a ER4118CF cryostat. Samples were placed into 1.4 mm outer diameter quartz Q-band EPR tubes.

Experimental Parameters

Modulation amplitude = 6 G, microwave power = 1.736 mW, receiver gain = 1 x 10^4, time constant = 40.96 ms. Microwave frequencies and number of scans are given in the figure captions.

Preparation of samples for EPR studies

A. KP1019, KP418, and NAMI-A in IBB

All EPR samples of the Ru(III)-complexes were prepared fresh prior to experiments were performed. The complexes were dissolved in IBB at a concentration of 6 mM. The concentration of NAMI-A was increased to 10 mM since no EPR signal was obtained from the 6 mM sample. The KP1019 solution was centrifuged briefly to remove any precipitate. 10% (by volume) glycerol was included in the samples as a glassing agent. All samples were immediately placed into the EPR tubes and frozen in liquid nitrogen.

B. KP1019, KP418, and NAMI-A in apo-hsTf

The Ru(III)-complex – protein binding studies were performed with diluted samples in 4 mL of total volume and the samples were concentrated 40 times to obtain 3 mM complex and 1.5 mM apo-hsTf in IBB at a final sample volume of 100 μL in the EPR tubes. First, 600 μL of 0.25 mM stock solution of apo-hsTf

was mixed with 2.8 mL of IBB in a 15 mL falcon tube. 600 μL of 0.5 mM stock solutions of the complexes, which were prepared in IBB, were added to the protein solutions. The final concentration of the complexes and apo-hsTf in the 4 mL total mixture volume were 0.075 mM and 0.0375 mM respectively. The complex/apo-hsTf mixtures were incubated at 37 °C for 40 minutes and concentrated down to 50 μL using 4 mL Amicon ultra centrifugal filter units at 8 °C. The concentrates were placed in 0.6 mL microcentrifuge tubes and mixed with 10 μL of glycerol. The filter units were rinsed with 40 μL of IBB to complete the total volume of the samples to 100 μL. The samples were then centrifuged briefly to remove any precipitate and frozen in liquid nitrogen in the EPR tubes with 3 mm outer diameter for measurements at 77 K.

C. KP1019 and KP418 in a solution of apo-hsTf/hsA mixture

To obtain 3 : 1.5 : 1.5 mM mixtures of the Ru(III)-complex : apo-hsTf : hsA, 1.8 mL each of the 0.25 mM apo-hsTf and hsA stock solutions were mixed in 15 mL falcon tubes. 400 μL of the 2.25 mM stock solution of the complexes were added onto the protein mixture. The resulting 4 mL samples were incubated at 37 °C for 1 hour and processed as described above. The final sample volume was 300 μL. 30 μL aliquots from each sample were transferred into 1 mm outer diameter Q-band quartz EPR tubes and frozen in liquid nitrogen. The rest of the samples were placed into 4 mm outer diameter X-band EPR tubes and frozen for EPR measurements at 20 K. Parallel experiments were done with 3 mM of each complexes with 1.5 mM apo-hsTf and 1.5 mM hsA one at a time as controls.

D. KP1019 and KP418 in rabbit serum

Ru(III)-complexes (KP1019: 4.3 mg; KP418: 3.5 mg) were dissolved in 8 mL IBB and mixed with 4 mL of rabbit serum. The final concentration of the complexes in 12 mL of complex/serum mixtures was 0.67 mM. 3 mL aliquots were taken and processed as described in section **C** above. The rest of the mixtures were incubated at 37 °C over a period of 24 hours. 3 mL aliquots were taken at 3 different time points; 2 hours, 6 hours, and 24 hours after incubation and processed as described in **C**. The final concentration of the complexes in the EPR tubes was 6.5 mM, which is reasonable considering the number of KP1019-binding sites on albumin and transferrin (several binding sites on each protein, albumin and transferrin concentration in the EPR samples are ~ 2 mM and 0.1 mM respectively).

E. KP1019 in solution with H249A site-directed mutant of N-terminal half molecule of recombinant hsTf (N/hsTf)

After purification by Cu^{2+}-affinity chromatography as described for the purification of full-length hsTf from the *P. pastoris* expression medium (4.4.2 of this thesis), the fractions containing the 37 kDa protein (determined by SDS-PAGE, data not shown) were pooled together and the buffer was exchanged into IBB using a centrifugal filter unit. The protein concentration of the resulting 5 mL solution was determined to be ~0.06 mM using a millimolar extinction coefficient of 38.4 for N/hsTf.[93] This solution was divided into two. One aliquot was concentrated down to ~60 μL and mixed with 10 μL of glycerol and the volume was completed to 100 μL. This sample was frozen in a 3 mm outer diameter EPR

tube in liquid nitrogen. The other aliquot was mixed with 600 μL of a 0.5 mM stock solution of KP1019 and the volume was completed to 4 mL with IBB. The resulting solution was incubated at 37 °C for 40 minutes and processed as described for the control sample. The final concentration of the KP1019 in the EPR tube was 3 mM.

F. KP1019 in a solution of Fe_2-hsTf

1.8 mL of 0.25 mM diferric-hsTf was mixed with 400 μL of 0.5 mM KP1019 in IBB and the volume was completed to 4 mL with IBB. After incubating at 37 °C for 40 minutes, this sample was processed as described in section **D** to give 3 mM KP1019 in 1.5 mM diferric-hsTf and frozen in a 4 mm outer diameter EPR tube.

2.3.8 UV-visible Spectroscopy

In order to investigate the KP1019 binding to apo-hsTf by UV-visible spectroscopy, the electronic absorption spectra of the samples were collected between 200 nm and 800 nm at room temperature. A 200 μM stock solution of the complex was prepared in reference buffer (IBB) immediately before the first scan and mixed with 1) IBB, 2) hsTf in IBB in 0.5 mL quartz cuvettes one at a time to a final concentration of 100 μM. The final concentration of hsTf in the cuvette was 50 μM. The data were collected at different time points (see figure 2.13) over a period of 24 hours after dissolving the complex.

The effect of temperature on the spectral behavior of KP1019 incubated in apo hsTf was also studied by UV-visible spectroscopy. 250 μL of the 200 μM

stock solution of the complex mixed with 100 μL of 250 μM stock solution of hsTf and 150 μL of IBB in a 1.5 mL microcentrifuge tube. This solution was incubated at 37 °C for 30 minutes and transferred to a 0.5 mL quartz cuvette to scan the UV-visible spectra between 200 and 800 nm at room temperature. A parallel experiment was performed with KP418 for comparison.

2.4 Results

2.4.1 X-band EPR analyses of KP1019, KP418, and NAMI-A in buffer and in apo-hsTf

The X-band EPR spectra of the frozen samples of KP1019 and KP418 in buffer (IBB) and in apo-hsTf were recorded at 77 K (figure 2.4) and the g-values are listed in table 2.1. The EPR signal of the NAMI-A complex both in buffer and apo-hsTf was very weak (data not shown) even at high concentrations up to 10 mM indicating that the ruthenium-centre in most of the complex is no longer in the +3 oxidation state, and addition of apo-hsTf does not prevent this change in the oxidation state. Therefore the g-values for this complex could not be assigned. KP1019 in buffer produced 3 lines with three distinct g-values (g_1 = 2.93, g_2 = 2.61, and g_3 = 2.20), which is typical for low-spin d^5 systems with rhombic symmetry.[94] KP418 also gave a spectrum for a rhombic system, however only two g-values could be assigned (g_1 = 3.07 and g_2 = 2.51). The EPR spectrum of KP418 in HEPES buffer at pH 7 was reported in the literature with similar observations.[94] When incubated with apo-hsTf at a 2:1 molar ratio in IBB at 37 °C for 40 minutes, both complexes gave spectra that were significantly changed from those of the buffer solutions. In both cases the EPR spectra were

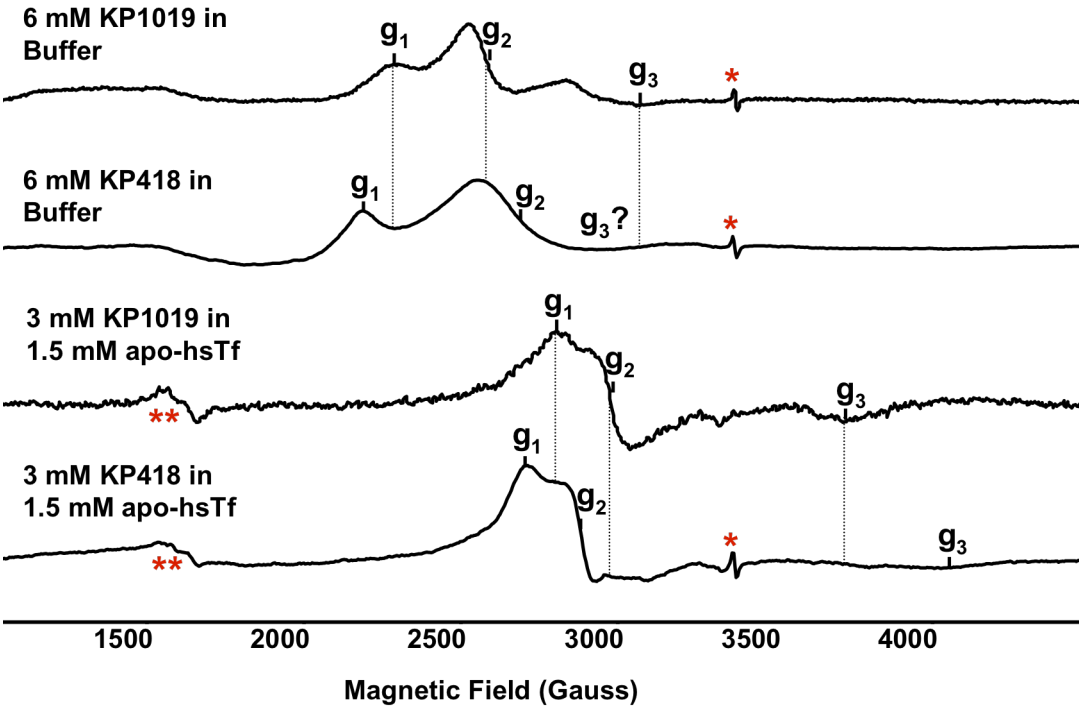

Figure 2-4 X-Band EPR spectra of KP1019 and KP418 in buffer and in apo-hsTf at 77 K. Both KP1019 and KP418 in buffer produce EPR spectra for a rhombic system. The complexes exhibit almost uniaxial EPR spectra upon binding to apo-hsTf. The g-values are given in table 2.1. *Background signal from a radical species in the finger dewar. **Characteristic EPR spectrum for Fe(III)-hsTf due to incomplete removal of Fe^{3+} from hsTf. (EPR parameters: microwave frequency = 9.43. The spectra were average of 10 scans).

Table 2.1 g-values of Ru(III)-complexes in buffer and in apo-hsTf obtained from X-band EPR experiments at 77 K.

Sample	g_1	g_2	g_3
KP1019 in buffer*	2.93	2.61	2.20
KP418 in buffer	3.07	2.51	Not assigned
KP1019 in apo-hsTf	2.38	2.27	1.84
KP418 in apo-hsTf	2.49	2.34	1.70

* **Buffer:** Iron binding buffer (50 mM HEPES, 150 mM NaCl, 20 mM $NaHCO_3$).

uniaxial, an indication of change in symmetry around the Ru(III)-centre. The large shifts in the g_3 values indicate a ligand exchange process between the complexes and the side-chains on the protein. Although the line shapes of the KP1019 and KP418 EPR spectra are similar to each other, the relatively small differences between the corresponding g-values suggest that the indazole and imidazole ligands are retained on the Ru(III)-centre after binding to apo-hsTf (If the complexes lost their heterocyclic ligands, the same spectra would be obtained from their protein adducts).

2.4.2 X-band EPR analyses of KP1019 and KP418 in serum

Based on the 'activation by reduction theory' perpetuation of KP1019 and KP418 in the +3 oxidation state before they enter cells is crucial to their anti-cancer activity. In this study, oxidation states of 6.5 mM KP1019 and KP418 in serum were examined by X-band EPR spectroscopy, which detects only the paramagnetic +3-state of ruthenium. Figures 2.5 and 2.6 show that the EPR signal of the complexes persisted over 24 hours, displaying the stability of +3 oxidation state of ruthenium in both KP1019 and KP418 in serum even after 24 hours. It was also possible to follow the time-dependent change in the structure of the complexes in serum by EPR analysis of the aliquots taken from the complexes incubated in serum at 37°C over a period of 24 hours. Figure 2.5 shows that at 0 time point, the KP1019 complex in serum has a very similar rhombic EPR spectrum with similar g-values to that of free- KP1019 in buffer. Incubation in serum at 37 °C for 6 hours and 24 hours both resulted in a dramatic

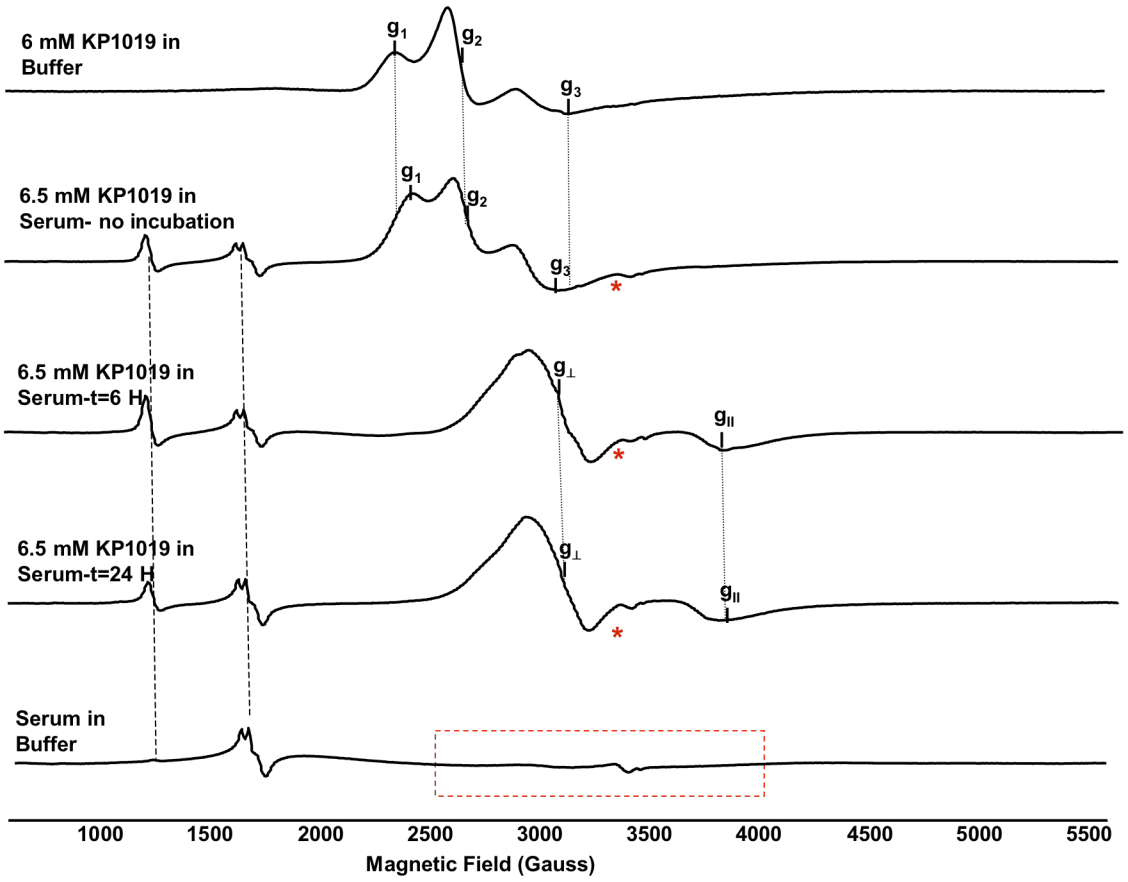

Figure 2-5 X-Band EPR spectra of KP1019 in buffer and in rabbit serum at 20 K. The g-values are given in table 2.2. An EPR signal of a high spin Fe(III) species with $g_{\perp}$= 5.80 (lowest field signal), and a characteristic Fe(III)-bound serum transferrin signal (second signal from the left) presents in all serum samples. *Background signal in the cavity of the instrument, which is more apparent in the serum control spectrum (serum in buffer, boxed region). (EPR parameters: microwave frequency = 9.38 GHz, the spectra were average of 20 scans)

change in the EPR spectra. The complex incubated in serum for 6 hours and 24 hours produced uniaxial spectra ($g_{\perp}$ = 2.25 and g_{II} = 1.79). There are some subtle changes in the EPR spectra of KP1019 incubated in serum for 6 hours and for 24 hours, suggesting some structural changes may occur after 6 hours of incubation in serum.

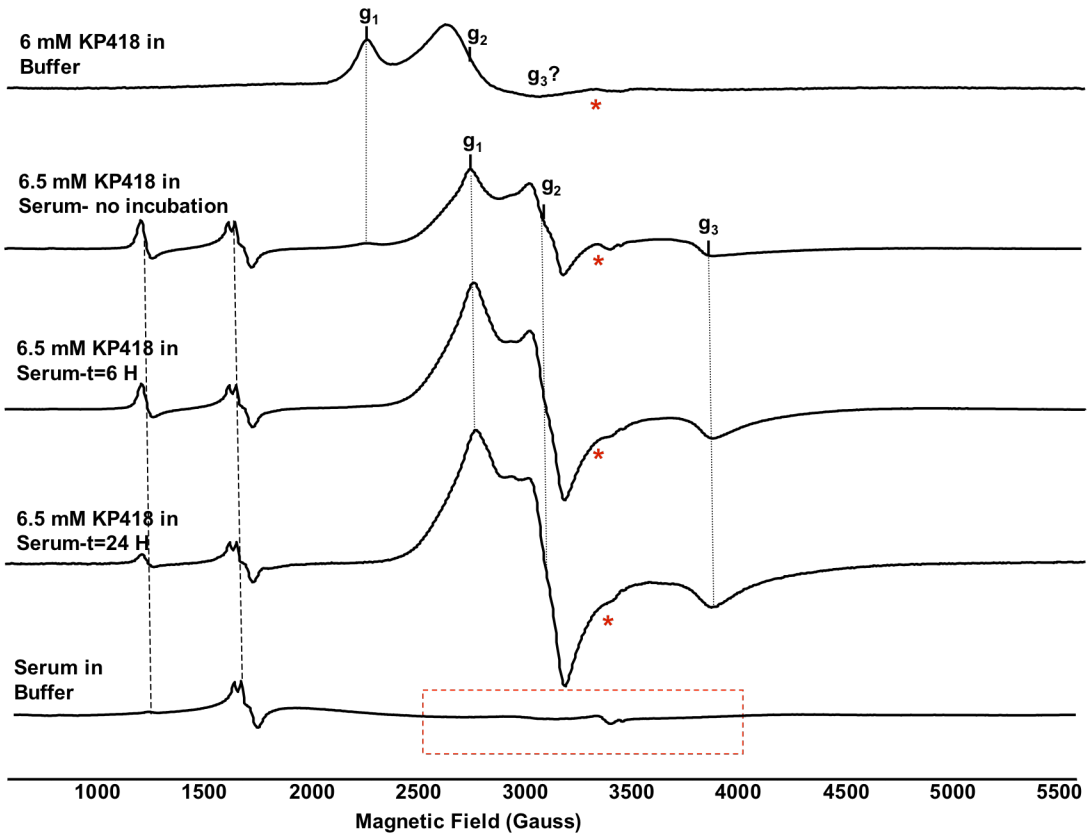

Figure 2-6 X-Band EPR spectra of KP418 in buffer and in rabbit serum at 20 K. The g-values are given in table 2.2. An EPR signal of a high spin Fe(III) species with $g_{\perp}$= 5.80 (lowest field signal), and a characteristic Fe(III)-bound serum transferrin signal (second signal from the left) is present in all serum samples. *Background signal in the cavity of the instrument, which is more apparent in the serum control spectrum (serum in buffer, boxed region). (EPR parameters: microwave frequency = 9.38 GHz, the spectra were average of 20 scans)

Figure 2.6 displays that the structural transformation of KP418 in serum follows a different path from that of KP1019. A significant deviation in the g values of KP418 as soon as it is introduced into the serum from those in buffer indicates a comperatively rapid ligand exchange, possibly by replacement of one or more of the chlorides on the Ru(III)-centre by side chains of available amino acid residues on the serum proteins. Unlike KP1019, KP418 maintains the same

Table 2.2 g-values of Ru(III)-complexes in buffer and in rabbit serum obtained from X-band EPR experiments at 20 K. The complexes were incubated in rabbit serum at 37 °C. Equal aliquots were taken at different times and analyzed by EPR spectroscopy.

Sample	g_1	g_2	g_3
KP1019 in buffer*	2.95	2.60	2.20
KP1019 in serum (t = 0)	2.87	2.60	2.25
KP1019 in serum (t = 6 h)**	2.25	2.25	1.79
KP1019 in serum (t = 24 h)**	2.25	2.25	1.79
KP418 in buffer	3.07	2.51	Not assigned
KP418 in serum (t = 0)	2.51	2.23	1.77
KP418 in serum (t = 6 h)	2.51	2.23	1.77
KP418 in serum (t = 24 h)	2.51	2.23	1.77

* **Buffer:** Iron binding buffer (50 mM HEPES, 150 mM NaCl, 20 mM $NaHCO_3$).
** Axial spectrum with $g_\perp$= 2.25 (g_1=g_2= $g_\perp$) and g_{II}=1.79 (g_3=g_{II}).

low symmetry rhombic structure in serum over an incubation time from 0 to 24 hours at 37 °C, which is evident from the unchanged g values obtained throughout the EPR analyses (see table 2.2 for the g values of KP418 in buffer and in serum).

2.4.3 X-band EPR analyses of KP1019 and KP418 in solution with equimolar mixture of apo-hsTf and hsA

EPR analyses of KP1019 and KP418 in serum showed that both Ru(III)-complexes are rapidly bound by serum proteins and are stabilized in the +3 oxidation state over a period of at least 24 hours. Two serum proteins; hsTf and hsA have been frequently implicated as the major Ru(III)-complex binding proteins in serum.[21, 22, 25, 26, 53-57] Considering the low concentration of transferrin in serum, detection of the complexes bound to transferrin in serum by EPR is

difficult (transferrin concentration in the EPR samples of the complexes in serum is ~0.1 mM). Thus, the observed EPR signals shown in figure 2.5 and 2.6 most probably arise from the complexes bound to albumin, which has ~20-fold greater concentration in serum compared to that of transferrin. To further investigate this, KP1019 and KP418 in hsA, in apo-hsTf, and in 1:1 mixture of apo-hsTf and hsA were analyzed by EPR spectroscopy. Comparison of the EPR spectra of KP1019 revealed three important results; **1**) Binding of KP1019 to hsA resulted in more than one structures, which is most likely due to the binding of the complex to different sites of hsA. This result was deduced from the shape of the EPR spectrum (figure 2.7, KP1019 in hsA) having many shoulders indicating an overlap of EPR spectra from more than one KP1019 derived species with similar g values. **2)** Binding to apo-hsTf resulted in an EPR spectrum of a single KP1019 species. **3)** The most interesting result from this analysis is the detection of a strong signal from a KP1019 species in the apo-hsTf/hsA mixture exactly at the same field as the complex in buffer. This signal was not observed in the apo-hsTf alone and only weakly observed in hsA (more apparent when the spectrum was amplified, data not shown). This EPR signal is attributed to KP1019 bound to hsA via hydrophobic interactions of the heterocyclic ligands with hydrophobic residues of hsA. Note that the EPR spectrum of KP1019 in serum without incubation displayed a similar feature (figure 2.5, second spectrum from the top). It may be argued that unbound KP1019 could not be removed successfully during the concentration process resulting in the same EPR signal for the complex in buffer. This is highly unlikely since free KP1019 almost completely

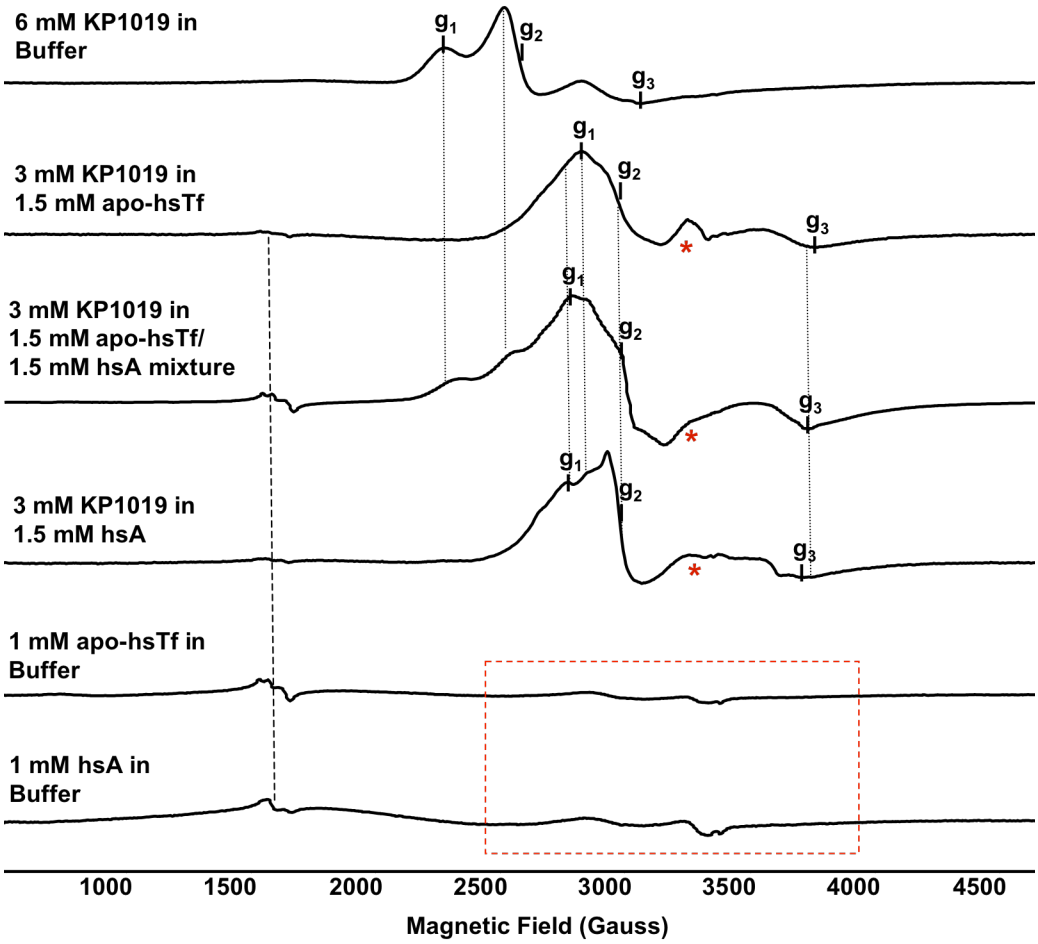

Figure 2-7 X-Band EPR spectra of KP1019 in hsTf, hsA, and hsTf/hsA mixture (1:1) at 20 K. The g-values are given in table 2.3. All complex/protein mixture samples were incubated at 37 °C for 1 hour. A characteristic Fe(III)-bound serum transferrin signal (on the left side of the spectra) is detected in all protein samples *Background signal in the cavity of the instrument, which is more apparent in the control spectra (apo-hsTf and hsA in buffer, boxed region). (EPR parameters: microwave frequency = 9.38 GHz, the spectra were average of 20 scans)

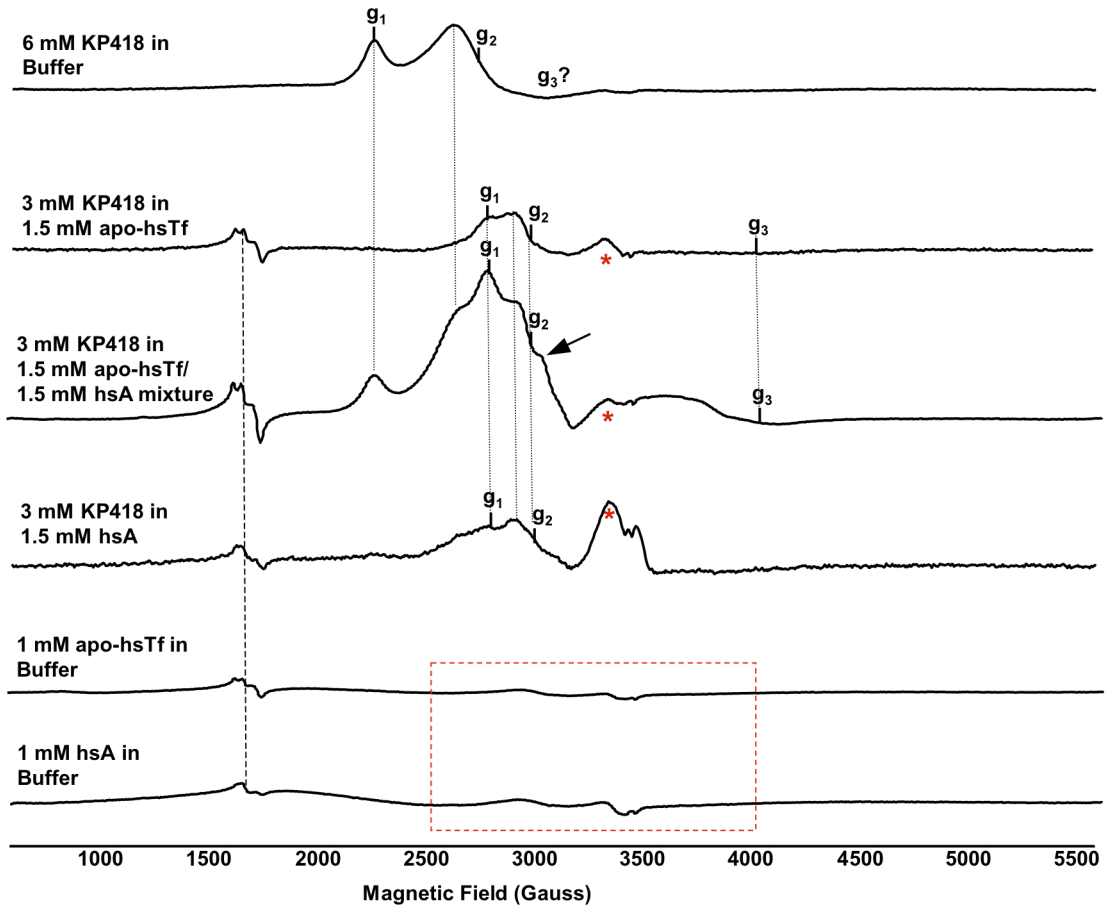

Figure 2-8 X-Band EPR spectra of KP418 in hsTf, hsA, and hsTf/hsA mixture (1:1) at 20 K. The g-values are given in table 2.3. All complex/protein mixture samples were incubated at 37 °C for 1 hour. A characteristic Fe(III)-bound serum transferrin signal (on the left side of the spectra) is detected in all protein samples *Background signal in the cavity of the instrument, which is more apparent in the control spectra (apo-hsTf and hsA in buffer, boxed region). (EPR parameters: microwave frequency = 9.38 GHz, the spectra were average of 30 scans)

Table 2.3 Comparison of the g-values of KP1019 and KP418 in buffer, in apo-hsTf, hsA, and in apo-hsTf/hsA (1:1) mixture obtained from X-band EPR experiments at 20 K. The complexes were incubated at 37 °C for 1 hour after mixing with proteins.

Sample	g_1	g_2	g_3
KP1019 in buffer*	2.95	2.60	2.20
KP1019 in apo-hsTf	2.37	2.24	1.78
KP1019 in has	2.41	2.24	1.79
KP1019 in apo-hsTf/hsA mixture	2.41	2.24	1.80
KP418 in buffer	3.07	2.51	Not assigned
KP418 in apo-hsTf	2.48	2.31	1.70
KP418 in has	2.48	2.31	Not assigned
KP418 in apo-hsTf/hsA mixture	2.48	2.31	1.69

* **Buffer: Iron binding buffer (50 mM HEPES, 150 mM NaCl, 20 mM $NaHCO_3$).**

precipitates in 1 hour at 37 °C. The precipitate can be removed by centrifugation leaving a colourless supernatant. On the other hand when serum proteins are present no precipitation occurs even after days of incubation at 37 °C. All complex/protein mixtures were centrifuged after the concentration step and the dark green colour (a characteristic feature of KP1019 bound to proteins[2, 86]) remained in the solution without giving any precipitate. Therefore maintenance of dark green colour without precipitation is strong evidence for the tight binding of KP1019 to the serum proteins. On the whole, the EPR spectrum of KP1019 incubated in a 1:1 mixture of apo-hsTf and hsA for 1 hour at 37 °C appears to be originating from the overlapping EPR signals of KP1019 coordinated to apo-hsTf and to hsA via ligand exchange as well as the KP1019 bound to hsA via hydrophobic interactions. Note that the g- values of the main signal from KP1019

incubated in the apo-hsTf/hsA mixture for 1 hour (g_1 = 2.41, g_2 = 2.24, g_3 = 1.79) are very close to the g-values of the complex incubated in serum for 6 hours (g_1=2.39, g_2=2.25, g_3=1.80), confirming that the apo-hsTf and hsA are the major binding proteins for KP1019 in serum.

The EPR spectra of KP418 in buffer, in apo-hsTf, hsA, and 1:1 mixture of apo-hsTf and hsA are shown in figure 2.8. Although the EPR signals from the KP418/apo-hsTf and KP418/hsA samples were weaker compared to that of KP418 in apo-hsTf/ hsA mixture, it was still possible to determine the g-values except for the g_3 of KP418 with hsA. The g_1 and g_2 values of KP418 with apo-hsTf, hsA, and apo-hsTf/hsA mixture were determined to be the same (g_1 =2.48, g_2 = 2.31). Since the g_1 and g_2 values of KP418 in apo-hsTf and in hsA are indistinguishable, the amount of the complex bound to apo-hsTf in the equimolar mixture of apo-hsTf and hsA cannot be estimated by EPR analysis. Although the EPR signal of KP418 in hsA with g_1 = 2.48, g_2 = 2.31 is similar to that of in apo-hsTf, two additional signals were observed only for the complex in hsA and in thprotein mixture; a shoulder (figure 2.8, marked with an arrow), and another signal matching the signal from the free complex (in buffer). These data suggest that there are more than one KP418 binding sites on hsA leading to three different KP418 species, and only one type of binding site on apo-hsTf since a single EPR signal from one KP418 species in apo-hsTf was observed. In addition, the same g_1 and g_2 values of KP418 in apo-hsTf and in hsA indicate that the major type of KP418 binding site on hsA is very similar to the binding site on apo-hsTf.

2.4.4 X-band EPR analysis of KP1019 in solution with H249A mutant of N-terminal half molecule of hsTf

In previous studies, binding of KP1019 to apo-hsTf has been suggested to be at the iron-binding sites, specifically via replacement of a chloride ligand on the Ru(III)-centre by the imidazole groups of the iron-binding site histidines (His249 in the N-lobe and His585 in the C-lobe).[2, 86, 86] Although the imidazole groups of histidine residues are well recognized as potential ligands for Ru(III) in the complexes, involvement of other three iron-binding residues (two tyrosines and an aspartate) cannot be ruled out. The strongest evidence to exclude or include the importance of the iron-binding residues of hsTf in anti-cancer Ru(III)-complex binding would be the investigation of the complex-binding ability of the iron-binding site mutants of hsTf. To address this issue, initially production of the N-lobe iron-binding site mutants of full-length hsTf was attempted in the methylotropic yeast *P. pastoris*. However, the yield of the functional protein was very low (see chapter 3 for details). Therefore, the recombinant DNA for the N-lobe of hsTf with and without the native signal sequence of hsTf was constructed for which a successful expression protocol using *P. pastoris* as host has been described in the literature.[95-97] Among four of the iron-binding site mutant DNA constructs (D63A, Y95A, Y188A, and H249A), only the H249A mutant with the native signal sequence of hsTf was expressed to a reasonable level.

Expression and analyses of the other three mutants were left to future research. The amount of H249A mutant of N-terminal half molecule of hsTf (H249A-N/hsTf) expressed in *P. pastoris* was sufficient for EPR analysis of only one complex.

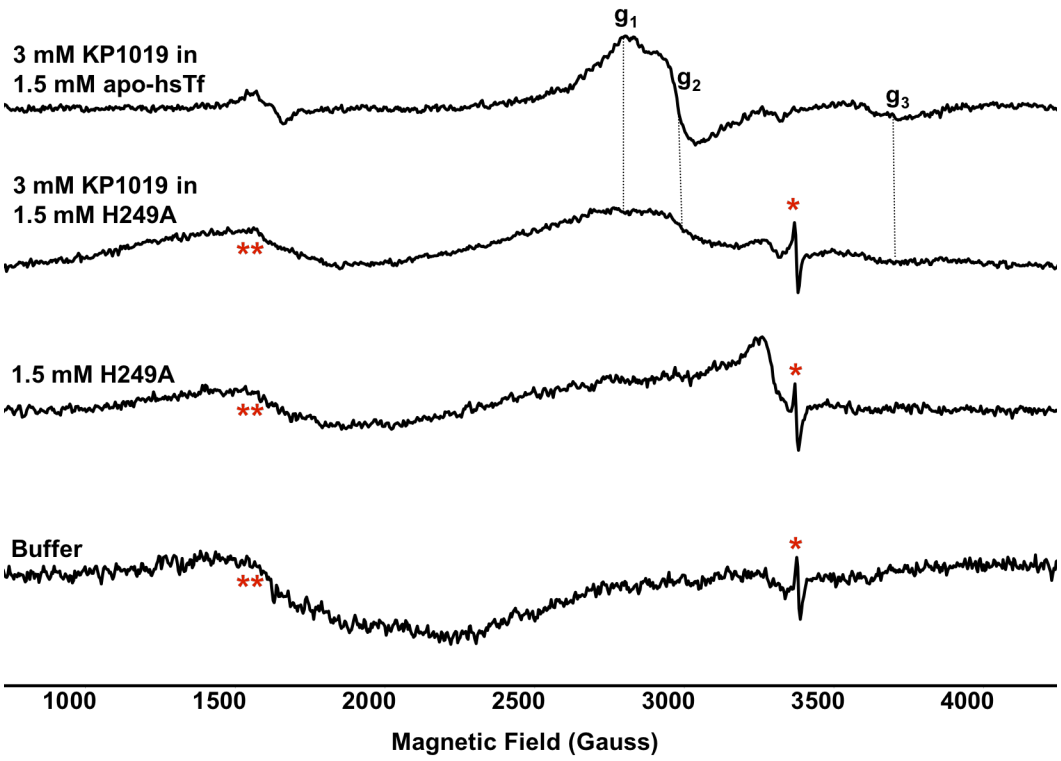

Figure 2-9 X-Band EPR analysis of KP1019 in H249A N-terminal half molecule of hsTf at 77 K. *Background EPR signal from a radical species in the finger dewar. **Background EPR signal in the cavity of the instrument. (EPR parameters: microwave frequency = 9.43 GHz, the spectra were average of 15 scans)

KP1019 was specifically chosen since its binding to hsTf has been suggested to be at His249 (N-lobe) and at His585 (C-lobe). The X-band EPR spectrum of KP1019 incubated in the H249A-N/hsTf at 37 °C for 40 minutes is shown in figure 2.9 (second spectrum from the top). Although the signal was very weak the shape of the spectrum and the g-values (g_1=2.38, g_2=2.27, g_3=1.84) were very similar to those of KP1019 in full-length apo-hsTf (figure 2.10, the first spectrum from the top). Despite the weak EPR signal of KP1019 in H249A-N/hsTf, its protein binding ability seemed to be unaffected since no precipitation

was observed after incubating KP1019 in H249A-N/hsTf for 40 minutes at 37 °C, and the dark green colour of the complex remained in the protein solution after the concentration process, which is a strong evidence of KP1019 binding to proteins. A reasonable explanation for the weak EPR signal of KP1019 in H249A-N/hsTf, despite its intact protein-binding ability, is that the interactions of the complex at the iron-binding pocket of hsTf is necessary for the stabilization of the EPR active +3 oxidation state. In the absence of the histidyl imidazole group at position 249 KP1019 may still bind to other histidine residues on H249A-N/hsTf, however, in this case the ruthenium centre in the majority of the complexes may be reduced to the EPR silent +2 oxidation state resulting in a weaker than expected signal.

2.4.5 X-band EPR analysis of KP1019 in solution with diferric-hsTf

In order to further investigate the importance of KP1019 binding at the iron-binding pocket of hsTf for stabilization of the +3 oxidation state of KP1019, both iron-binding pockets of 1.5 mM hsTf were saturated with Fe^{3+} and incubated with 3 mM KP1019 at 37 °C for 40 minutes. Again, no precipitation was observed throughout sample preparation and the dark green colour of the complex remained in the protein solution indicating that the complex is bound to diferric-hsTf. As shown in figure 2.10 KP1019 in diferric-hsTf contains two paramagnetic species. The strong EPR signal around g = 4.4 (magnetic field ~1600 gauss) is characteristic for diferric-hsTf. The second paramagnetic species produced is expanded in the inset. The g-values and the line shape of this weak signal were determined to be very similar to those of KP1019 in apo-hsTf. Despite its intact

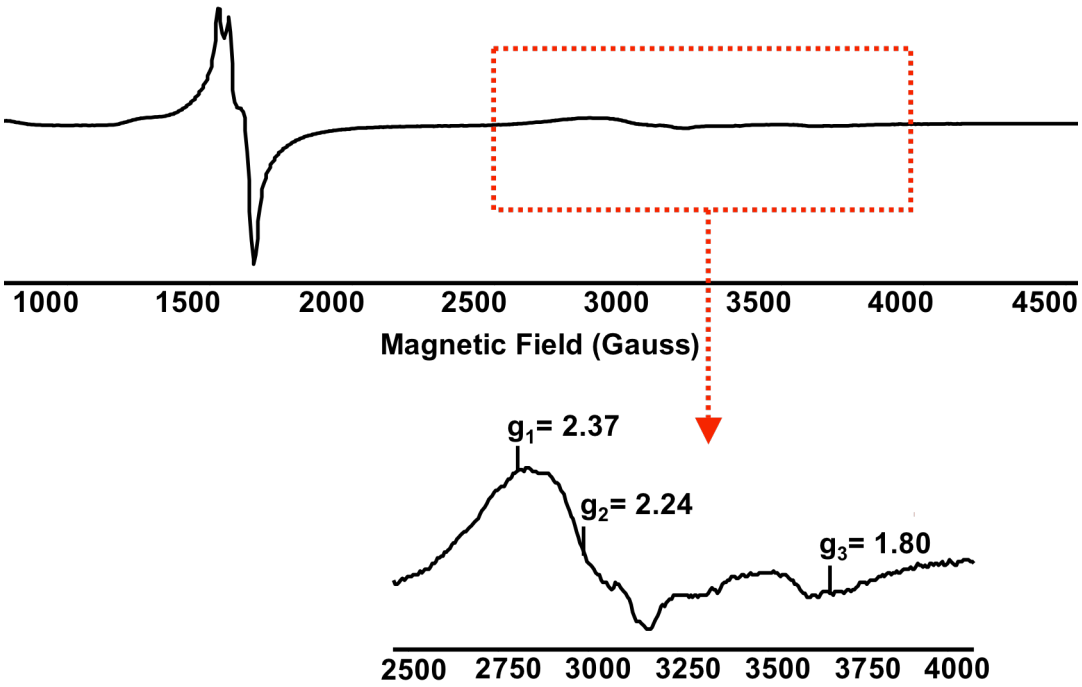

Figure 2-10 X-Band EPR analysis of KP1019 in diferric-hsTf at 20 K. The strong EPR signal around 1600 gauss is the characteristic EPR signal for diferric-hsTf. The expanded region (boxed) shows the weak EPR signal around 3250 gauss with similar g-values as KP1019 in apo-hsTf (see table 2.3 for the g-values and figure 2.8 for the line shape of KP1019 in apo-hsTf). (EPR parameters: microwave frequency = 9.38 GHz, the spectra were average of 20 scans)

protein-binding ability, the weak EPR signal of KP1019 in diferric-hsTf strongly suggests that majority of the ruthenium centres in KP1019 bound to diferric-hsTf outside the iron-binding pocket are in the EPR silent +2 oxidation state. The result of this study supports the findings of the EPR analysis of KP1019 in solution with H249A-N/hsTf that interaction of KP1019 with hsTf at the iron-binding pockets is important for stabilization of the +3 oxidation state under physiological conditions (37 °C, pH 7.4), which has important implications for the anti-cancer activity of KP1019.

2.4.6 Q-band EPR analysis of KP1019 in buffer

In Q-band (34 GHz) EPR spectroscopy a ~4 times higher frequency is used and ~4 times larger magnetic field is scanned than in X-band (9-10 GHz). This allows greater resolution of g-values, which is particularly helpful when spectral peaks partially or completely overlap in X-band EPR spectra. In order to confirm the correct assignment of the g-values of KP1019 in buffer by X-band EPR spectroscopy, Q-band EPR spectroscopy was employed. As shown in figure 2.11, the g-values obtained from Q-band EPR spectrum of KP1019 in buffer (g_1 = 2.96, g_2 = 2.62, g_2 = 2.22) are very similar to those obtained from X-band EPR spectrum (g_1 = 2.95, g_2 = 2.60, g_2 = 2.20). This result demonstrates the proof of principle for this approach, but such measurements of other samples are left to future work. The Q-band instrument has intrinsically lower sensitivity. In addition, sample volumes are significantly smaller: ~30 μL for Q-band EPR as compared to 300 μL for X-band EPR. Thus, there are technical challenges involved in these measurements. The similarity of the g-values of KP1019 in buffer measured by Q-band EPR and X-band EPR spectroscopies implies that the g-values of the other samples measured by X-band EPR spectroscopy given in this study are correctly analyzed.

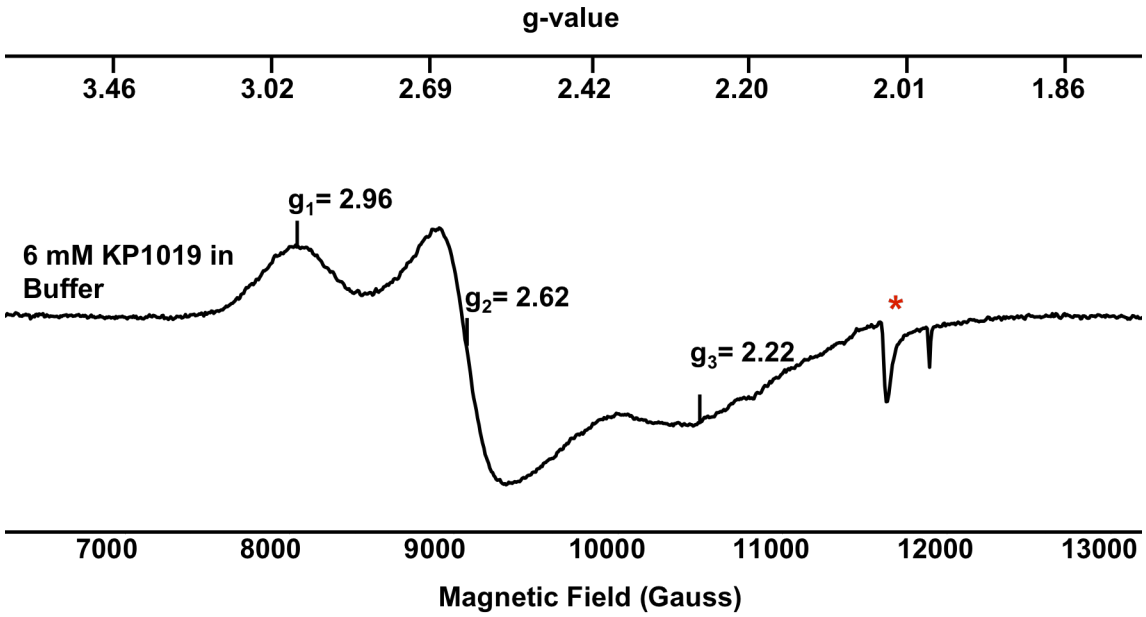

Figure 2-11 Q-Band EPR spectrum of KP1019 in buffer at 20 K. The g-values are very similar to those obtained from X-band EPR analysis of KP1019 in buffer at 77 K (table 2.1) and at 20 K (table 2.2). *EPR signal from an impurity in the KP1019. (EPR parameters: microwave frequency = 34 GHz, the spectrum was an average of 20 scans)

2.4.7 UV-visible spectroscopic analysis of KP1019 hydrolysis in buffer and in apo-hsTf solution

The structural transformation of KP1019, i.e. replacement of chloro-ligands, in buffer and in apo-hsTf at room temperature was followed by the changes in the UV-visible spectra over a period of 24 hours (figure 2.12). KP1019 both in buffer and in apo-hsTf exhibits two bands at 356 nm and 420 nm, which remain unchanged during the first 20 minutes. These bands correspond to the ligand to metal charge transfer (LMCT) transitions that are within the typical region for octahedral Ru(III)-complexes.[86] After 1 hour, both LMCT bands started to broaden, and a new band in the visible region started to develop. Development

of this new band was attributed to a d-d transition an indication of a significant lowering in the symmetry of KP1019 complex which was has been used to characterize the hydrolysis of KP1019 and KP418.[22, 27] After 5 hours, the LMCT bands for KP1019 in both buffer and apo-hsTf disappeared and intensity of the d-d transition bands increased. The position of d-d transition band for KP1019 was found to be different in buffer and in apo-hsTf solution (574 nm and 586 nm respectively) suggesting that binding to apo-hsTf causes a marked change in the hydrolysis profile of KP1019.

Using capillary electrophoresis, a previous study showed that the kinetics of hydrolysis of KP1019 is temperature dependent being significantly faster at 37 °C.[12] In order to investigate the spectral behavior of KP1019 when incubated in apo-hsTf at 37 °C for 30 minutes, the UV-absorption spectrum was scanned between 325 nm and 650 nm (figure 2.13, red line). None of the two LMCT bands was observed for KP1019 while the d-d transition band was present at a different wavelength (595 nm) compared to KP1019 incubated in apo-hsTf at room temperature for at least 5 hours (585 nm). Therefore incubation at 37 °C not only accelerates the chemical transformation of KP1019 in apo-hsTf but also it leads to formation of a different complex/protein adduct. Hydrolysis of KP418 in apo-hsTf under the same conditions was also investigated since it is known to exhibit a slower hydrolysis rate compared to KP1019.[12] As shown in figure 2.13 (blue line), hydrolysis of KP418 did not take place when it was incubated in apo-hsTf at 37 °C for 30 minutes. Development of the d-d transition band at 598 nm took several hours (> 5 hours) when KP418 was incubated in apo-hsTf at room

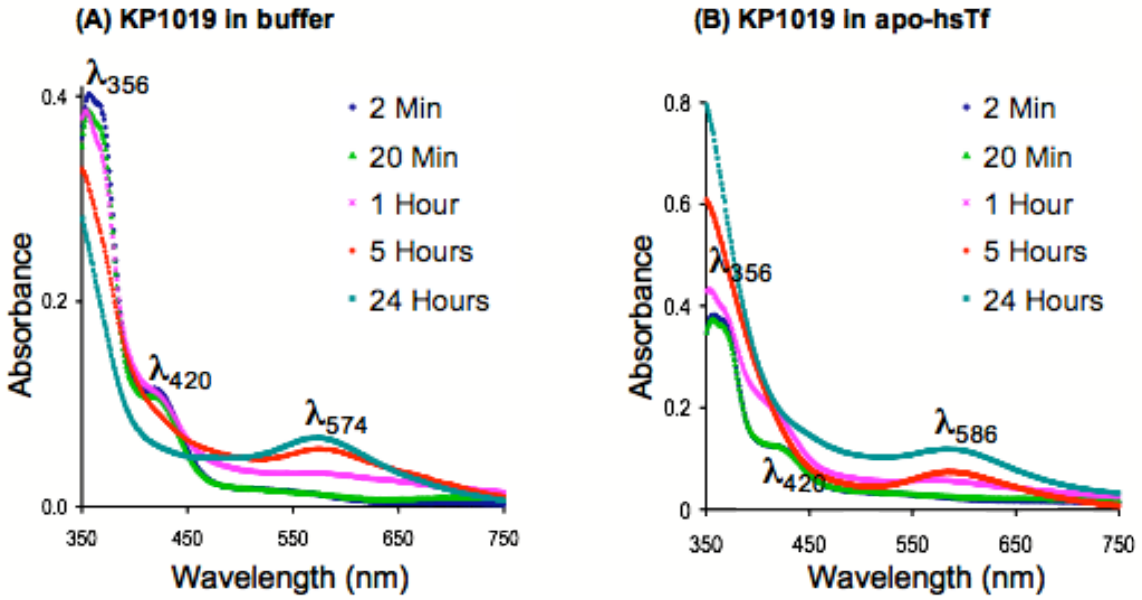

Figure 2-12 UV-visible spectroscopic analysis of time-dependent hydrolysis of KP1019 in buffer **(A)** and in apo-hsTf **(B)** at room temperature. Concentrations of KP1019 and apo-hsTf were 100 μM and 50 μM respectively.

temperature over a period of 48 hours, after which the intensity of this band was still very low (data not shown). The slower hydrolysis of KP418 even in the presence of apo-hsTf under physiological conditions, i.e. 37 °C, pH 7.4, compared to that of KP1019 may be one of the reasons why KP1019 is a more efficient anti-cancer agent over KP418.

2.5 Discussion

Electronic and structural properties of Ru(III)-complexes in buffer, in apo-hsTf, hsA, and in serum

Several groups have studied the behavior of KP1019, KP418, and NAMI-A under physiological conditions as well as their binding to two serum proteins;

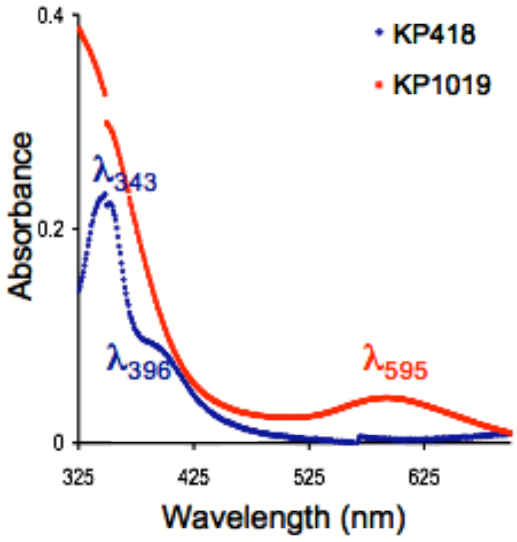

Figure 2-13 UV-visible spectra showing the effect of temperature on the hydrolysis KP1019 and KP418 incubated in apo-hsTf at 37 °C for 30 minutes. 100 μM of the complexes and 50 μM of apo-hsTf were used.

apo-hsTf and hsA by various spectroscopic and chromatographic techniques.[12, 14, 15, 20-22, 27, 29, 53, 94, 98] Although these studies have established the binding of the complexes to serum proteins, details of these interactions remain largely unknown. In this study the nature of the interactions between the Ru(III)-complexes and serum proteins was investigated by EPR spectroscopy, which provided valuable information about the local environment surrounding the Ruthenium-centre. Unlike KP1019 and KP418, the anti-metastatic agent NAMI-A produced a very weak EPR signal both in buffer and in apo-hsTf (data not shown) suggesting that the +3 oxidation state of Ru(III) in NAMI-A is not very stable in buffer and binding to apo-hsTf does not prevent its reduction to Ru(II). Therefore this complex was not studied any further by EPR. The EPR profiles of

KP1019 and KP418 were found to be similar as both complexes exhibited marked change in their spectra in buffer and in apo-hsTf solution, suggesting that the structure of the Ru(III)-complexes changes, indicating binding to apo-hsTf.

Binding studies with KP1019 and KP418 in an equimolar mixture of apo-hsTf and hsA solution by EPR spectroscopy (figures 2.6 and 2.7) suggested more than one complex-binding site on hsA, and only one binding site on apo-hsTf. This finding was reasoned from the observation of several distinct sets of EPR signals for the complexes in hsA and in the apo-hsTf/hsA mixture, whereas only one set of EPR signals was observed in apo-hsTf (it is also possible that there may be more than one set of EPR signals but these may not be resolved due to the broadness of the spectrum). The g-values and the general appearance of the two sets of EPR signals of the complexes in hsA and in the apo-hsTf/hsA mixture were significantly different from those observed in buffer indicating that the complexes interact with hsA by direct coordination of the Ru(III)-centre to amino acid residues at two different sites. One clear component of EPR spectrum matched the signal from the complexes in buffer. This signal presumably arises from the binding of the complexes to hsA through hydrophobic interactions between their heterocyclic ligands and a hydrophobic binding pocket of hsA rather than through exchange of a chloro-ligand of the Ru(III)-centre by an amino acid side-chain.

EPR analysis of KP1019 incubated in serum at 37 °C over a period of 24 hours strongly suggests that KP1019 undergoes several structural changes in serum and its interaction with serum proteins is a multi-step process (see figure

2.6). The first step appears to be the binding to serum protein(s) as soon as it is introduced into the serum (without incubation at 37 °C) possibly through hydrophobic interactions between the heterocyclic ligands of the complex and hydrophobic binding pockets in serum protein(s). hsA is the most likely candidate in serum responsible for this hydrophobic interaction since the same feature was observed in the EPR spectrum of the complex incubated in a solution with hsA and apo-hsTf/hsA mixture at 37 °C for 1 hour. A dramatic change in the EPR spectrum of KP1019 when incubated in serum at 37 °C is strong evidence of ligand exchange in the following steps. This is assigned to exchange of a chloro ligand of the Ru(III)-centre by an amino acid side chain of the serum protein(s).

The structural transformation of KP418 in serum was found to be different from that of KP1019 (see figure 2.7). The EPR signal from the initial hydrophobic interaction between the complex and serum proteins observed for KP1019 was not very strong for KP418. Instead, an almost complete ligand exchange took place as soon as the complex was introduced into the serum (no incubation at 37 °C) giving an EPR spectrum with significantly different g-values from those observed in buffer. The same signal for a low symmetry rhombic system persisted after incubation at 37 °C even after 24 hours.

EPR studies of each complex in serum at 37 °C over 24 hours not only allowed for observation of the time dependent structural transformation of the complexes in serum, but also confirmed that Ru(III) / Ru(II) reduction is not significant in serum. The anti-cancer activities of KP1019 and KP418 have been correlated to the selective reduction of the Ru(III)-centre to Ru(II) within cancer

cells.[2, 6, 43] Thus, establishment of the oxidation states of these complexes outside the cells (in serum) is vital to gain further insight into their mechanism of action. Previously, the oxidation state of KP1019 in the presence of ascorbic acid was investigated by cyclic voltametry[33] and it was shown that Ru(III)-centre in KP1019 can be reduced to Ru(II) by this reducing agent, which naturally occurs in blood. On the other hand only a portion of the Ru(III)-centres was reduced when complex-protein adducts were formed. The stability of the +3 oxidation state of ruthenium in the presence of serum proteins was claimed in another study using UV-visible spectroscopy.[22] However, EPR spectroscopy is the most reliable technique to unambiguously assign the oxidation state of Ruthenium centre in the complexes, since only the paramagnetic Ru(III) produces an EPR signal, whereas the diamagnetic Ru(II) does not. To our knowledge, the results given in this study are the first to establish the stability of the +3 oxidation state of KP1019 and KP418 in serum.

One of the most interesting results of this study is the observation of a strong signal that developed at g = 5.80 (figures 2.6 and 2.7, first signal from the left in all serum-containing samples) after addition of the complexes into serum. High spin Fe(III)-heme is known to have a characteristic axial EPR signal at $g_{\perp}$ ~ 5.8 and g_{II} ~ 2.0.[99-101] Therefore, the signal at g = 5.8 ($g_{\perp}$) observed in the EPR spectra of the complexes in serum was assigned to a high spin Fe(III)-heme species. In most cases the second g value (g_{II} = 2.0) is usually weak and in this case it was obscured by the background cavity signal. Either free heme or heme bound to hemoglobin could have been released due to red blood cell lysis during

serum preparation from whole rabbit blood. Remarkably, this signal is much weaker in the serum control sample when the intensity of this signal is compared to the intensity of the Fe(III)-hsTf signal (characteristic at g ~ 4.3). Since non-protein bound small molecules were removed from the sample by ultrafiltration, this high spin Fe(III)-heme species must be bound to a serum protein to be detected by EPR. It is apparent that complex-binding to a serum protein results in the development of a strong EPR signal at g = 5.80. A reasonable explanation for this phenomenon is a change in the spin state of iron in the heme from EPR silent to EPR active high-spin Fe(III) induced by addition of the complexes into serum. It is anticipated that in the absence of the Ru(III)-complexes most of the iron-heme is in the +2 oxidation state, (low-spin Fe(II); EPR silent,). Upon addition to serum, a small portion of the Ru(III)-centre in the complexes may be reduced to Ru(II) causing oxidation of low-spin Fe(II)-heme to high-spin Fe(III)-heme, which produces an axial EPR spectrum at g ~5.8. Nevertheless, a conclusion cannot be drawn without further investigation. However, even if this is the case, clearly Ru(III) / Ru(II) reduction is not significant since the signal from the complexes is much stronger than that from the high spin Fe(III)-heme species.

EPR analysis of the interactions of KP1019 with H249A mutant of N/hsTf and diferric-hsTf

hsTf provides a highly effective route for specific delivery of anti-cancer Ru(III)-complexes to tumor cells. Elucidation of the binding sites in hsTf is of great importance to categorize the Ru(III)-complexes with respect to their

binding sites on hsTf, which in turn would help design more effective metal-based anti-cancer drugs. A previous study reported that two moles of KP1019 binds to 1 mole of apo-hsTf at the histidyl imidazoles in the iron binding sites, whereas KP418 binding was found to be less specific having a higher molar ratio of KP418 per mole of apo-hsTf.[27] In a follow up study, crystallographic evidence was cited for secondary binding sites in lactoferrin at other histidine residues in addition to the primary binding sites in the iron binding pockets.[86] Although lactoferrin (an iron binding protein in secreted fluids) shares many similar features with hsTf, such as tight but reversible iron binding, a highly-conserved three-dimensional structure, and essentially identical iron-binding sites, some functional and structural differences exist.[102] Consequently, lactoferrin/complex-binding studies may not reflect the actual Ru(III)-complex binding sites in hsTf. The most reliable approach to determine whether the complexes bind to apo-hsTf specifically at the iron-binding sites would be the analysis of the complex-binding ability of iron-binding site mutants of hsTf. In this study, binding of KP1019 to the iron binding site histidine mutant of the N-terminal half molecule of hsTf (H249A-N/hsTf) was investigated by means of X-band EPR spectroscopy.

An important feature of KP1019 chemistry is that it precipitates within minutes of dissolving in aqueous buffer at pH 7.4 at room temperature giving a dark green coloured solid; incubation at 37 °C accelerates this process. In contrast, when serum proteins are present no precipitation is observed even after long time incubation for several hours at 37 °C. This behavior of KP1019 has been cited in many literature reports as an evidence of protein binding.[22, 27, 86]

Thus, evidenced from the experimental observations (maintenance of dark-green colour) during this study, KP1019 binding to the mutant protein at a 2:1 molar ratio was found to be almost intact. Despite its intact protein binding ability, KP1019 incubated in H249A-N/hsTf at 37 °C for 40 minutes produced only a weak EPR signal suggesting a significant amount of reduction of Ru(III)-centres in KP1019 to Ru(II). Therefore it is proposed that in the absence of the iron-binding site histidyl imidazole group, KP1019 binds to other histidyl imidazoles outside the iron binding site of H249A-N/hsTf, but that the +3 oxidation state of KP1019 is no longer stabilized. The validity of this theory was tested by performing KP1019 / differric-hsTf binding studies and it was found that KP1019 binds to hsTf even when the iron binding sites are occupied with iron but it is no longer in its EPR active +3 oxidation state. This result has important implications for the anti-tumor activity of KP1019 with respect to its oxidation state when bound hsTf. A previous study showed that KP1019/diferric-hsTf adducts exhibit an approximately 80-fold higher efficacy in inhibiting growth of human colon cancer cells in culture compared to the complex alone, while the anti-tumor activity of apo-hsTf adducts was lower than that of the free-complex.[85] The results of that previous study combined with the results presented here strongly suggest that KP1019 bound to hsTf outside the iron-binding sites in the Ru(II)-state has the highest anti-cancer activity. Therefore it is suggested that, as opposed to the general opinion, preservation of the Ru(III)-state of KP1019 when bound to hsTf is not necessary for its anti-cancer activity. Nevertheless, further studies are needed to provide additional proof for this novel finding.

Effect of apo-transferrin on the hydrolysis of KP1019 and KP418

A brief analysis of the electronic absorption spectra of KP1019 in water (no incubation) and in apo-hsTf (20 minutes incubation) were reported by Kratz et al.[86] More recently, the spectral profile of KP1019 in buffer (50 mM NaH_2PO_4, 100 mM NaCl, pH 7.4) and in apo-hsTf at room temperature over a period of 24 hours was described.[22] However, in the former study only one time point was taken and the UV-visible spectrum of KP1019 in buffer was not given. The latter study, although more detailed, reported a spectral range of only between 400 nm - 680 nm, and therefore the change in one of the LMCT bands was not observed. In addition, the spectral behaviour of KP1019 in apo-hsTf at 37 °C was not investigated. Therefore, this study represents a more thorough analysis of the time-dependent changes in the UV-visible spectra of KP1019 in buffer and in apo-hsTf. The spectral data collected in this study suggest that the hydrolysis of KP1019 in the presence of apo-hsTf is affected significantly. Most importantly, the difference between the position of the d-d transition bands for KP1019 in apo-hsTf at room temperature and at 37 °C suggests the formation of distinct KP1019/apo-hsTf adducts at different temperatures. Therefore, the experimental conditions should be considered carefully when evaluating the reactions of KP1019 in biologically relevant media since the results of experiments performed at room temperature may not reflect actual events under physiological conditions.

CHAPTER 3: EXPRESSION OF FULL-LENGTH RECOMBINANT HUMAN SERUM TRANSFERRIN IN *PICHIA PASTORIS*

3.1 Abstract

Production of recombinant human serum transferrin (hsTf) is a difficult task due to the large number of disulphide linkages that need to be formed for proper folding of the protein. The presence of carbohydrate attachment sites, necessity to remove the signal sequence, and in some cases toxicity of the protein to the host cells, exacerbates the difficulty of expression. Due to its strong iron-chelating nature, hsTf inhibits growth of *E.coli*. In addition, *E.coli* cannot carry out formation of disulphide bonds. For these reasons, the *E.coli* expression system, the easiest and fastest system for expressing recombinant proteins, is not suitable for production of hsTf. Therefore, an alternative expression system was sought. The methylotrophic yeast *Pichia pastoris* (*P. pastoris*) was chosen for production of high levels of hsTf as it is generally considered an excellent alternative to mammalian expression systems for proteins that require post-translational modifications or are toxic to host bacteria cells.

This chapter describes a protocol for expression, purification and partial characterization of full-length hsTf in *P. pastoris*. The ultimate goal of this study was to produce high levels of site-directed mutants of hsTf in order to investigate the possible involvement of iron-binding residues in the binding of anti-cancer Ru(III)-complexes. The yield of the functional full-length hsTf expressed in *P.*

pastoris was not sufficient for use in the subsequent experiments although the expression levels were high. The stability and the yield of the functional recombinant protein were increased significantly by addition of iron to the secretion medium either during the expression or immediately after the cell-harvesting step. However, addition of iron also caused formation of radical species in the recombinant hsTf. It was concluded that the recombinant hsTf expressed in *P. pastoris* is unstable in the absence of an additional iron source. The key factor in the high-level expression of functional full-length hsTf in *P. pastoris* will be discovering an efficient way of supplementing iron to the secretion medium without causing radical formation in the protein.

3.2 Introduction

3.2.1 Expression systems for recombinant hsTf

hsTf plays crucial roles in biological processes ranging from iron metabolism to metal-based drug transport. Due to its importance, extensive efforts have been made to develop and optimize expression systems for members of Tf family of proteins, including human serum Tf (hsTf), human lactoferrin (hLf), and chicken ovotransferrin (oTf). Such systems enable the production of site-directed mutants of Tfs to study their function, structure, and interactions with other biomolecules or drugs. These expression systems include *E.coli*, filamentous fungi, insect cells, mammalian cells, yeast cells, and the milk of transgenic animals. Table 3.1 displays the yield of recombinant Tfs produced in different types of expression systems. Although the full length hsTf was expressed in *E. coli* at a level of 60 mg/L, the yield after renaturation of the

Table 3.1 Expression systems for recombinant Tfs.

Expression system	Protein	Yield (mg/L)
E. coli	hsTf (full-length)[106]	NG*
E. coli	hsTf [107]	NG
E. coli	hsTf/N-lobe[108], hTf/C-lobe[108]	NG
E. coli	hsTf[109], hsTf/N-lobe[109], hTf/C-lobe[109]	3
P. pastoris	hsTf/N-lobe[95]	14
P. pastoris	hsTf/N-lobe[96]	166
P. pastoris	porcineLf[110], equineLf[111], goatLf[112]	NG; 40; 2
P. pastoris	oTf[113]	57
A. nidulans	hLf[114]	1.5
A. oryzae	hLf[115]	25
A. awamori	hLf[105, 116]	1,700
Insect cells	hsTf[117]	20
Insect cells	hLf[118]	10
BHK cells	hsTf (glycosylated)[119]	125
BHK cells	hsTf (nonglycosylated)[119-121]	25; 50; 50
BHK cells	hsTf/N-lobe[122]	100
BHK cells	oTf[123]	80
Transgenic animals	hLf[124, 125]	NG; 750

Table was adopted from reference[62]
Abbreviations: **hsTf**, human serum transferrin**; hLf**, human lactoferrin; **oTf**, ovotransferrin; **BHK cells**, baby hamster kidney cells; **NG**, not given.

protein (found in the insoluble inclusion bodies) was only 3 mg/L.[103] Expression of hLf in filamentous fungus *A. awamori* was reported at very high levels (~2 g/L),[104] and shown to possess the same structure as native hLf.[105] There are several advantages of this system including high level protein expression in a relatively short time at a low cost and the ability of the cells to perform post-

translational modifications. However, the components of filamentous fungi expression systems are not easily available. Both hsTf and hLf has been expressed in baculovirus-infected insect cells at the levels of 20 mg/L and 10 mg/L respectively.[117, 118] The recombinant proteins were shown to be equivalent to the native proteins with regard to their functional and structural properties. The highest yield of full-length hsTf expression (150-200 mg/L) was obtained from the mammalian expression system (baby hamster kidney cells).[119] This system has particular advantages with regard to production of recombinant mammalian proteins that are almost indistinguishable from the native ones. On the other hand, the time and cost of the expression is not as favorable compared to other eukaryotic systems. The methylotrophic yeast *P. pastoris* has been employed for expression of the N-terminal half molecule of hsTf (hsTf/N-lobe),[95, 96] full length porcine,[126] equine,[111] and goat,[112] Lf and ovoTransferrin.[113] Although the full-length Lf and oTf expression levels were relatively low (2-57 mg/L), N-lobe of hsTf expression level in *P. pastoris* was as high as ~170 mg/L. By using a fermentor equipped with a methanol sensor, approximately 1 g/L hsTf/N-lobe was produced in *P. pastoris.*[127] Despite the successful expression of hsTf/N-lobe, full-length Lf, and oTf in *P. pastoris*, expression of functional full-length hsTf in this system has not been reported.

Protein expression in *P. pastoris,* a unicellular eukaryote, is economical in terms of time, cost, and labour compared to higher eukaryotic systems, such as insect and mammalian expression systems.[128] *P. pastoris* grows faster, and the cost of the media and equipment used for this system is much lower than that of

mammalian expression systems. *P. pastoris* is particularly useful for expression of proteins that can only be expressed in *E. coli* as inclusion bodies, which requires unfolding of the proteins for recovery and after refolding the yield of functional proteins is usually very low. In the case of hsTf expression, *P. pastoris* is capable of forming disulphide bridges that are necessary for proper folding of hsTf, which *E. coli* cannot carry out. Because of these advantageous properties, *P. pastoris* was chosen as host for expression of full-length hsTf.

3.2.2 General features of *P. pastoris* expression system

The methylotrophic yeast *P. pastoris* is a unicellular microorganism and hence can be easily manipulated in a way similar to *E. coli*. As a eukaryote, it is capable of performing post-translational modifications, which can be important for production of properly folded, functional proteins. Expression of a foreign gene is driven by the alcohol oxidase-1 (*AOX1*) promoter, which also regulates the production of alcohol oxidase. *P. pastoris* can utilize the alcohol oxidase to metabolize methanol as its sole carbon source. Expression of genes that are under the control of *AOX1* promoter is tightly regulated by methanol in a two-step process: a repression/derepression and an induction mechanism.[129] Transcription of the *AOX1* gene is repressed in the presence of glucose and addition of the inducer methanol cannot overcome this repression. For this reason the derepressor glycerol is used in the growth medium as a carbon source instead of glucose. Switching the carbon source to methanol induces the expression of alcohol oxidase and the downstream recombinant genes of interest.

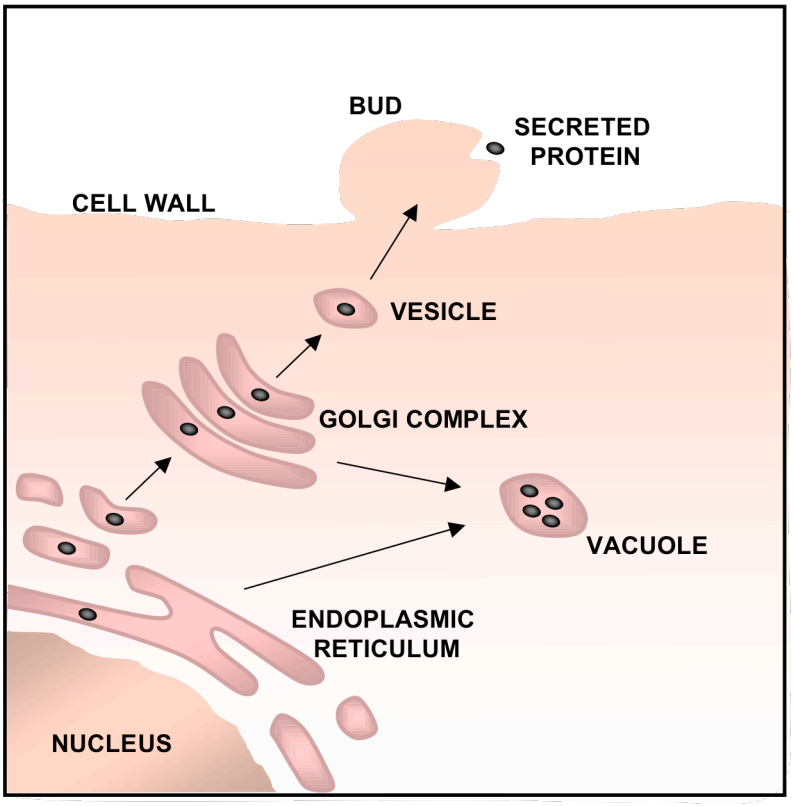

Figure 3-1 A schematic representation of secretory pathway in yeast. Proteins containing certain signal sequences translocate to the endoplasmic reticulum (ER) either co- or post-translationally. Folding and some of the post-translational modifications, such as formation of disulphide bridges and glycosylation take place in the ER. These proteins can then be moved to the Golgi complex via transport vesicles for further processing and eventually to the cell surface through growing bud.[130] Protein folding in the ER lumen is the rate-limiting step in the secretory expression and misfolded proteins are generally subject to vacuolar degradation.[131] In some instances, misfolded proteins due to a mutation in their disulphide bond-forming cysteines escape from the ER but are targeted to vacuole from the Golgi complex.[132]

3.2.3 Protein expression in *P. pastoris*

Recombinant proteins can be expressed either intracellularly or can be targeted for secretion in *P. pastoris*. The original location of the protein in its source should be considered when choosing the type of expression. Proteins that

are normally secreted in their original source usually require post-translational modifications, such as N-glycosylation and disulphide bridge formation. This is why these proteins must be targeted for secretion when expressed heterologously since the disulphide bond formation is most efficiently carried out in the lumen of endoplasmic reticulum, the first compartment of the secretory pathway (figure 3.1). Secretory expression also allows for fast and easy recovery of a recombinant protein from the secretion media since *P. pastoris* secretes very low levels of its own native proteins. In order for a protein to be targeted to the secretory pathway a secretion signal sequence must be included on the protein. One of the most successfully used secretion signals in *P. pastoris* is the yeast mating alpha factor, which consists of a 19 amino acid 'Pre' signal sequence followed by a 66-amino acid 'Pro' sequence.[129, 133-135] Removal of the prepro-signal sequence (also called the secretion leader) from the protein is carried out in three steps: The pre-sequence is cleaved by a signal peptidase in the ER followed by removal of the pro-sequence at the C-terminal dibasic lysine-arginine sequence by the Kex2 endopeptidase in the late Golgi. A dipeptidyl aminopeptidase, STE13, then cleaves the N-terminal glutamine-alanine repeats[136]. The correct processing of the prepro-leader sequence is necessary for secretion of the mature protein and requires the Kex2 signal sequence cleavage site to be located downstream of the α-factor signal sequence.

3.2.4 Experimental outline

Protein expression process in *P. pastoris* (figure 3.2) is similar to that in any other host cells, consisting of cloning of the gene of interest in an expression

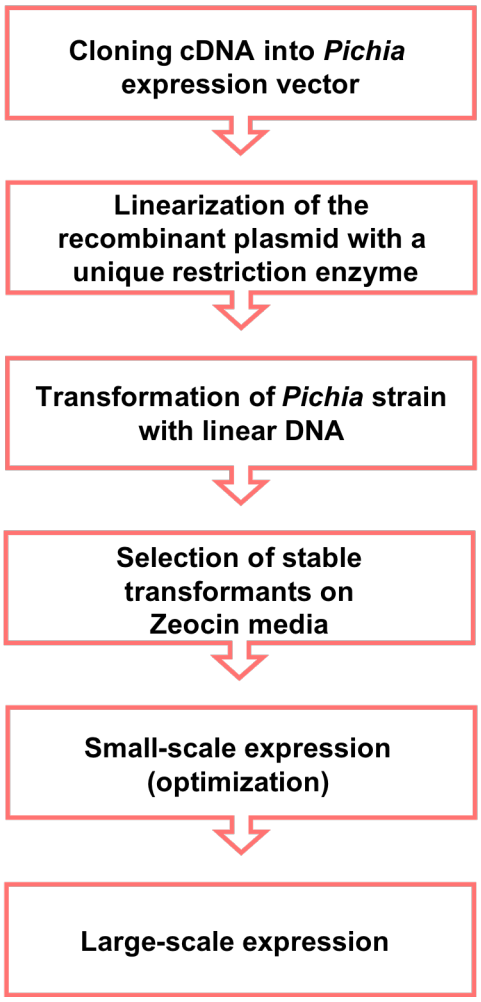

Figure 3-2 Experimental outline of protein expression in *P. pastoris*. The gene of interest is inserted into a *P. pastoris* expression vector and the *P. pastoris* strain of choice is transformed with either a linearized or circular recombinant plasmid. *Pichia* transformants are selected on zeocin-containing media and screened for the expression of the recombinant proteins. After optimizing the conditions for expression, the recombinant protein can be expressed in *P. pastoris* in large-scale.

vector to yield a recombinant plasmid followed by transformation of host *P. pastoris* cells with either the linearized or circular recombinant construct. *P. pastoris* transformants are isolated on media containing a selection marker, which is included in the recombinant construct. Although circular recombinant

constructs can be used to transform the host cells, stable transformants of *P. pastoris* are generated more efficiently with linear DNA via homologous recombination between the transforming DNA and the homologous regions of the *P. pastoris* genome.[129, 135] After recombinant *P. pastoris* strains bearing the recombinant DNA construct integrated into their genome are isolated, several colonies are tested for the expression of the recombinant gene of interest. The expression conditions are optimized in low culture volumes and following that the protein can be expressed in large-scale in shake flasks.

3.3 Materials and Methods

3.3.1 Materials

The plasmid bearing the full-length hsTf gene was obtained from American Type Culture Collection (ATCC# 53106). *Pfu* DNA polymerase, dNTPs, Dpn1, and restriction endonucleases were from Fermentas. T4 DNA ligase was purchased from Invitrogen. *E. coli* competent cells (XL-1 Blue) were from Stratagene. DNA fragment and plasmid purification kits were obtained from Qiagen. Synthesis of oligonucleotides was performed by Sigma-Genosys. DNA sequencing was performed by the Nucleic Acids and Peptide Service (NAPS) Unit at University of British Columbia. All media and buffer components were purchased from Bioshops Canada. EasySelect™ *Pichia* Expression kit was obtained from Invitrogen which included *E. coli* Top10F′ cells, *P. pastoris* host strains GS115(*his4*) and KM71H, pPICZα-A secreted expression vector, and the antibiotic Zeocin™. Pre-packed DEAE or CM Sepharose™ Fast Flow columns

(HiTrap) were purchased from GE Health Care. Amicon® Stirred Cell and Amicon®Ultra-4 (or Ultra-15) Centrifugal Filter Units were from Millipore.

3.3.2 Construction of the recombinant plasmids

pPICZα-A/TF (with hsTf native signal sequence)

The cDNA encoding the full-length human serum transferrin (including the signal sequence) was amplified from the pKT218 vector by polymerase chain reaction (PCR) using the forward and reverse primers:

TF-Xho1F (5′-GCTC**CTCGAG**ATGAGGCTCGCCGTGG-3′)

TF-Xba1R (5′-GCACAC**TCTAGA**GCAGGTCTACGGAAAGTGC-3′).

Restriction sites are shown in bold and underlined. The forward primer was designed to introduce the *XhoI* restriction site to the 5′ end of the gene. The reverse primer was designed to introduce the *Xba I* site to the 3′ end of the gene. The stop codon was removed and two more nucleotides were added to enable in-frame cloning of the gene with the C-terminal His-tag. The resulting ~2.1 kb PCR product, flanking the 5′-*XhoI* and 3′-*Xba I* sites, was cleaved with *Xho I* and *Xba I* restriction endonucleases and purified from 1% agarose gel along with the *Xho I* / *Xba I* digested pPICZα-A vector. T4 DNA ligase was used to ligate the fragment into the *Xho I* and *Xba I* sites of the vector. The pPICZα-A vector contains the Zeocin resistance gene for positive selection in both *E.coli* and *P. pastoris*. The ligation mixture was used to transform either *E.coli* XL-1 blue or TOP10F′ competent cells and colonies were selected on low salt LB/agar plates

Table 3.2 Components used in the PCR amplifications.

Components	Final Concentration
Sterile ddH_2O	---
DMSO	5 x
10 x *Pfu* DNA polymerase buffer	1 x
Forward primer	0.5 μM
Reverse primer	0.5 μM
Template DNA	60 ng/50 mL
2.5 mM dNTP mixture	0.25 mM
Pfu DNA polymerase	2.5 Units/50 μL
Total reaction volume: 50 μL	

DMSO: Dimethyl sulphoxide, **dNTP**: deoxynucleotide triphosphate

Table 3.3 Thermal cycling parameters used in PCR amplifications.

Temperature (°C)	Time length	Number of cycles
95 (Initial denaturation)*	1 minute	1
95 (Denaturation)	30 seconds	7
70 (Primer annealing)**	1 minute	
74 (Extension)	4 minutes	
95 (Denaturation)	30 seconds	28
65 (Primer annealing)**	1 minute	
74 (Extension)	4 minutes	
74 (Final extension)	2 minutes	1

*The thermal cycler is preheated to 95 °C.

**10 °C temperature gradient is used.

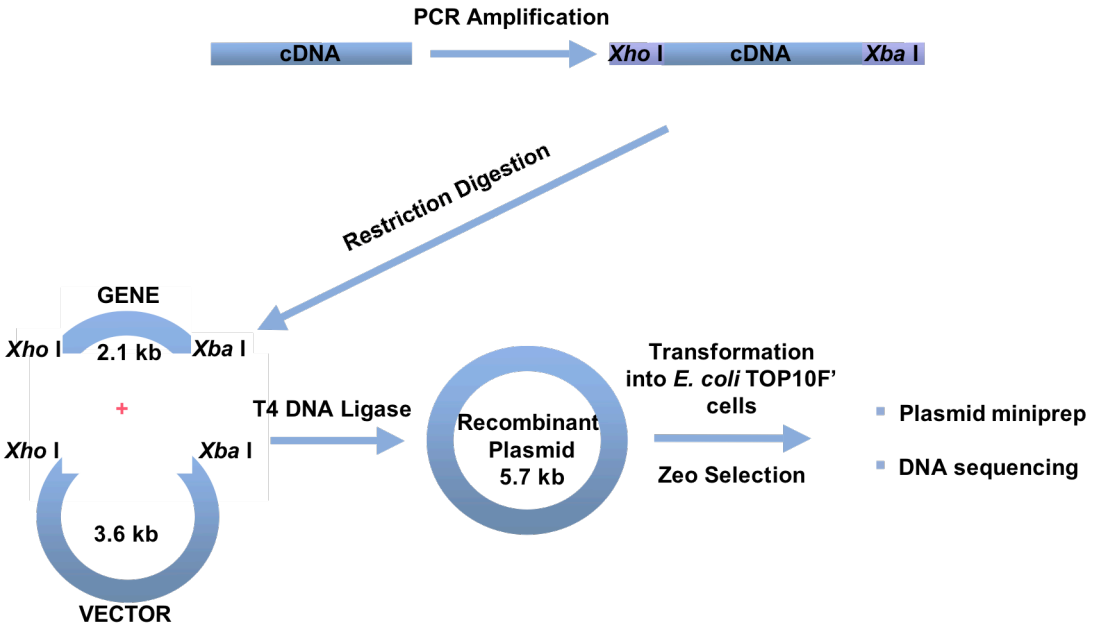

Figure 3-3 An illustration of the experimental procedure for cloning the hsTf gene into the pPICZα-A expression vector.

containing 25 μg/ml Zeocin. Isolated transformants were analyzed by restriction mapping for the presence of the insert. Correct orientation and in-frame insertion of the gene with the α-factor signal sequence and C-terminal His-tag was confirmed by DNA sequencing using

5′ AOX1: (5′- GACTGGTTCCAATTGACAAGC -3′)

3′ AOX1: (5′- GCAAATGGCATTCTGACATCC- 3′)

sequencing primers. This recombinant plasmid construct was designated as pPICZα-A/Tf. The experimental procedure for cloning is illustrated in figure 3.3.

pPICZα-A/TfNS (without hsTf native signal sequence)

The native signal sequence of hsTf was removed by PCR amplification using pPICZα-A/Tf as template. The forward and reverse primers were:

Tf-NS-Xho1F (5′-GCTC**CTCGAG**GTCCCTGATAAAACTG-3′)

Tf-Xba1+Stop (5′-GAAG**TCTAGA*TTA***AGGTCTACGGAAAGTGC-3′)

The forward primer introduces the *Xho I* site just upstream of the codon for the N-terminal valine residue of hsTf. The reverse primer reintroduces the stop codon (shown in bold and italic) at the C-terminal of hsTf. After restriction digestion with *Xho I* and *Xba I*, the ~ 2.1 kb fragment coding for the full-length hsTf without its native signal sequence was cloned into the *Xho I* and *Xba I* sites of the pPICZα-A vector as described above. DNA sequencing results proved the removal of the signal sequence. This recombinant construct was designated as pPICZα-A/TfNS.

pPICZα-A/Tf-Kex2

The Kex2 signal peptidase cleavage site was inserted into pPICZα-A/Tf between the C-terminal of hsTf signal sequence and the codon for the N-terminal valine residue of hsTf by two subsequent site-directed mutagenesis reactions. The PCR components and the cycling parameters are given in table 3.4 and table 3.5. The mutagenic primers were:

Table 3.4 Components used in the PCR mutagenesis.

Components	Final Concentration
Sterile ddH_2O	---
10 x *Pfu* DNA polymerase buffer	1 x
Forward primer	125 ng / 50 μL
Reverse primer	125 ng / 50 μL
Template DNA	50 ng/50 μL
2 mM each dNTP mixture	0.2 mM each
Pfu DNA polymerase	2.5 Units/50 μL
Total reaction volume: 50 μL	

dNTP: deoxynucleotide triphosphate

Table 3.5 Thermal cycling parameters used in PCR mutagenesis.

Temperature (°C)	Time length	Number of cycles
95 (Denaturation)	30 seconds	
55 (Primer annealing)	1 minute	20
68 (Extension)	13 minutes	

*The thermal cycler is preheated to 95 °C.

Reaction 1: (first codon for Kex2 site)

Tf-Kex2F-1(5′-GCTGTGTCTGGCT**GAGAAA**GTCCCTGATAAAACTG-3′)

Tf-Kex2R-1 (5′-CAGTTTTATCAGGGAC**TTTCTC**AGCCAGACACAGC-3′)

Reaction 2: (second two codons for Kex2 site)

Tf-Kex2F-2(5′-GTCTGGCTGAGAAA**AGAGAG**GTCCCTGATAAAACTG-3′)

Tf-Kex2R-2 (5′- CAGTTTTATCAGGGAC**TTTCTC**AGCCAGACACAGC-3′)

In the first PCR, pPICZα-A/Tf was used as template. At the end of the reaction 1 μL of *Dpn I* was added to the reaction mixture to digest the parental DNA and incubated at 37 °C for 3 hours. 5 μL of this mixture was used to transform 150 μL of the *E. coli* TOP10F′ competent cells, which were prepared according to the supplier's protocol. The transformation reaction was plated on low salt LB/agar plates containing 25 μg/mL Zeocin. Plasmid DNA was purified from the overnight culture of a single colony using Qiagen plasmid miniprep kit. Insertion of the mutagenic codons was confirmed by DNA sequencing. This plasmid DNA was then used as a template in the second PCR for insertion of the second part of the Kex2 site and the correct insertion was confirmed by DNA sequencing. This final plasmid DNA was designated as pPICZα-A/Tf-Kex2.

pPICZα-A/TfNS-Kex2

The Kex2 site was inserted into the pPICZα-A/TfNS between the *Xho I* site and the N-terminal valine residue of hsTf by site-directed mutagenesis. Mutagenesis was performed in a single step using a single set of mutagenic primers, which inserted 3 of the 4 codons for the Kex2 site. The forward and reverse primers were:

TfNS-Kex2F: (5′-GGTATCTCTCGAG**AAAAGAGAG**GTCCCTGATAAAACTG -3′)

TfNS-Kex2R: (5′-CAGTTTTATCAGGGAC**CTCTCTTTTT**CTCGAGAGATACC- 3′)

Note that the first codon for Kex2 site (GAG) was part of the *Xho I* site which was already in the template DNA. The mutant plasmid DNA (pPICZα-A/TfNS-Kex2) was prepared as described above. The correct insertion of the Kex2 site was

confirmed by DNA sequencing.

3.3.3 Site-directed mutagenesis of glycosylation sites

hsTf has two glycosylation sites, Asn413 and Asn611, located at the C-terminal of the protein. A double mutant was generated using two sets of mutagenic primers in two subsequent site-directed mutagenesis reactions by PCR. The first primer set was used to mutate the Asn413 to Asp.

TfN413D-F: (5′- CTTGGCAGAAAACTA**GAT**AAGAGCGATAATTGTG -3′)

TfN413D-R: (5′- CACAATTATCGCTCTT**ATC**TAGTTTTCTGCCAAG -3′)

After confirming the mutation by DNA sequencing, this plasmid was used as template to generate the second mutant Asn611Asp using mutagenic primers:

TfN611D-F: (5′-GCACCTATTTGGAAGC**GAC**GTAACTGACTGCTCG -3′)

TfN611D-R: (5′-CGAGCAGTCAGTTAC**GTC**GCTTCCAAATAGGTGC -3′)

The correct mutation was verified by DNA sequencing. The components and the cycling parameters of PCR were the same as described for the Kex2 site insertion reactions (table 3.4 and 3.5). The template DNAs were either pPICZα-A/Tf, pPICZα-A/Tf-Kex2, or pPICZα-A/TfNS-Kex2. The resulting plasmids were designated as pPICZα-A/NGTf, pPICZα-A/NGTf-Kex2, and pPICZα-A/NGTfNS-Kex2.

3.3.4 Transformation of *P. pastoris* host strains

Preparation of transforming DNAs

Approximately 12 μg of plasmid DNAs of each construct to be used in the transformation of *P. pastoris* strains, were prepared from the 2 x 5 mL low-salt LB overnight cultures containing 25 μg/mL Zeocin. The restriction endonuclease *Sac I*, which cuts only at the 5′ *AOX1* region was used to linearize the plasmid DNAs. In order to ensure complete linearization, an excess amount of the enzyme was used in the total volume (250 μL) of reaction mixture. After 8 hours of incubation at 37 °C, the completion of the linearization was checked by agarose gel electrophoresis. The linearized plasmid constructs were then purified from the reaction mixture by phenol/chloroform extraction. Briefly, 250 μL of 1:1 phenol/chloroform mixture was added to the reaction mixtures, mixed and centrifuged at 13,000 rpm for 10 minutes. The aqueous phase containing the DNA was taken into a clean eppendorf tube and mixed with 25 μL (1/10 volume of the initial reaction mixture volume) of 3 M Sodium acetate and 600 μL (2.5 volume) of 100% ethanol. This solution was left at -20 °C overnight or at -80 °C for 1 hour. The DNA was pelleted by centrifugation at 13,000 rpm for 20 minutes at 4 °C. The pellet was washed with 80% ethanol and air (or vacuum) dried. Finally, the DNA pellet was resuspended in 10 μL of sterile, double- distilled water.

Electroporation of *P. pastoris* strains

Electrocompetent *P. pastoris* cells, GS115(*his4*) and KM71H, were prepared as described in the supplier's manual. A 5 mL overnight culture of YPD

was started at 29 °C with 20 μL of frozen glycerol stock that was generated from a single colony. 500 mL of fresh YPD medium in a 2 L flask was inoculated with 100 μL of overnight culture and grown overnight at 29 °C to an OD_{600} of ~1.5. After centrifugation at 2,500 rpm for 5 minutes at 4 °C, the cell pellet was resuspended in 500 mL of ice-cold sterile water. Following another centrifugation the pellet was resuspended in 250 mL of ice-cold sterile water and repelleted by centrifugation. 20 mL of 1 M ice-cold sterile sorbitol was used to resuspend the pellet. After this final centrifugation, 2/3 of the volume of 1 M ice-cold sorbitol was used to resuspend the pellet. The cells were kept on ice and used within the same day.

10 μL of at least 10 μg linear recombinant DNA constructs as well as the linearized pPICZα-A DNA (as control for background expression) were mixed gently with 100 μL of electro competent *P. pastoris* cells and transferred into a 0.2 cm ice-cold electroporation cuvette. After incubation on ice for 5 min, the cells were pulsed for 5 ms at 1.5 kV using a Bio-Rad gene pulser. 1 mL of 1 M ice-cold sorbitol was added gently to the cells and the resulting solution was incubated at 30 °C for 2 hours without shaking. The transformation mixtures were then plated on YPDS/agar plates containing 100, 250, 500, and 1000 μg/mL Zeocin for isolation of integrants as well as the multicopy integrants on increasing concentrations of Zeocin plates. Plates were incubated at 30 °C for 3-6 days. 10 colonies from each plate were picked and purified on fresh YPD/agar plates containing corresponding concentrations of Zeocin followed by incubation at 30 °C for another 3 days. 6-10 colonies of GS115-recombinants were tested for their

Mut (Methanol utilization) phenotypes as described in the EasySelect *Pichia* expression manual. Since KM71H-recombinants are all Mut^s (Methanol utilization slow) phenotype, no Mut phenotype screen was necessary for this strain. In order to confirm the integration of the gene into the *P. pastoris* genome, genomic DNAs of Mut^+ (Methanol utilization plus) and Mut^s phenotypes of recombinants were isolated and used as templates in the PCR analysis.

Isolation of *P. pastoris* genomic DNA

5 mL of overnight cultures of single colonies from the Mut^+ and Mut^s strains were grown as described earlier. The cells were pelleted and resuspended in 50 μL of STES buffer and mixed with 20 μL of TE buffer (pH 7.6) and 50 μL of acid-washed glass beads (Sigma-Aldrich) in small test tubes. 60 μL of 1:1 phenol/chloroform mixture was added and the tubes vortexed for 1-2 minutes. The cell lysate was centrifuged at 13,000 rpm for 5 minutes at room temperature and the aqueous phase was collected. Genomic DNA was pelleted by ethanol precipitation as described above and resuspended in 40 μL of TE buffer. Integration of the DNA constructs into the *P. pastoris* genome was confirmed by PCR analysis using the conditions given in table 3.6 and 3.7.

Table 3.6 Components used in the PCR amplification of *P. pastoris* genomic DNA.

Components	Final Concentration
Sterile ddH_2O	---
10 x *Pfu* DNA polymerase buffer	1 x
Forward primer (5' AOX1)	0.1 μg /50 μL
Reverse primer (3' AOX1)	0.1 μg /50 μL
Genomic DNA	~1 μg/50 μL
25 mM each dNTP mixture	0.5 mM each
Pfu DNA polymerase	5 Units/50 μL
Total reaction volume: 50 μL	

dNTP: deoxynucleotide triphosphate

Table 3.7 Thermal cycling parameters used in PCR amplification of *P. pastoris* genomic DNA.

Temperature (°C)	Time length	Number of cycles
95 (Initial denaturation)*	4 minutes	1
95 (Denaturation)	1 minute	30
55 (Primer annealing)	1 minute	
72 (Extension)	2 minutes	
74 (Final extension)	10 minutes	1

*The thermal cycler is preheated to 95 °C.

3.3.5 Small scale expression and optimization of expression conditions

6-10 colonies of Mut^+ (GS115) and Mut^S (KM71H) recombinants were tested for small-scale protein expression. GS115 and KM71H cells transformed with the pPICZα-A vector (without the insert) were tested for background expression. GS115/Albumin/Mut^S, which grows slowly in methanol medium and secretes albumin in to the medium, was included in the *P. pastoris* expression kit, and used to test the effectiveness of the conditions for secretion.

Briefly, 50 mL of BMGY in 500 mL baffled flasks and 100 mL of BMGY in 1 L baffled flasks were inoculated with single colonies of Mut^+ and Mut^S recombinants respectively. Following incubation at 29 °C in a shaking incubator (250 rpm) for approximately 20 hours (OD_{600}= 2-6), cells were harvested by centrifuging at 4,000 rpm for 5 min. To induce expression, the cell pellets were resuspended in 200 mL of BMMY (0.5% methanol) in 1 L baffled flasks (Mut^+) and 20 mL of BMMY in 250 mL flasks (Mut^S). The flasks were covered with 2 layers of sterile cheese cloth and incubated under the same conditions for 4 days. In order to maintain induction, 100% methanol was added to a final concentration of 0.8% every 24 hours. This methanol concentration (0.8% per day) was determined to be the optimum after testing 0.5-1% methanol concentrations. Each day 1 mL aliquots of expression cultures were taken and centrifuged at 14,000 rpm at room temperature for 5 minutes. The supernatants were analyzed by SDS-PAGE and Western blots. Glycerol stocks of overnight cultures from the best expressing colonies were prepared in small aliquots and stored at –80 °C for future use.

3.3.6 SDS-PAGE and Western blot analysis

SDS-PAGE (Sodium dodecyl sulphate- polyacrylamide gel electrophoresis) analysis was performed using 10% mini gels according to the Laemmli method.[137] Protein samples were mixed with equal volumes of sample buffer (Bio-Rad) in 600 μL centrifuge tubes, spun down, and left in a boiling water bath for ~3 minutes. The samples were then loaded on SDS-polyacrylamide gel in running buffer and run at 90 volts for 20 minutes. The voltage was increased to 120 and run for a further 1 hour. The gel was microwaved in Coomassie blue staining solution and stained on a rocking platform for a few hours or alternatively stained overnight without microwaving. The gel was destained on a rocking platform with several changes of destaining solution until the gel background was clear.

For Western blot analysis, staining and destaining steps were omitted and the proteins on the SDS-polyacrylamide gel were transferred onto a nitrocellulose membrane using a semi-dry electroblotting apparatus (Bio-Rad) at 15 V for 20 minutes. After transfer, the membrane was blocked with blocking buffer (3% BSA in PBS-T buffer) for 1 hour at room temperature. The membrane was then probed with goat anti-hsTf IgG (Sigma-Aldrich # T6265), which was diluted (1:8000) in blocking buffer, overnight at 4 °C. After washing several times with PBS-T, the membrane was blocked with blocking buffer for 30 min at room temperature and incubated with horseradish peroxidase-conjugated rabbit anti-goat IgG (Sigma-Aldrich # A5420) at a concentration of 1:40,000 for 1 hour at room temperature. The membrane was washed several times with PBS-T buffer

and detection of the secondary antibody was accomplished using the Super Signal West Pico chemiluminescent detection kit (Pierce) and film (Kodak Biomax MR).

3.3.7 Large-scale expression in shake flasks

After optimizing the conditions, the expression was scaled-up to larger volumes. 20 μL of the frozen glycerol stocks of overnight cultures, which were prepared from the best expressing single colonies, were grown overnight in BMGY media in a shaking incubator at 250 rpm and 29 °C to an OD_{600} of 2. The volumes of BMGY media for growth of Mut^+ and Mut^s recombinants were determined according to the easy select *Pichia* expression kit manual. The overnight cultures were then used to inoculate BMGY media and grown under the same conditions to an OD_{600} of 2. Cells were harvested by centrifugation at 4,000 rpm for 10 minutes at room temperature. The pellet was resuspended in BMMY to an OD_{600} of 1 (for Mut^+) or 1/6 of the original volume (for Mut^s), to induce protein expression. The flasks were returned to the shaking incubator (250 rpm, 29 °C) and the induction was continued by daily addition of 100% methanol to a final concentration of 0.8% for four days. At the end of the fourth day the culture media was centrifuged at 4 °C and 6,000 rpm for 20 minutes. The resulting pellet was discarded and the supernatant was concentrated to less than 50 mL using an Amicon stirred cell with a PM-10 membrane followed by centrifugation for clarification. However, a large amount of white precipitate was observed during the concentration with the Amicon cell. To prevent or reduce

precipitation, iron-binding buffer (1/3 of the supernatant volume) was added to the supernatant before the concentration step.

Effect of iron addition to the expression medium

In hopes of improving the expression levels, the effect of feeding iron to cells during expression was evaluated. To do this, Fe^{3+} was fed to cells either in free form ($FeCl_3$) or in the chelated form (Fe^{3+}-nitrilotriecetic acid - $FeNTA_2$, or ferric citrate) to a concentration of 5-50 mM. In addition a ferri-siderophore, N',N'', N'''-triacetylfusarinine C (TAF) chelated 1:1 with Fe^{3+} (generously supplied by Dr. Margo Moore) was tested for any possible increase in the yield of functional full-length hsTf. The KM71H cells transformed with pPICZα-A/TfNS-Kex2 were grown from the same colony and split into two baffled flasks followed by resuspension and induction with methanol media as described above. 50 mM ferric-TAF (final concentration in the culture medium) was added into one of the culture flasks. In the fourth day of expression the cells were harvested and the same culture volume of iron-binding buffer was added to the supernatants followed by iron saturation (chapter 2.3.3). Purification was carried out as described below.

3.3.8 Purification of recombinant hsTf from the *P. pastoris* secretion media

Anion-exchange chromatography

Prior to purification, the recombinant protein was prepared using two different protocols:

1) The culture supernatant was exchanged into the start buffer (20 mM

Tris-HCl pH 8.1) and concentrated down to 50 mL using an Amicon stirred cell. The sample was clarified through a 40 mM syringe filter and loaded onto a 5 mL, prepacked HiTrap DEAE FF column (GE Healthcare). Purification was carried out with 5 column volumes of start buffer containing increasing concentrations of salt (0-500 mM NaCl) either manually with a syringe or using a gradient pump and a fraction collector (Bio-Rad). The fractions were analyzed by SDS-PAGE.

2) After centrifuging the cells, 2/3 volume of iron-binding buffer was added on the culture supernantant. The concentration of the hsTf expressed by *P. pastoris* was roughly determined from the SDS-polyacryl amide gel and approximately 50 μM of $FeNTA_2$ (excess amount) was added on the sample in iron-binding buffer to saturate the protein with Fe^{3+}. The reason for Fe^{3+}-saturation was to render the protein homogenous prior to purification, which would reduce the isoelectric point shifts and hence also reduce the spread of the protein into the wash step fractions during purification. Following saturation, the buffer was exchanged into the start buffer and the sample was purified as described in protocol 1.

Ni^{2+}-affinity chromatography

The supernatant from the secretion medium was taken into the binding buffer (20 mM sodium phosphate, 20 mM imidazole, 150 mM NaCl, pH 7.4) using the Amicon stirred cell, filtered, and applied to a 5 mL of prepacked His-Trap FF column. The column was washed with 30 mL of 50 mM imidazole in binding buffer and the protein was eluted with 300 mM imidazole in binding buffer. Purification was carried out manually using a syringe. Fractions were analyzed

by SDS-PAGE.

3.3.9 Spectroscopic studies

Electron Paramagnetic Resonance (EPR) Spectroscopy

Iron-loaded (Fe_2-hsTf) recombinant hsTf expressed in *P. pastoris* and the commercial hsTf were prepared as described in chapter 2. The concentrated samples (1 mM commercial hsTf, 0.5 mM recombinant hsTf) were mixed with 10% glycerol, frozen in liquid nitrogen in 3 mm outer diameter quartz EPR tubes (Wilmad, Buena, NJ), and analyzed by X-band EPR spectroscopy as described in chapter 2.3.7.

UV-visible spectroscopy

UV-Visible absorption spectra of the iron-free and iron-loaded forms of both recombinant and commercial hsTf were scanned between 280 and 680 nm and recorded at room temperature using Varian Cary100 spectrophotometer. 2 mg/mL samples in iron binding buffer (50 mM HEPES, 20 mM $NaHCO_3$, 150 mM NaCl, pH 7.4) were used in the assays.

3.3.10 Determination of protein concentration

Protein concentrations were determined by UV spectroscopy at 280 nm using the millimolar absorption coefficients at 280 nm for Apo-hsTf (86.7) and diferric-hsTf (111.4).[119]

3.3.11 Buffers and media recipes

PBS (phosphate buffered saline) buffer: 8 g of NaCl, 0.2 g of KCl, 1.44 g of Na_2HPO_4, and 0.24 g of KH_2PO_4 were dissolved in 800 mL of double distilled water. pH was adjusted to 7.4 and the volume was completed to 1 L with water. For PBS-T 0.1% tween 20 was added.

SDS-PAGE running buffer: 14.4 g of glycine, 3.03 g of Tris-base, and 1 g of SDS were dissolved in 800 mL of double distilled water. pH was adjusted to 8.3 and the volume was completed to 1 L with water.

Coomassie blue staining solution: 1 g of coomassie blue R-250 was stirred in 450 mL of ethanol for 1 hour. 100 mL of glacial acetic acid and 450 mL of water was added and the solution was stirred for 30 minutes.

Destaining solution: 450 mL ethanol, 100 mL glacial acetic acid, and 450 mL water.

Low salt LB medium: 10 g of tryptone, 5 g of yeast extract, and 5 g of NaCl were dissolved in 950 mL of double distilled water. pH was adjusted to 7.5 and the volume was completed to 1 L with water. The solution was autoclaved at 121 °C for 20 minutes. The antibiotic was added after cooling to ~55 °C. For agar plates 15 g/L agar was added before autoclaving.

YPD media: 10 g of yeast extract and 20 g of peptone were dissolved in 900 mL of double distilled water. After autoclaving, 100 mL of 20% dextrose (autoclaved previously) was added. For YPDS media 182.2 g of sorbitol was added before autoclaving. For agar plates 20 g/L agar was also added before autoclaving.

BMGY and BMMY media: 10 g of yeast extract and 20 g of peptone were dissolved in 700 mL of double distilled water. After autoclaving, 100 mL of filter

sterilized 1 M potassium phosphate buffer (pH 6.0), 100 mL of 13.4% yeast nitrogen base, 2 mL of 0.02% biotin, and 100 mL of 10% glycerol for BMGY medium or 100 mL of 5% methanol for BMMY medium were added and mixed well.

3.4 Results

3.4.1 Construction of the expression vectors

Selection of the expression vector largely depends on the type of recombinant protein to be expressed. The pPICZα-A expression vector (figure 3.4) was chosen specifically for the secreted expression of recombinant hsTf in *P. pastoris* since it contains the *S. cerevisiae* mating α-factor prepro-leading sequence. In order to efficiently target the hsTf to the secretory pathway where the disulphide bonds are formed, the cDNAs encoding hsTf, including the native N-terminal signal sequence of hsTf, were cloned in-frame with the α-factor signal sequence in the pPICZα-A vector. As explained in 3.2.1, the α-factor signal sequence is removed in the secretory pathway by the endopeptidase Kex2. The Kex2 cleavage site is located at the C-terminal of the α-factor signal sequence and flanked by 2 *Xho I* sites. Note that when the *Xho I* site was utilized for insertion of the gene into the vector, the Kex2 cleavage site was removed from the vector.

Although the α-factor has been the most successfully used secretion signal for secreted expression of recombinant proteins in *P. pastoris*, in some cases combined use of the native secretion signal of the protein of interest

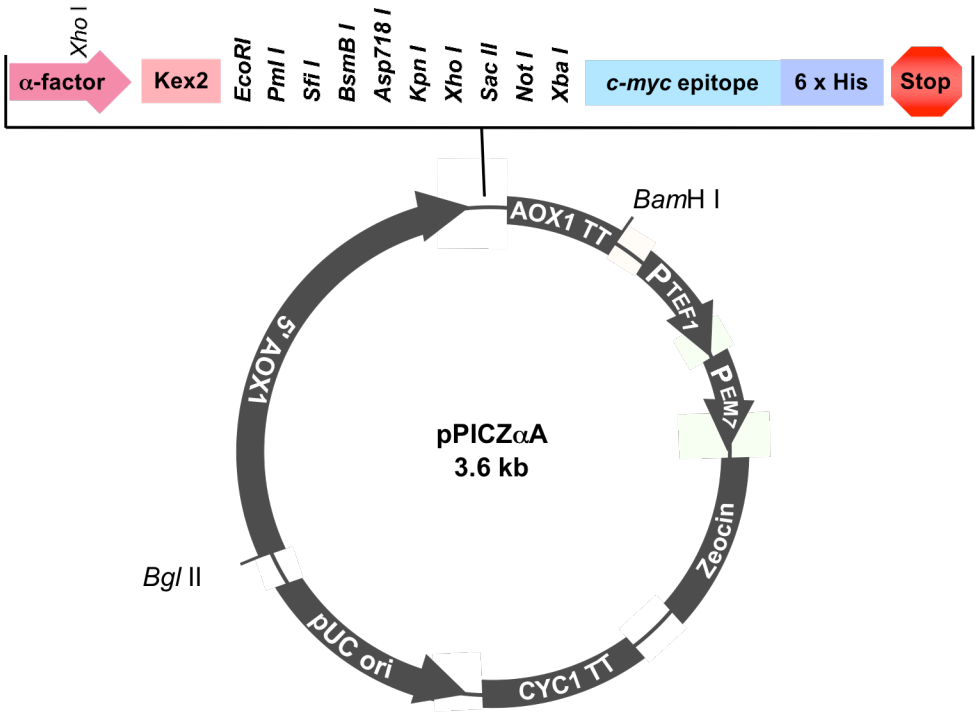

Figure 3-4 pPICZα-A *P. pastoris* expression vector. *5′ AOX1* region contains the P_{AOX1} promoter site that allows induction of high-level expression by methanol. The α-factor secretion signal enables efficient secretion of downstream proteins. The KEX-2 cleavage site resides between the α-factor signal sequence and the multiple cloning-site of 10 unique restriction sites. Downstream of the cloning-site is the C-terminal *myc* epitope tag for detection of the fusion protein by an antibody for *myc*. The C-terminal polyhistidine tag is included as an option for purification of fusion proteins by metal-chelate affinity chromatography. *AOX1 TT* is the transcription termination from the *AOX1* gene. The P_{TEF1} promoter from *S. cerevisiae* and constitutive P_{EM7} synthetic prokaryotic promoter drives the expression of the *Sh ble* gene (*Zeocin*™ resistance gene) in *P. pastoris* and *E. coli* respectively. The *CYC1* transcription termination region ensures the efficient 3′ mRNA processing of the *Zeocin*™ resistance gene. pUC origin of replication is necessary for maintenance of the plasmid in *E. coli*. There are three unique restriction sites in the 5′ AOX1 region (*Sac I*, *Pme I*, *BstX I*) for linearization of the plasmid, which increases the efficiency of the DNA integration into *P. pastoris* genome. For more details see the EasySelect™ *Pichia* Expression Kit manual (Invitrogen, Catalog no. K1740-01).

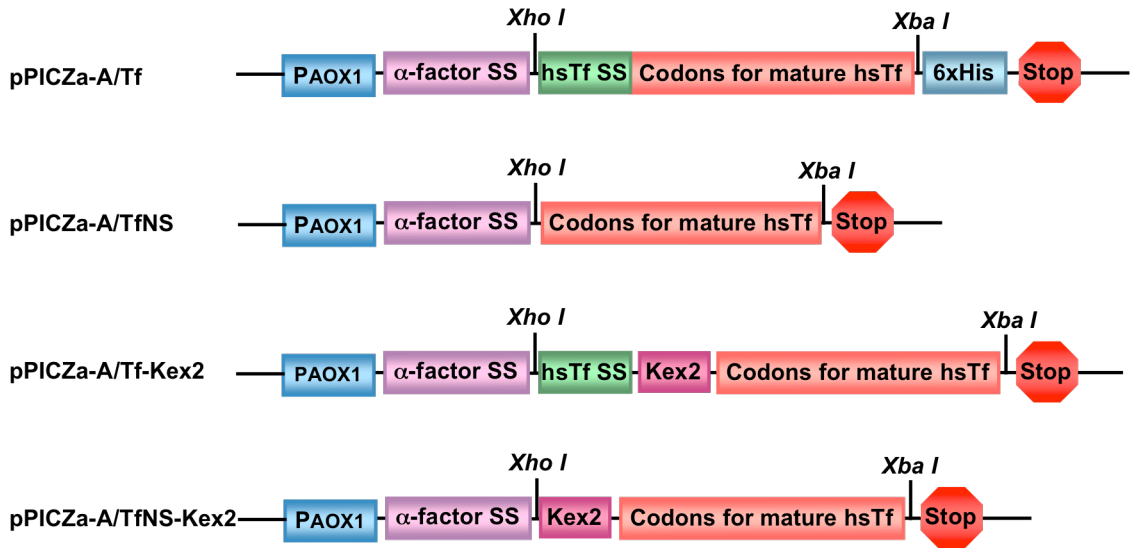

Figure 3-5 An illustration of the recombinant plasmid constructs for secreted expression of hsTf. P_{AOX1}: 5′ AOX1 promoter region; α-factor SS: α-factor secretion signal; hsTf SS: native secretion signal of hsTf; Kex2: Kex2 endo peptidase cleavage site; 6xHis: polyhistidine tag. Nonglycosylated (NG) hsTf constructs were also generated for all of the constructs and designated as pPICZα-A/NGTf, pPICZα-A/NGTfNS, pPICZα-A/NGTf-Kex2, and pPICZα-A/NGTfNS-Kex2.

significantly improved or inhibited the secretion from *P. pastoris.*[138] In order to compare the expression levels of recombinant hsTf in *P. pastoris*, the native secretion signal of hsTf was removed as described in the materials and methods section of this chapter to generate the recombinant plasmid pPICZα-A/TfNS. To ensure the correct processing of the signal sequences, the Kex2 cleavage sitewas reconstructed into the recombinant plasmids just upstream of the codon for the N-terminal valine residue of mature hsTf to obtain pPICZα-A/Tf-Kex2 (with the native secretion signal of hsTf) and pPICZα-A/TfNS-Kex2 (without the native secretion signal of hsTF). The recombinant constructs are illustrated in figure 3.5.

Figure 3-6 Agarose gel electrophoresis analysis of recombinant DNA constructs digested with *Sac I* restriction endonuclease. The complete linearization of the recombinant DNA constructs pPICZα-A/Tf (lane 3) and pPICZα-A/NGTf-nonglycosylated (lane 4), as well as the pPICZα-A vector (without insert, lane 5) was analyzed by agarose gel electrophoresis. The undigested DNAs; pPICZα-A/Tf (lane 2) and pPICZα-A vector (lane 6) were included as controls. A 10 kb DNA ladder was run in lane 1.

3.4.2 Transformation of *P. pastoris* host strains

The *P. pastoris* strains GS115 and KM71H were transformed with linearized recombinant DNA constructs and the pPICZα-A vector (without the insert). Complete linearization of the plasmid DNAs with the restriction endonuclease Sac I was analyzed by agarose gel electrophoresis. Linear DNA can be detected on agarose gel since it migrates more slowly than circular or supercoiled DNA. As shown in the representative agarose gel image (figure 3.6), the DNA constructs pPICZα-A/Tf and the pPICZα-A/NGTf, as well as the pPICZα-A vector were almost completely linearized as they migrated more slowly than the undigested control DNAs pPICZα-A/Tf and pPICZα-A vector.

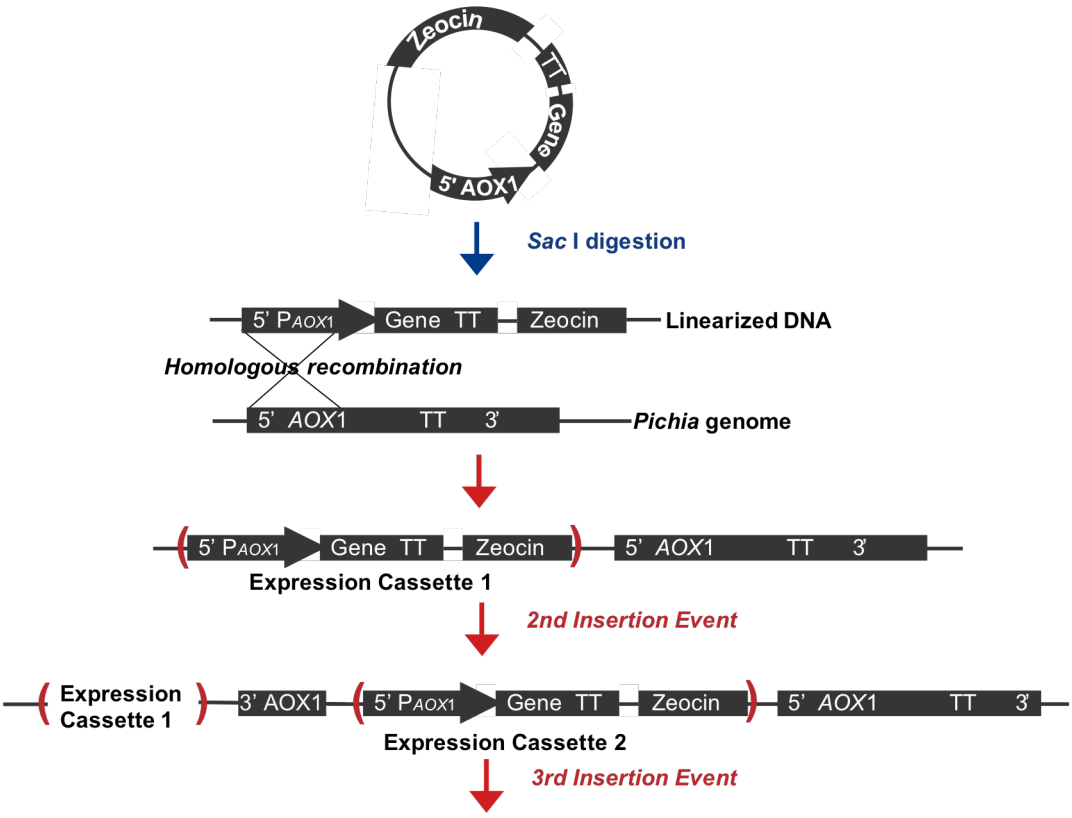

Figure 3-7 A schematic representation of gene integration into *P. pastoris* genome.

The linear DNAs stably integrate into the *P. pastoris* genome via homologous recombination. This single crossover event takes place at the *AOX1* (GS115) or the *aox1::ARG4* (KM71H) loci between the homologous regions of the host genome and the pPICZα-A vector (*AOX1* promoter or the *AOX1*transcription termination (TT) region). Multiple gene insertions may occur with low frequency. Figure 3.7 represents the integration of a linear DNA into the *P. pastoris* genome. pPICZα-A contains the *Streptoalloteichus hindustanus* bleomycin gene (*Sh ble*)encoding a 13.66 kDa Zeocin resistance protein that binds stoichiometric amounts of Zeocin, a member of the bleomycin/phleomycin-type antibiotics.[139,

[140] This gene product serves as a positive selection marker to isolate the *P. pastoris* transformants that harbour the recombinant DNA along with the Zeocin resistance gene. Growth on high Zeocin plates is made possible by the multiple insertions of the Zeocin resistance gene into the host genome. In order to isolate the multicopy integrants, the *P. pastoris* cells electroporated with the recombinant DNAs were plated on increasing concentrations of Zeocin plates (100 - 1000 μg/mL). However, the highest Zeocin concentration that allowed colony growth was 500 μg/mL indicating that only a few copies of the Zeocin resistance gene were integrated into the *P. pastoris* genome. The control cells (wild type cells) did not grow at all even on the low Zeocin plates. All of the GS115 transformants tested were Mut^+ phenotype. In order to confirm the integrations of the DNAs into the P. pastoris genome, genomic DNAs were isolated from the Mut^+ clones (GS115 transformants) and the Mut^s clones (KM71H transformants). Using the AOX1 forward and reverse primers the *AOX1* gene was amplified by PCR. Figure 3.8 shows the agarose gel electrophoresis analysis of the PCR products of the genomic DNAs from the two different pPICZα-A/Tf – GS115 transformants (lanes 2-3), pPICZα-A/NGTf – GS115 transformants (lanes 4-5), and a pPICZα-A vector – GS115 transformant. The two bands were detected easily in the lanes for the pPICZα-A/NGTf – GS115 transformants corresponding to the size of the AOX1 region in the vector plus the hsTf gene (2650 bp), and the *AOX1* gene in the *P. pastoris* genome (2200 bp). On the other hand, these bands in the lanes for pPICZα-A/Tf – GS115 transformants (lanes 2-3) were very faint and are invisible in the figure 3.8 indicating low levels of PCR product. In lane 6, two

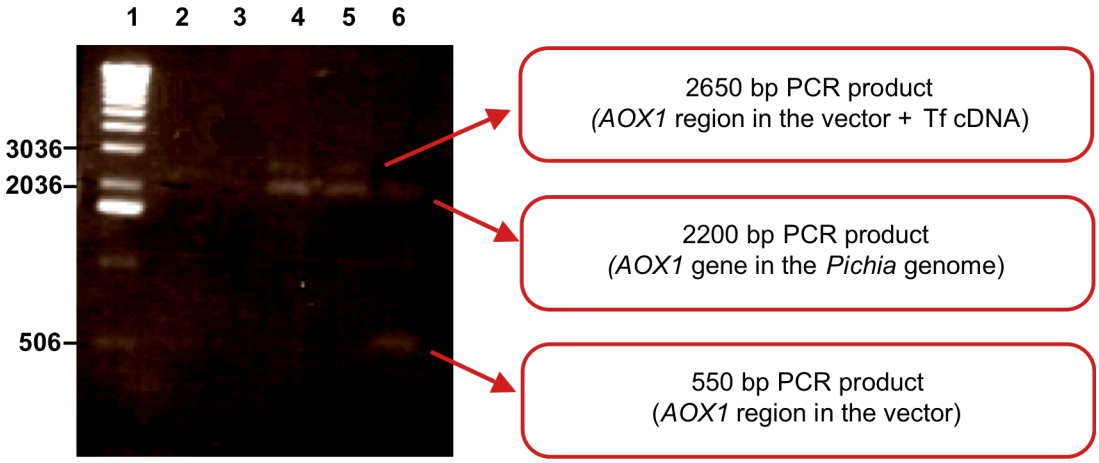

Figure 3-8 Agarose gel electrophoresis analysis of the PCR amplified genomic DNAs from *P. pastoris* (GS115) transformants. Lane 1 is a 10 kb DNA ladder; lane 2 and 3 are the PCR products of genomic DNAs isolated from two different pPICZα-A/Tf Mut$^+$ transformants, lane 4 and 5 are from the two different pPICZα-A/NGTf Mut$^+$ transformants, and lane 6 is from a pPICZα-A vector Mut$^+$ transformant.

bands corresponding to the *AOX1* gene in the *P. pastoris* genome (2200 bp) and the AOX1 region in the vector (550 bp) are visible. These results confirm that the transforming DNAs have integrated into the *P. pastoris* genome, which is consistent with the ability of the transformants to grow on Zeocin-containing media. PCR analysis was not performed for all of the clones carrying the recombinant constructs given in figure 3.5 since growth on Zeocin plates provided sufficient proof for recombination of the gene constructs into the *P. pastoris* genome.

3.4.3 Expression, purification, and partial characterization of the Wild type (WT) and nonglycosylated (NG) recombinant hsTfs

pPICZα-A/Tf and pPICZα-A/NGTf constructs in GS115 cells

The GS115 (Mut^+) cells transformed with pPICZα-A/Tf (WT hsTf) and pPICZα-A/NGTf (NG hsTf) were grown in BMGY media and the recombinant proteins were expressed in BMMY media as described in the materials and methods section of this chapter. After induction with methanol, the optimum expression time was determined to be four days after which protein degradation was observed (data not shown). The SDS-PAGE analysis of the secretion media is given in figure 3.9. 1 mL of culture supernatants from the third and the fourth days of each expression were concentrated down to 0.2 mL, and 15 mL of these samples were used in the SDS-PAGE. As shown in figure 3.9, the recombinant proteins NG and WT hsTf with an approximately 75 kDa molecular mass were efficiently secreted from *P. pastoris* comprising most of the proteins in the secretion media. The amount of the secreted proteins increased on the fourth day of the expression. The lack of hsTf background expression in GS115 cells was confirmed by analysis of the negative control in which the GS115 cells were transformed with pPICZα-A vector (lanes 6, 7). The efficiency of the experimental conditions for successful protein secretion was demonstrated by high-level secretion of albumin by GS115/Mut^s-Albumin cells (lanes 8, 9), which were included in the *Pichia* expression kit. The amount of albumin secretion was much higher than that of the recombinant hsTfs.

The identities of the secreted proteins corresponding to the 75 kDa bands on SDS-polyacrylamide gel were confirmed as recombinant hsTfs by Western

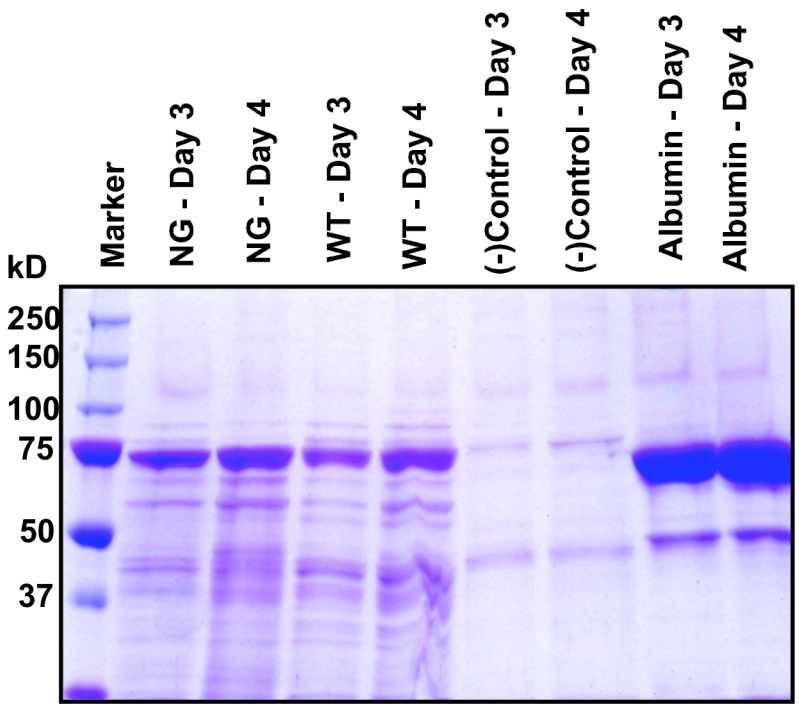

Figure 3-9 SDS-PAGE analysis of the recombinant wild type (WT) and nonglycosylated (NG) hsTfs secreted by GS115 transformants. On the third and fourth days of the expression, 1 mL of culture supernatants from each expression were concentrated down to 0.2 mL and 15 mL of these samples were used in SDS-PAGE. (-)Control represents the control for background expression (GS115 cells transformed with pPICZα-A vector). 15 mL of the supernatant from the albumin expression (included as secretion control) was used without concentrating.

blot analysis using a primary antibody for hsTf (figure 3.10). Protein detection was achieved by chemiluminescence using horseradish peroxidase-conjugated secondary antibody (A), and by direct infrared fluorescence using infrared fluorophore-conjugated secondary antibody (B) as described in materials and methods. Both detection techniques revealed that the WT recombinant hsTfsecreted by GS115 cells was heterogeneous with molecular masses varying from 75 kDa to 100 kDa whereas a single band at 75 kDa was obtained from the

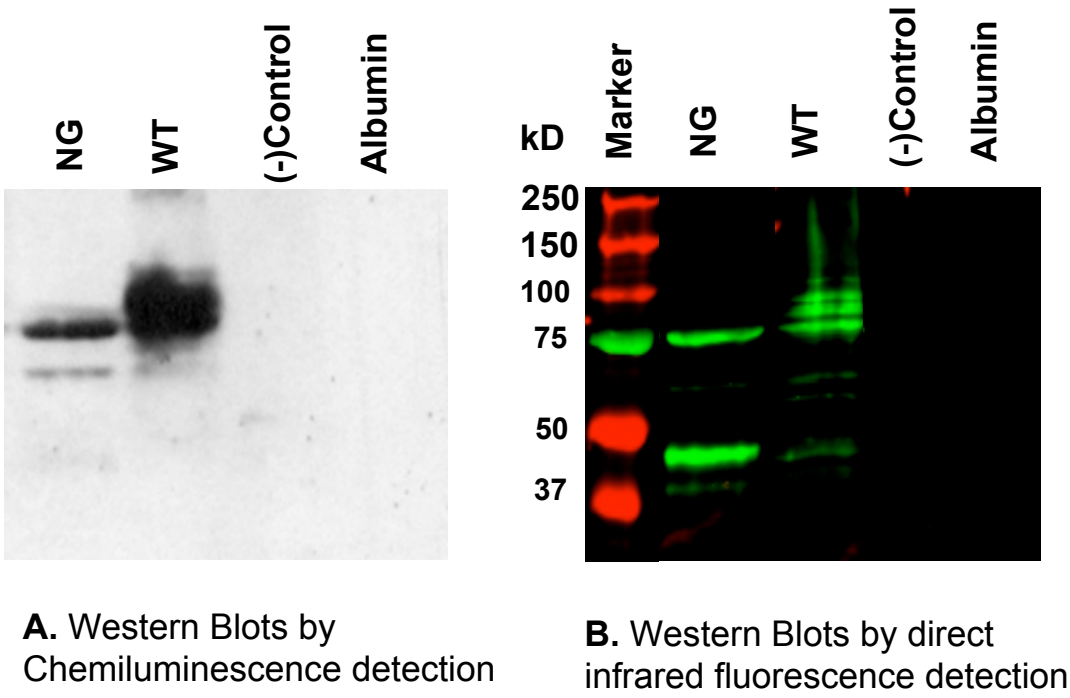

Figure 3-10 Western blot analysis. 5 mL of samples from the culture supernatants were run on SDS-polyacrylamide gel and blotted on nitrocellulose membrane. Protein detection was achieved by chemiluminescence using horseradish peroxidase-conjugated secondary antibody (A), and by direct infrared fluorescence using infrared fluorophore-conjugated secondary antibody (B).

NG hsTf. Low molecular mass protein fragments were also detected by Western blot for both of the recombinant proteins indicating proteolysis or early transcription termination.

Although the culture supernatants contained mostly the recombinant proteins, removal of the culture media was required for functional characterization of the proteins. In addition, purification also increases the concentration of the proteins of interest by eliminating the contaminating proteins.

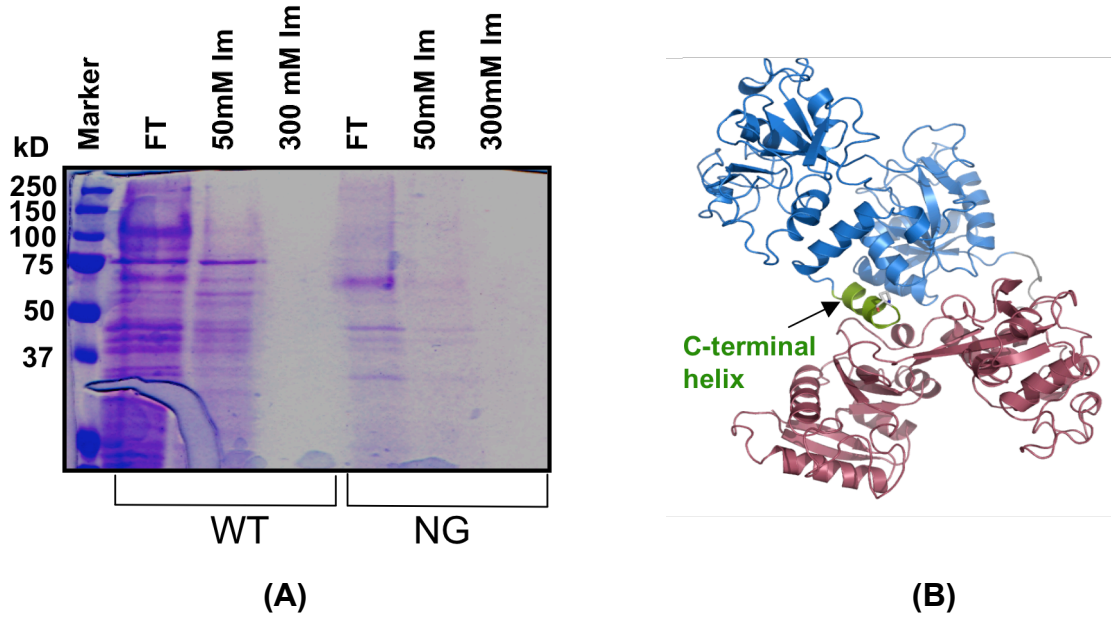

Figure 3-11 **(A)** SDS-PAGE analysis of fractions from the purification of WT and NG hsTf by Ni^{2+}-afinity chromatography. The poly-His tagged recombinant proteins did not bind to the column efficiently. (FT: flow through; Im: imidazole). **(B)** Cartoon representation of the hsTf. The C-terminal a-helix is shown in green. Inability of the poly-His tagged proteins to bind to the Ni^{2+}-charged column may be due to the hindrance of the tag by the interiorly folded C-terminal helix.

Initially Ni^{2+}-affinity chromatography was used to purify the WT and NG recombinant proteins, which contained the C-terminal poly-His tag (pPICZα-A/Tf and pPICZα-A/NGTf constructs, see figure 3.5). SDS-PAGE analysis of the fractions (figure 3-11 – A) shows that both the WT and NG hsTf did not bind to the column since tmost of the proteins were found in the flow-through fractionsand the fractions of the wash step with 50 mM imidazole. No proteins were detected in the elution fractions with 300 mM imidazole. This might be due to the hindrance of the poly-His tag by the C-terminal α-helix of hsTf (figure 3.11–B). For this reason, anion exchange chromatography was employed by either

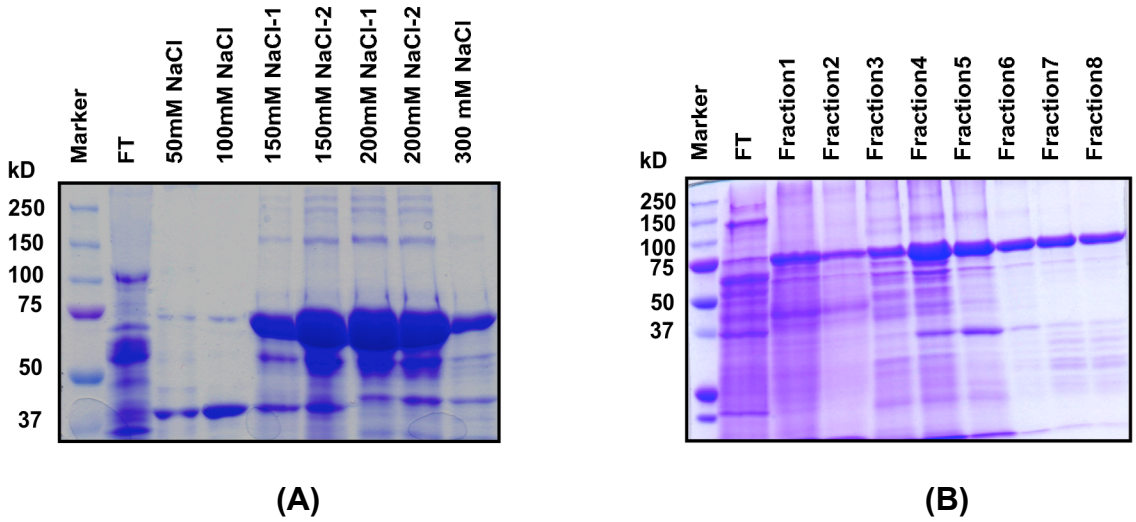

Figure 3-12 SDS-PAGE analysis of fractions from the purification of WT hsTf by anion exchange chromatography. Purification was carried out **(A)** manually using a syringe filter or **(B)** automatically using a gradient pump and a fraction collector. The total amount of recombinant protein purified by either technique was estimated to be 5 mg/L.

manual or gradient pump purification. The samples were prepared as described in the 3.3.7 – protocol 1. In figure 3.12 – A, SDS-PAGE analysis of the concentrated fractions from the manual purification of the WT hsTf is shown. The protein bound to the column efficiently and the wash steps with 50 and 100 mM NaCl eliminated some of the impurities. Although the elution step with 300 mM NaCl yielded >95% pure protein, the majority of the total protein from the culture supernatant was found in the fractions from wash steps with 150, 200, and 250 mM NaCl along with contaminating proteins. Therefore a gradient pump and a fraction collector were used for purification to enable a better separation of the recombinant protein from the contaminants (figure 3.12 – B). This method was determined to be more efficient compared to manual purification. However, ~50%

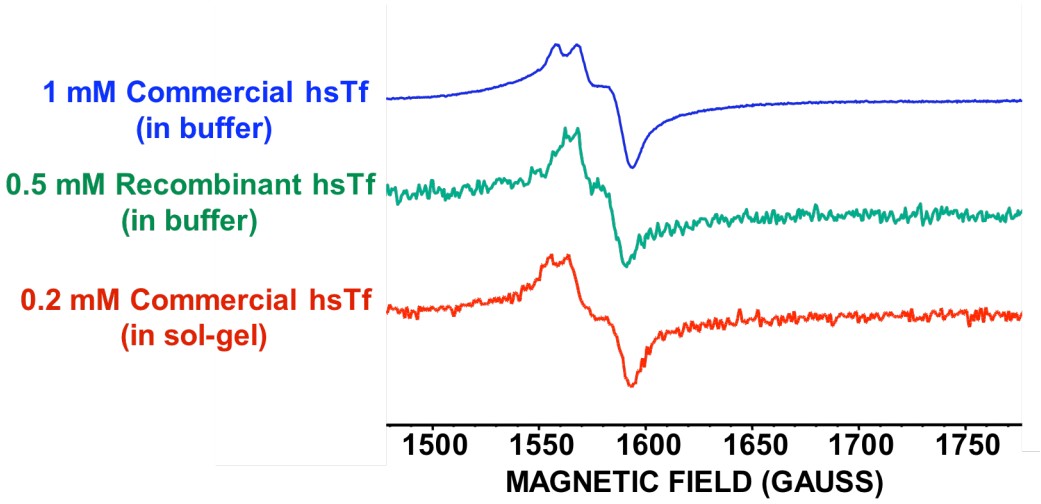

Figure 3-13 X-band EPR spectra of recombinant and commercial hsTfs at 77 K. (EPR parameters: microwave frequency = 9.4, modulation amplitude = 6 G, microwave power = 1.74 mW, receiver gain = 1x 10^4, time constant = 40.96 ms. The spectra were an average of 15 scans).

of the total protein was still present in the wash step fractions. This was attributed to the heterogeneity of WT hsTf secreted by *P. pastoris* arising from the differential glycosylation. It is also possible that the culture medium contains iron-bound and iron-free protein populations, which may cause differences in their isoelectric points. For this reason, iron-saturation prior to purification wasconsidered. However, iron-saturation (by using protocol 2) caused radical formation in the protein, which is discussed in the following sections.

The results given above prove that both WT and NG full-length hsTfs can be produced in the *P. pastoris* expression system. In order to verify the integrity of iron binding by the recombinant hsTf EPR spectroscopy was employed. Fe^{3+}-bound hsTf has a characteristic rhombic EPR signal arising from the coordination

of the paramagnetic Fe^{3+} to the four iron-binding residues of hsTf and to the synergistic carbonate anion. In figure 3.12 the EPR spectrum of the Fe^{3+}-loaded hsTf produced in *P. pastoris* is compared to the spectra of Fe^{3+}-loaded commercial hsTfs (Sigma). Protein concentrations in the EPR tubes were estimated to be 0.5 mM (recombinant,) and 1 mM (commercial) in iron binding buffer. The EPR spectrum of a 0.2 mM sample of commercial hsTf measured in sol-gel medium was included in the comparison to evaluate the yield of functional recombinant protein. The EPR spectra of all three Fe^{3+}-loaded hsTfs are very similar. The spectrum of 1 mM commercial hsTf is essentially noiseless owing to its high concentration. 0.5 mM recombinant hsTf was expected to produce a relatively noiseless spectrum compared to the 0.2 mM commercial hsTf, however an opposite result was obtained indicating that the concentration of the functional recombinant protein in the EPR tube is less than 0.2 mM. This is most likely due to the instability of the recombinant hsTf produced in *P. pastoris* leading to non-functional protein populations during the isolation processes. Consequently, the concentration of the recombinant protein was not sufficient for a thorough EPR analysis. Therefore expression of different constructs outlined in the figure 3.5 was evaluated for increased levels of expression.

pPICZα-A/TfNS, pPICZα-A/Tf-Kex2, and pPICZα-A/TfNS-Kex2 constructs in GS115 cells and KM71H cells

Secretion levels of functional recombinant proteins from yeast differ depending on the protein. In addition, the type of the signal sequence used has a significant effect on the level of secretion. For instance, secretion levels of the

recombinant human insulin-like growth factor from *Saccharomyces cerevisiae* and *P. pastoris* varied greatly when different secretion signal sequences were used.[141, 142] Recombinant human serum albumin (hsA) and human lysozyme were successfully secreted from *P. pastoris* at high levels using only the native signal sequence of hsA.[143-145] Therefore different DNA constructs (figure 3.5) with and without the native signal sequence of hsTf were tested for high-level secreted expression in the two *P. pastoris* strains GS115 (Mut^+) and KM71H (Mut^s). It is recommended by the *Pichia* expression kit supplier (Invitrogen) that both Mut^+ and Mut^s phenotypes should be tested since either phenotype may produce higher levels of recombinant proteins depending on the protein being expressed. Expression levels of the constructs in KM71H cells were higher than in the GS115 cells. However, these proteins expressed in KM71H cells were very unstable and precipitated during the initial processing (concentration of the secretion media, buffer exchange for purification). The white precipitate was completely removed by centrifugation and the supernatant was purified by anion exchange chromatography. Despite a ~100-fold concentration of the fractions, SDS-PAGE analysis revealed only faint bands at 75 kDa (data not shown). Detection of the proteins were possible only by Western blots analysis. The analysis of the fractions from the purification of the recombinant hsTf construct, pPICZα-A/TfNS-Kex2, expressed in KM71H cells is given in figure 3.14 as an example. Analysis of the other constructs were similar and are not given here.

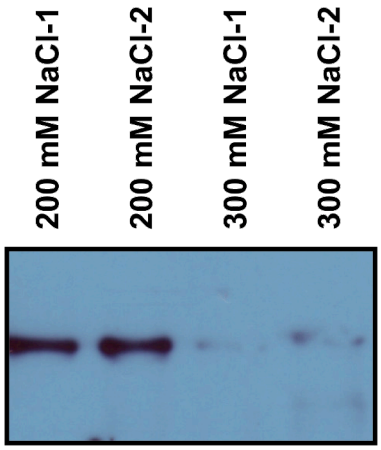

Figure 3-14 Western blot analysis of the fractions from DEAE/sepharose column purification of recombinant hsTf (pPICZα-A/TfNS-Kex2 construct) in KM71H cells. Only 4 fractions were included in the analysis. All fractions were concentrated 100-fold using Amicon centrifugal filter units.

3.4.4 Effect of iron addition on the yield of recombinant hsTf

Addition of iron into the expression media during expression

Expression of recombinant porcine lactoferrin in *P. pastoris* has been shown to increase significantly when 100 mM $FeCl_3$ was added to the culture medium during expression.[110] Therefore the effect of iron addition to the expression culture on the yield of recombinant hsTf in *P. pastoris* GS115 cells (transformed with pPICZα-A/Tf construct) was evaluated. Addition of iron, either in the free form or chelated form, increased the expression levels remarkably as determined by SDS-PAGE and Western blot analysis (data not shown). Moreover, The characteristic salmon pink color of iron-bound hsTf was readily observed in the fractions after purification. When iron was removed from the recombinant hsTf the color disappeared and reappeared upon iron addition indicating that the

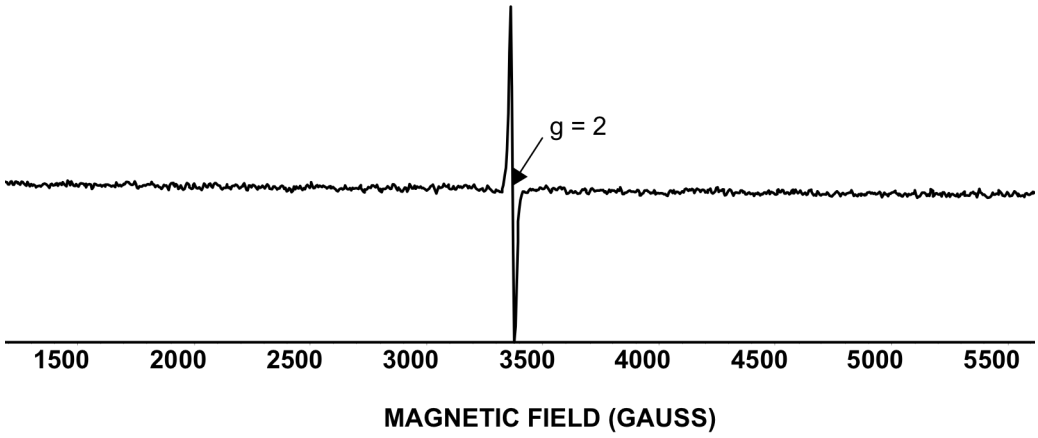

Figure 3-15 EPR spectroscopy analysis of the purified recombinant hsTf expressed in iron-fed *P. pastoris*. A single signal was obtained with a g value of 2 demonstrating the formation of a radical species by added iron during expression.

recombinant protein binds and releases iron in a pH dependent manner, an evidence of its functionality. However, addition of iron (free or chelated) into the culture medium caused radical formation as shown by EPR analysis of the purified recombinant hsTf fractions (figure 3.15). Furthermore, UV-visible spectroscopy revealed that the maximum absorbance at 465 nm, a characteristic of iron-bound hsTf, is shifted to 476 nm in the radical species of hsTf (figure 3.16). The salmon pink colour stems from the ligand to metal charge transfer between Fe^{3+} and tyrosine ligand in the iron binding sites of hsTf. The salmon pink colour of the recombinant protein is therefore an evidence of iron-binding at the correct site. The wavelength shift may be due to the formation of tyrosine radicals since the iron-coordinating tyrosine residues are easily accessible by radical oxygen species. The absence of the absorbance at 476 nm in the iron-free (apo-hsTf) form of the recombinant protein proves the source of this

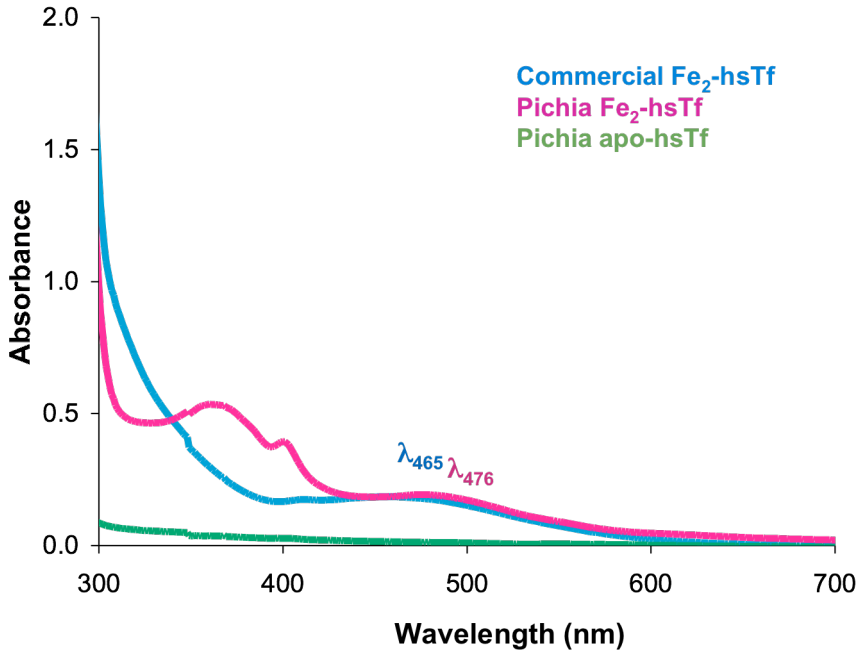

Figure 3-16 Analysis of iron-bound radical species of recombinant hsTf by UV-visible spectroscopy. UV-visible spectra of the sample used in the EPR analysis (pink) and the commercial hsTf (blue) was recorded in the range of 300-700 nm. Iron-bound recombinant hsTf expressed in *P. pastoris* has an absorbance at 476 nm which is absent in the iron-free form.

absorbance as iron bound to hsTf.

Addition of iron to the supernatant from the expression media

The purpose of feeding iron to the *P. pastoris* cells during expression was to provide the cells with additional iron since the secreted hsTf chelates the available iron in the culture media. For this reason, another expression was performed using a ferri-siderophore (ferric-TAF) to provide iron to the cells. A single colony of the KM71H cells transformed with pPICZα-A/TfNS-Kex2 was grown and divided into two. In the second day of expression, 50 μM ferric-TAF

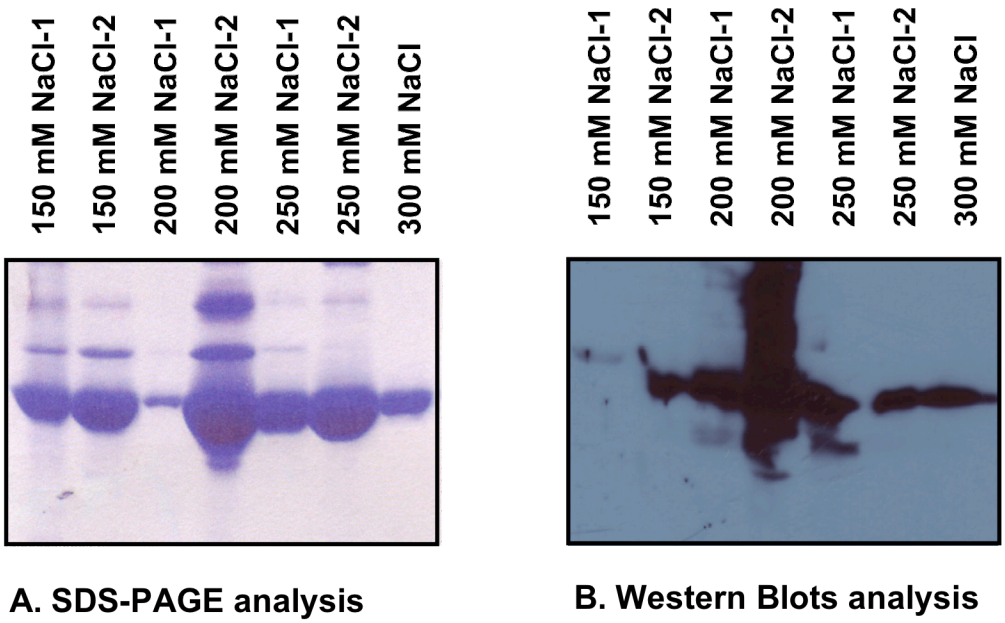

Figure 3-17 SDS-PAGE and Western Blot analysis of recombinant hsTf saturated with iron following the cell-harvesting step. When the expression was complete the cells were harvested and the supernatant was saturated with iron. After purification the fractions with salmon pink color were analyzed by SDS-PAGE **(A)** and Western Blot **(B)**.

was added into one of the flasks. The other expression media served as controls (without ferric-TAF). At the end of the expression, supernatants from both cultures were saturated with iron and purified by ion-exchange chromatography. No precipitation was observed in any of the supernatants. Interestingly, the fractions from the control sample (without ferric-TAF) had intense salmon pink colour, indicating the presence of iron-bound hsTf, whereas the fractions from the purification of the sample (with ferric-TAF) did not. SDS-PAGE and Western blot analysis revealed that addition of ferric-TAF into the expression media decreases the yield of recombinant protein since no bands were obtained at 75 kDa (data not shown). As shown in figure 3.17 - A, iron-saturation as soon as the cell

harvesting step resulted in a striking increase in the yield of recombinant hsTf. Western blot analysis proved the identity of the protein corresponding to the bands at 75 kDa on the SDS-polyacrylamide gel as hsTf (figure 3.17 – B). Interestingly, the EPR spectroscopy analysis of these fractions disclosed a single signal of a radical species similar to that of shown in figure 3.15.

3.5 Discussion

Production of functional full-length hsTf in *P. pastoris* has been reported to be challenging.[62, 146] In this study, a protocol for expression of functional hsTf in *P. pastoris* was described. Initially, a recombinant construct in which the Kex2 site was removed and the hsTf cDNA including the codons for the native signal sequence of hsTf was fused in-frame with the yeast mating α-factor signal sequence, was used to transform the GS115 *P. pastoris* cells. As explained in 3.2.3 of this chapter, removal of the a-factor signal sequence requires the Kex2 cleavage site. Thus, it can be argued that the recombinant hsTf expressed from this construct may not be processed properly and may carry the α-factor signal sequence in its N-terminal along with its native signal sequence. However, the C-terminal native signal sequence of hsTf, Leu-Ala-Val-Pro, is very similar to the C-terminal pre-signal sequence of α-factor, Leu-Ala-Ala-Pro, which is recognized and cleaved by the signal peptidase in the yeast ER.[147-149] Since this event takes place before the pro-signal sequence is removed by Kex2 in the late Golgi, it is likely that the C-terminal native signal sequence of hsTf is recognized by the *P. pastoris* signal peptidase and removed along with the a-factor signal sequence. Therefore, the recombinant hsTf corresponding to the band at ~75 kDa obtained

from the SDS-PAGE and Western blots analysis, should be the mature full-length hsTf. Nevertheless, N-terminal peptide sequencing must be performed to confirm that this protein is in fact the correctly processed mature full-length hsTf, and not a short form due to an early transcription termination, carrying the ~100 amino acid residues long α-factor signal sequence and the hsTf's native signal sequence.

This recombinant construct was expressed in 500 mL of BMMY media in reasonable quantities (~10 mg/L), but after purification the yield reduced to ~5 mg/L. 0.5 mM recombinant protein produced an EPR spectrum similar to that of commercial hsTf. However, the weak signal compared to that of 1 mM and 0.2 mM commercial hsTf suggested that the concentration of the functional recombinant protein was below 0.2 mM. Attempts were made to improve the yield of functional recombinant protein by expressing different DNA constructs of hsTf in which the Kex2 site was rebuilt between the α-factor signal sequence and either the hsTf native signal sequence or the codon for the first amino acid residue (Val) of mature hsTf. Note that, the poly-His tag was absent in these constructs since the purification utilizing this tag was not efficient. Moreover, the six His residues at the C-terminal of the recombinant hsTf may interfere with the Ru(III)-complex-binding experiments. Therefore, the poly-His tag was excluded from these constructs by rebuilding the hsTf's stop codon at its C-terminal. The *P. pastoris* strains GS115 and KM71H were transformed with these constructs and the KM71H cells secreted higher levels of recombinant protein compared to the GS115 cells. Unfortunately, the recombinant hsTf produced in KM71H cells

were unstable and precipitated after the cell-harvesting step.

The low level expression of hsTf in *P. pastoris* was initially correlated to the iron depletion in the expression medium due to the strong iron-chelating nature of hsTf. For this reason, various iron sources were added to the culture medium during expression, as an iron-supplement for the cells. $FeCl_3$, $FeNTA_2$, and ferric-citrate addition resulted in a significant increase in the yield of recombinant hsTf regardless of the recombinant DNA constructs, and the *P. pastoris* strain used. In addition, the characteristic salmon pink colour of iron-bound hsTf was readily observed in the fractions of purified recombinant protein. However, the EPR analysis revealed that all of the recombinant hsTfs expressed in the presence of $FeCl_3$, $FeNTA_2$, or ferric-contained radical species. This result is expected when $FeCl_3$ is added to the culture medium since the unprotected Fe^{3+} is highly insoluble in neutral aqueous media and produces the very reactive hydroxyl radical and eventually the protein radicals.[66] On the other hand, formation of radical species caused by addition of citrate-chelated Fe^{3+} to the culture medium is surprising since citrate is a physiological iron chelator.[66]

In order to overcome the Fe^{3+}-mediated radical formation, a ferric siderophore, ferric-TAF, was used to provide cells with additional iron. Although yeast cells do not secrete or synthesize siderophores they can take up iron-siderophore complexes.[150] Thus, *P. pastoris* cells should be able to utilize ferric-TAF in which the ferric ion is strongly sequestered by the siderophore molecule TAF. Interestingly, when ferric-TAF was added to the culture medium no recombinant hsTf was observed by SDS-PAGE or Western blots analysis. On the

contrary, the control expression (i.e. without ferric-TAF) from the same colony produced very high levels of recombinant hsTf. The only difference between this control expression and the previous expressions (from the same colony) is that iron saturation was performed as soon as the cells were harvested. Despite a very high yield, the purified recombinant protein contained radical species as shown by EPR spectroscopy. No radical species were observed for ferric-TAF-containing either the culture medium or the fractions from the purification of this medium. Note that, the supernatants from both expression cultures (with and without TAF) were processed the same way.

Taken together, these results suggest that the recombinant full-length hsTf is secreted from *P. pastoris* cells at very high levels, but it is unstable in the absence of Fe^{3+}. The ferric-TAF experiment also supports this argument. Natural siderophores are very strong iron chelators, synthesized by bacterial pathogens to sequester iron from the bacteriostatic proteins such as transferrin and lactoferrin.[151] Therefore, no recombinant hsTf expression in the presence of TAF can be attributed to the sequestration of the iron from hsTf. Even if the protein is secreted, it is likely to precipitate in a free-iron deficient environment. TAF experiments also suggest that Fe^{3+}-mediated radical formation is independent of the cells, since the radical protein species were also obtained when $FeNTA_2$ was added after the cells were removed from the expression medium. However, when TAF was present, no radical species were observed. This indicates that Fe^{3+} interacts with the components of BMMY media possibly producing reactive oxygen species, which can be prevented by a strong iron-chelating agent such

as a siderophore. Since addition of a strong chelating agent prevents recovery of the recombinant hsTf from the *P. pastoris* secretion medium, an alternative expression media should be considered, to which $FeNTA_2$ can be safely added without causing radical formation. A basal salt medium has been reported to be more suitable for the expression of N-terminal half molecule of hsTf in *P. pastoris.*[96] Thus, future studies should include expression of full-length hsTf in *P. pastoris* using a basal salt medium or alternative expression media in which the recombinant protein can be rendered stable by safe addition of Fe^{3+}.

CHAPTER 4: A SIMPLE AND COST-EFFECTIVE METHOD FOR PURIFICATION OF TRANSFERRIN

4.1 Abstract

Obtaining pure proteins from complex mixtures in high yields using simple, easily accessible, and cost-effective purification methods is highly desirable in protein research. In this study, progress towards such method was made for purification of recombinant human serum transferrin (hsTf). The motivation for this work was the low efficiency of the most common purification methods (i.e. poly-His-tag / Ni^{2+}- affinity and ion-exchange chromatographies) for the reasons explained in chapter 3. The method described here utilizes immobilized metal ion affinity chromatography (IMAC) and exploits the functional properties of hsTf as a metal-binding protein. The purification procedure is fairly simple consisting of: 1) sample loading at optimum pH, 2) elimination of the nonspecifically bound proteins by washing with binding buffer containing varying concentrations of imidazole, and 3) elution with either binding buffer containing 50 mM EDTA or low pH buffer. IMAC media charged with two different metal ions, Fe^{3+} and Cu^{2+} was tested for isolation of recombinant hsTf from the *P. pastoris* expression culture. The Cu^{2+} - affinity chromatography was found to be the most efficient.

IMAC with Fe^{3+} and Cu^{2+} was also evaluated for purification of Transferrin (Tf) from rabbit serum, but it was found to be unsuitable for one-step purification of Tf from serum due to contamination from high albumin concentration.

However, a serum protein, histidine-rich glycoprotein, was obtained with >95% purity from purification of rabbit serum by IMAC with Cu^{2+}.

4.2 Introduction

IMAC was first introduced by Porath et al. in 1975 as a new approach to fractionate proteins by using iminodiacetic acid (IDA) as a chelating ligand.[152] IMAC employs a multidentate chelator such as IDA or NTA (nitrilotriacedic acid) coupled to a cross-linked chromatographic support via a spacer arm (figure 4.1). The principle of this method is to separate proteins with respect to their affinities for metal ions. Initially it was thought that proteins coordinate to metal ions such as Zn^{2+} and Cu^{2+} mostly with their surface-exposed imidazole and thiol groups.[153, 154] Later it was shown that side-chains of surface-exposed hydrophobic residues such as tryptophan could also form relatively stable coordination structures with metal ions.[155] Further studies have revealed more specifics of the interactions between proteins and the metal ions on the IMAC adsorbents. It has been shown, for example, that within the pH range of 4.5 and 7.5, soft metal ions such as Cu^{2+}, Zn^{2+}, or Ni^{2+} primarily interact with accessible imidazole group of histidine residues, while the N-terminal α-amino groups and side-chains of tryptophan or cysteine residues play a secondary role in protein binding to the immobilized soft metal ions.[156-159] On the other hand, immobilized hard metal ions, such as Fe^{3+}, favor oxygen-rich side chains of aspartic and glutamic acid or phosphate groups on the surface of proteins.[158-165]

By a method developed by Roche, IMAC with soft metal ions was applied to purification of recombinant proteins with a poly-histidine tag engineered at

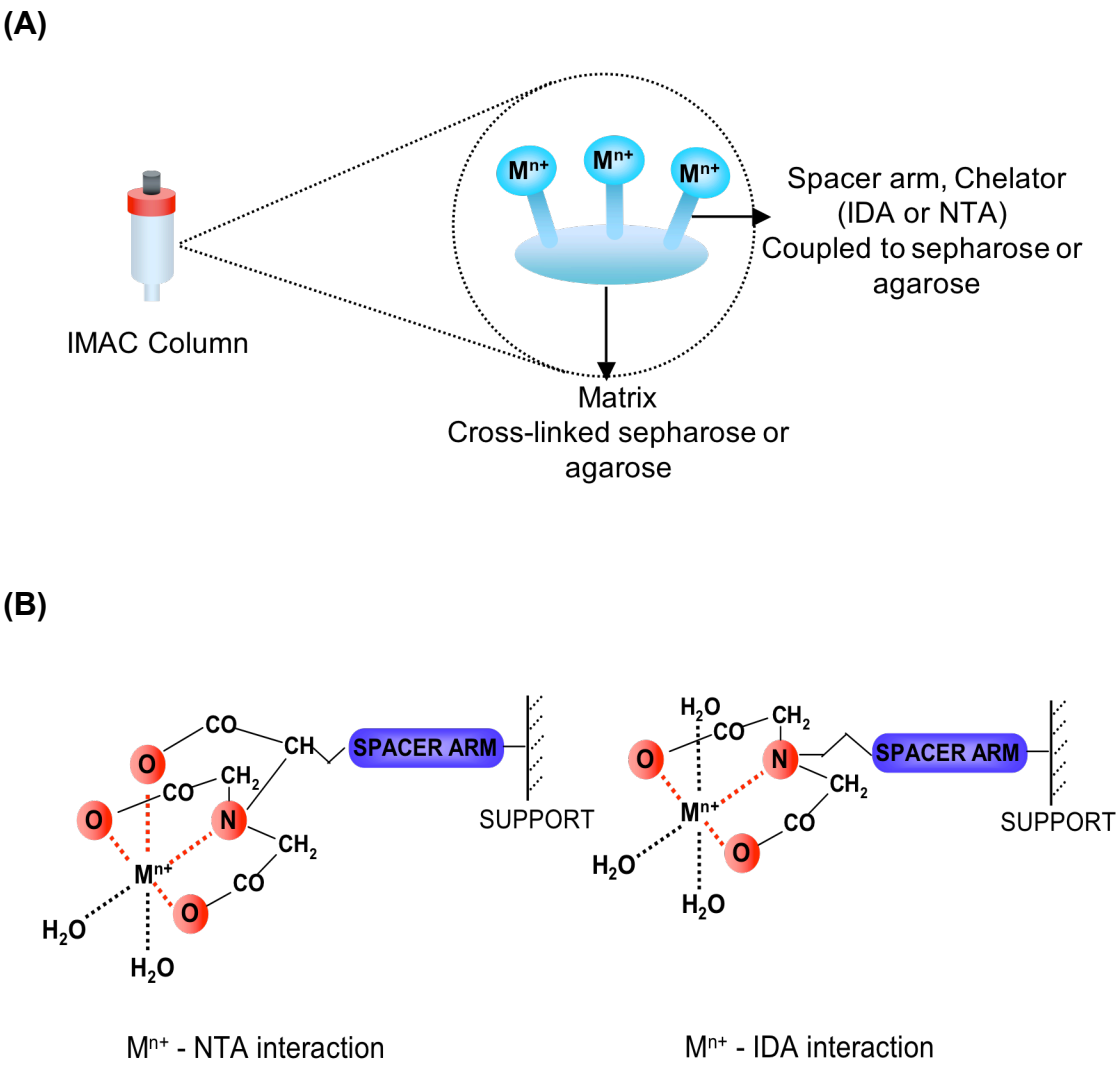

Figure 4-1 **(A)** A schematic representation of IMAC adsorbent. The metal ion is immobilized by a multidentate chelator, which is covalently attached to a chromatographic support via a spacer arm. **(B)** Interactions of the NTA and IDA metal chelate matrices with metal ions (adapted from the QIAexpressionist, handbook for high-level expression and purification of 6xHis-tagged proteins, QIAGEN). NTA is a tetradendate chelating agent and binds and retains metal ions more strongly than the tridentate chelating agent IDA.

either their N- or C-terminal. Two or three histidine residues on the tag coordinate to the metal ion on the chelating resin with their imidazole groups allowing strong binding of the His-tagged protein to the resin. Unwanted proteins generally bind

nonspecifically and can be removed from the column by washing with buffer containing low concentrations of imidazole. The tagged protein is then eluted with a higher concentration of imidazole, which competes with histidine residues on the protein, resulting in protein release from the adsorption media.

In this study, IMAC was employed for purification of hsTf from complex mixtures such as expression media and serum. The aim was to apply the function of hsTf as an iron-binding protein to its separation from other proteins by using IMAC (figure 4.2). In principle, hsTf should bind to immobilized Fe^{3+} with much higher affinity than that of other proteins, which should only bind nonspecifically with their surface exposed imidazole, thiol, or hydrophobic groups. Buffers containing varying concentrations of imidazole should readily eliminate these nonspecifically bound proteins from the purification media. In apo-hsTf both iron-binding sites should be accessible with four iron-binding residues in each binding pocket. Therefore hsTf should remain attached to Fe^{3+} on the resin even after washing with high concentrations of imidazole. Elution of hsTf can then be accomplished by passing a low pH buffer through the column, since hsTf releases Fe^{3+} below pH 4.8.[63, 64, 166] In addition, EDTA could also be included in the elution buffer to ensure efficient elution of Tf from the column. This hypothesis was tested using IMAC with Fe^{3+} and Cu^{2+} to purify recombinant hsTf expressed in *P. pastoris* as well as the native Tf from rabbit serum.

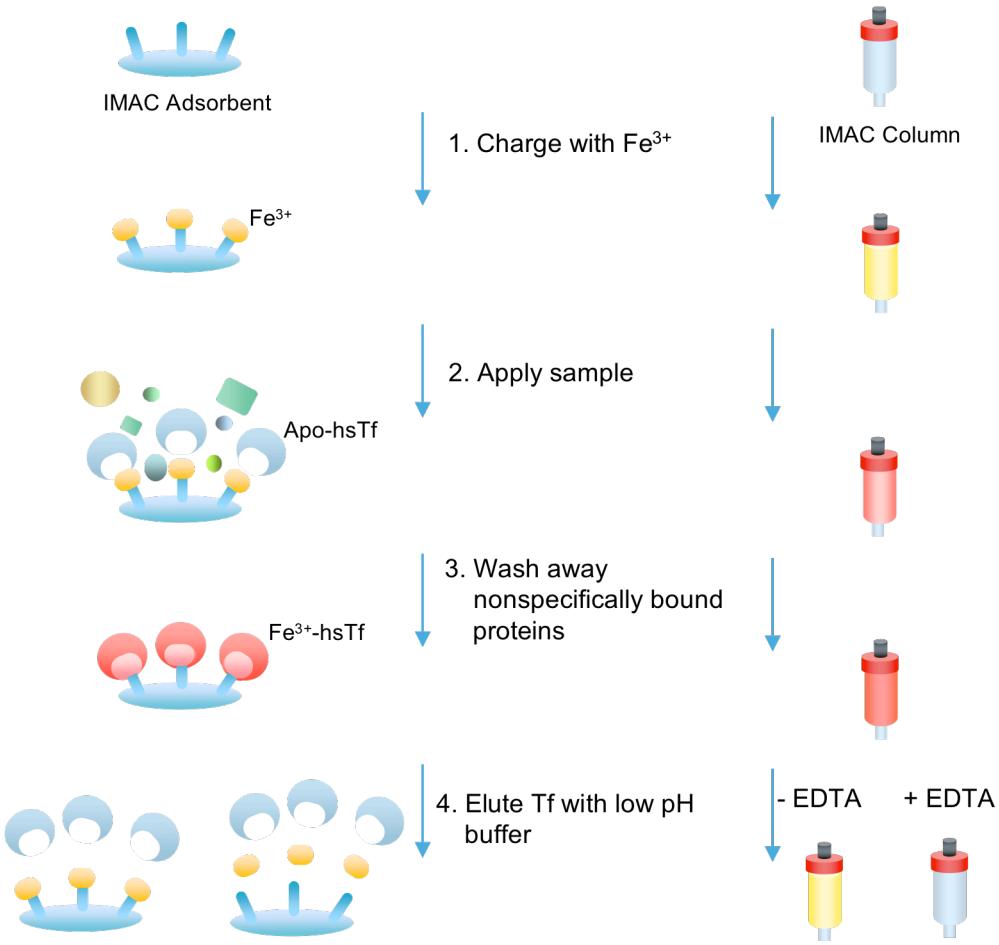

Figure 4-2 Schematic representation of the proposed hsTf purification by immobilized Fe^{3+}-affinity chromatography. The colour of the Fe^{3+}-charged column changes from pale yellow to salmon pink upon loading hsTf, which is characteristic for Fe^{3+}-bound hsTf. When low pH buffer is applied to the column, Tf is expected to be released from the immobilized Fe^{3+} and the colour of the column should change back to pale yellow. When EDTA is included in the elution buffer, it will cause removal of the metal ion and hsTf from the column.

4.3 Materials and methods

4.3.1 Optimization of the purification procedure using hsTf and BSA mixture

The purification procedure was optimized by using either NTA-agarose media (Qiagen Inc. catalog # 30210, ON, Canada) for Ni^{2+}- and Fe^{3+}-affinity chromatography, or IMAC sepharose^{TM} high performance media (GE Healthcare, catalog # 17-0920-06, NJ, USA) for Cu^{2+}-affinity chromatography. First, commercial human serum transferrin (hsTf, Sigma-Aldrich catalog # T2252) was used to test the proposed purification procedure by Fe^{3+}-affinity chromatography. Initially, IMAC sepharose^{TM} high-performance beads were utilized for purification of hsTf. However, this media was found to be unsuitable because of the weak chelating agent, IDA, on the beads. IDA has only three metal-chelating sites and cannot compete with strong Fe^{3+}-binding proteins such as hsTf (see figure 4.1 – B). Consequently, the Fe^{3+} ion dissociates from the beads when these proteins are present. In addition, it was found to be more difficult to charge the beads with Fe^{3+} because of the unavailability of a chelating agent to protect Fe^{3+} that is weaker than IDA. For this reason, NTA-agarose beads were chosen. NTA is a tetradentate ligand and under conditions where hsTf binds weakly, such as at low pH, it can compete with Tf for Fe^{3+}. NTA-agarose beads were charged with Fe^{3+} by incubation with $Fe(IDA)_3$. $Fe(IDA)_3$ was prepared by dissolving $FeCl_3$ in IDA at a molar ratio of 1:3. pH was increased to ~ 2 by drop-wise addition of 1 M NaOH. The solution was centrifuged at max. speed to remove insoluble iron species that were formed during pH adjustment. 3 mL of the supernatant consisting of ~50 mM $Fe(IDA)_3$ was used to charge 0.75 mL of the NTA-agarose beads, which

enabled a stable Fe^{3+}-release from IDA to NTA without precipitating. Low pH was necessary during the purification procedure due to strong binding of hsTf to Fe^{3+} at neutral pH, which caused leaching of the metal ion. A wide range of pH points was tested and the optimum pH for protein binding was found to be 5.8. In a 2 mL microcentrifuge tube, 0.5 mL of 0.25 M (10 mg) hsTf in binding buffer (see table 4.1) was added to 0.75 mL of Fe^{3+}-charged NTA-agarose beads. The beads had been previously equilibrated with 7.5 mL of the binding buffer. The sample was incubated with the beads for 1-2 minutes and centrifuged at 6,000 RPM for 1 min. The supernatant was saved and designated as flow through. Any non-specifically bound hsTf was eliminated by washing with buffer containing 10-20 mM imidazole. Finally, 3 mL of three different elution buffers (table 4.1) each were tested for their ability to remove hsTf from the beads. 1.5 mL fractions were taken at each step and analyzed by SDS-PAGE. The buffers used in the purification steps are described in table 4.1.

In order to optimize this procedure for purification of Tf from complex mixtures, a 1:1 mixture of commercial hsTf (0.5 mL, 0.25 mM) and bovine serum albumin (0.5 mL, 0.25 mM) was studied by Fe^{3+}- and Cu^{2+}-affinity chromatography methods. The purification steps were similar to those detailed above. For Cu^{2+}-affinity chromatography, 0.75 mL IDA-sepharose beads were charged with Cu^{2+} by applying 5 mL of 0.1 M $CuSO_4$ solution. In order to remove the unbound metal ions, the beads were washed with 5 mL of water. The beads were then equilibrated with 7.5 mL of binding buffer. The same purification procedure was followed as described for Fe^{3+}-affinity purification.

Table 4.1 Buffers used in the optimization of commercial hsTf purification by Fe^{3+}-affinity chromatography.

Buffer Name	Buffer Components	pH
Binding Buffer (BB)	50 mM MES, 20 mM $NaHCO_3$, 150 mM NaCl	5.8
Wash Buffer 1	BB, 5 mM imidazole	5.8
Wash Buffer 2	BB, 10 mM imidazole	5.8
Wash Buffer 3	BB, 20 mM imidazole	5.8
Elution Buffer 1*	500 mM acetate buffer	4.5
Elution Buffer 2*	500 mM acetate buffer, 5 mM EDTA	4.5
Elution Buffer 3*	BB, 50 mM EDTA	5.8

* Three separate purifications were carried out with each of the three elution buffers.

The buffers used in Fe^{3+}- and Cu^{2+}-affinity purification of sample mixture are given in table 4.2 and table 4.3 respectively.

4.3.2 Purification of recombinant hsTf expressed in *P. pastoris* by IMAC with Fe^{3+} and Cu^{2+}

IMAC with Fe^{3+}

Full-length hsTf was expressed in *P. pastoris* KM71H cells as described in chapter 3.3.6. In the fourth day of expression cells were spun down and the supernatant containing the secreted protein was collected. 100 mL of binding buffer (table 4.4) was added to 100 mL of the secretion media. 5 mL of NTA-agarose beads charged with Fe^{3+} was mixed with this solution and incubated for 30 min. at 4 °C with gentle shaking. The beads were then allowed to settle. Supernatant was removed carefully without disturbing the beads. The proteins trapped on the beads were fractionated by the procedure described for Fe^{3+}-affinity chromatography purification of commercial hsTf. Since the complete

Table 4.2 Buffers used to optimize the purification of Tf from 1:1 mixture of hsTf and BSA by Fe^{3+}-affinity chromatography.

Buffer Name	Buffer Components	pH
Binding Buffer (BB)	50 mM MES, 20 mM $NaHCO_3$, 150 mM NaCl	5.8
Wash Buffer 1	500 mM acetate buffer	4.5
Wash Buffer 2	BB, 5 mM imidazole	5.8
Wash Buffer 3	BB, 10 mM imidazole	5.8
Wash Buffer 4	BB, 15 mM imidazole	5.8
Wash Buffer 5	BB, 20 mM imidazole	5.8
Elution Buffer	BB, 50 mM EDTA	5.8

Table 4.3 Buffers used to optimize the purification of hsTf from 1:1 mixture of hsTf and BSA by Cu^{2+}-affinity chromatography.

Buffer Name	Buffer Components	pH
Binding Buffer (BB)	IBB	7.4
Wash Buffer 1	BB, 4 mM imidazole	7.4
Wash Buffer 2	BB, 5 mM imidazole	7.4
Wash Buffer 3	BB, 15 mM imidazole	7.4
Elution Buffer	BB, 50 mM EDTA	7.4

*__IBB:__ Iron Binding Buffer (50 mM HEPES, 150 mM NaCl, 20 mM $NaHCO_3$)

removal of EDTA from the protein sample is essential for experiments such as Ru(III)-complex binding, a higher concentration of imidazole was used during the wash steps to assess the possibility of eluting hsTf without the need for EDTA. The buffers used in this procedure are described in table 4.4.

Table 4.4 Buffers used for purification of full-length recombinant hsTf expressed in *P. pastoris* by Fe^{3+}-affinity chromatography.

Buffer Name	Buffer Components	pH
Binding Buffer (BB)	50 mM MES, 20 mM $NaHCO_3$, 150 mM NaCl, 10 mM imidazole	5.8
Wash Buffer 1	BB, 40 mM imidazole	5.8
Wash Buffer 2	BB, 60 mM imidazole	5.8
Wash Buffer 3	BB, 100 mM imidazole	5.8
Wash Buffer 4	BB, 300 mM imidazole	5.8
Elution Buffer	BB, 50 mM EDTA	5.8

IMAC with Cu^{2+}

The sample preparation and purification procedure with Cu^{2+}-charged IMAC media was the same as described above except for the following changes: IBB (50 mM HEPES, 150 mM NaCl, 20 mM $NaHCO_3$, pH 7.4) was used as binding buffer and the purification was performed at pH 7.4. Imidazole concentrations were the same throughout purification.

4.3.3 Metal removal from rabbit serum

Rabbit serum was prepared from whole rabbit blood as described in chapter 2.3.5. Metal chelate affinity column purification required metal-free proteins for maximum binding to the metal-charged resin. For this reason, any possible metal ions bound to Tf in serum were removed by using the iron-removal protocol as described in chapter 2.3.3. Following iron-removal, a stock solution of rabbit serum was exchanged into IBB.

4.3.4 Application of IMAC to purification of rsTf from rabbit serum

IMAC with Fe^{3+}

0.5 mL of serum was exchanged into the binding buffer at pH 5.8 using amicon centrifugal filter units and rsTf separation from other serum proteins was attempted as outlined for commercial hsTf purification from 1:1 hsTf/BSA mixture. The wash step with 500 mM acetate buffer (pH 4.5) was omitted since it had no effect on the hsTf purification from a 1:1 hsTf/BSA mixture. The buffers used in the procedure are described in table 4.5.

IMAC with Cu^{2+}

Cu^{2+}-IDA-sepharose beads were prepared by the method described in 4.4.1. The purification procedure was also the same except for small differences in the buffers used, which are specified in table 4.6 (at pH 7.4) and table 4.7 (at pH 5.8). A Cu^{2+}-affinity column was tested to assess a possible enhancement of rabbit serum fractionation. The column was prepared by processing a 5 mL Ni^{2+}-charged HisTrap FF crude sepharose column to remove Ni^{2+} from the resin. 50 mL of metal-stripping buffer (20 mM sodium phosphate, 500 mM NaCl, 50 mM EDTA, pH 7.4) was passed through the column as recommended by the supplier (GE Healthcare). After washing with excess of water, 20 mL of 100 mM $CuSO_4$ solution was applied to charge the column with Cu^{2+}. To eliminate unbound Cu^{2+}, the column was washed with 100 mL of water. For removal of any weakly bound metal ions, a blank run was performed by passing 100 mM imidazole-containing binding buffer through the column. The column was then equilibrated with 10 column volumes of binding buffer. 1 mL of rabbit serum in 9 mL of binding buffer

Table 4.5 Buffers used for fractionation of rabbit serum by Fe^{3+}-affinity chromatography.

Buffer Name	Buffer Components	pH
Binding Buffer (BB)	50 mM MES, 20 mM $NaHCO_3$, 150 mM NaCl	5.8
Wash Buffer 1	BB, 10 mM imidazole	5.8
Wash Buffer 2	BB, 15 mM imidazole	5.8
Wash Buffer 3	BB, 20 mM imidazole	5.8
Elution Buffer	BB, 50 mM EDTA	5.8

Table 4.6 Buffers used for fractionation of rabbit serum by Cu^{2+}-affinity chromatography at pH 7.4.

Buffer Name	Buffer Components	pH
Binding Buffer	IBB*, 1 mM imidazole	7.4
Wash Buffer 1	IBB, 2 mM imidazole	7.4
Wash Buffer 2	IBB, 3 mM imidazole	7.4
Wash Buffer 3	IBB, 3.5 mM imidazole	7.4
Wash Buffer 4	IBB, 4 mM imidazole	7.4
Wash Buffer 5	IBB, 5 mM imidazole	7.4
Wash Buffer 6	IBB, 6 mM imidazole	7.4
Wash Buffer 7	IBB, 10 mM imidazole	7.4
Wash Buffer 8	IBB, 15 mM imidazole	7.4
Wash Buffer 9	IBB, 20 mM imidazole	7.4
Elution Buffer	IBB, 50 mM EDTA	7.4

*__IBB:__ Iron Binding Buffer (50 mM HEPES, 150 mM NaCl, 20 mM $NaHCO_3$)

was loaded on the column and purification was performed as described for hsTf purification from 1:1 hsTf/BSA mixture by Cu^{2+}-IDA-sepharose beads (at pH 7.4) but with 5 times larger buffer volumes (table 4.8). The flow rate for the sample loading step was 5 mL/min and for wash/elution steps was 10 mL/min.

Table 4.7 Buffers used for fractionation of rabbit serum by Cu^{2+}-affinity chromatography at pH 5.8.

Buffer Name	Buffer Components	pH
Binding Buffer (BB)	50 mM MES, 20 mM $NaHCO_3$, 150 mM NaCl	5.8
Wash Buffer	BB, 20 mM imidazole	5.8
Elution Buffer	BB, 50 mM EDTA	5.8

Table 4.8 Buffers used for fractionation of rabbit serum by Cu^{2+}-IDA-sepharose column and Ni^{2+}-NTA-agarose media.

Buffer Name	Buffer Components	pH
Binding Buffer	IBB*, 5 mM imidazole	7.4
Wash Buffer 1	IBB, 40 mM imidazole	7.4
Wash Buffer 2	IBB, 60 mM imidazole	7.4
Wash Buffer 3	IBB, 100 mM imidazole	7.4
Elution Buffer	IBB, 50 mM EDTA	7.4

*__IBB:__ Iron Binding Buffer (50 mM HEPES, 150 mM NaCl, 20 mM $NaHCO_3$)

IMAC with Ni^{2+}

0.5 mL of metal-free rabbit serum was fractionated by using Ni^{2+}-NTA-agarose beads as described for rabbit serum fractionation with immobilized Cu^{2+}-affinity chromatography. The buffers used in the process are given in table 4.8.

4.3.5 SDS-Polyacrylamide gel electrophoresis (SDS-PAGE)

All fractions were analyzed by SDS-PAGE as described in chapter 3.3.5. Rabbit serum and/or hsTf/albumin were included as controls.

4.3.6 Protein identification

The identity of the histidine-rich glycoprotein that was obtained with very high purity from rabbit serum by Ni^{2+}- and Cu^{2+}-affinity purification was confirmed by peptide sequencing. The elution fractions containing the histidine-rich glycoprotein were run on SDS-polyacrylamide gel. The gel was stained with coomassie blue staining solution, and destained with standard destaining solution as described in chapter 3.3.5. Peptide sequencing and protein identification was performed at University of Victoria-Genome BC Proteomics Centre using in-gel digestion followed by high-performance liquid chromatography system coupled with tandem mass spectrometer (LC-MS/MS).

4.4 Results

4.4.1 Optimization of hsTf purification by IMAC

IMAC with Fe^{3+}

Prior to purification of Tf from complex mixtures, commercial hsTf was used to determine the optimum conditions for Fe^{3+}-affinity chromatography. Among several pH points tested, pH 5.8 was found to be optimal for hsTf-binding. Above pH 5.8, hsTf chelated Fe^{3+} from beads, and below pH 5.8 it did not bind to the beads (data not shown). SDS-PAGE analysis (figure 4.3) indicates hsTf-binding to the Fe^{3+}-charged NTA-agarose beads efficiently as very little hsTf was observed in the flow through (lane 1). Washing with binding buffer removed all of the unbound hsTf from the beads, but no hsTf was detected in the

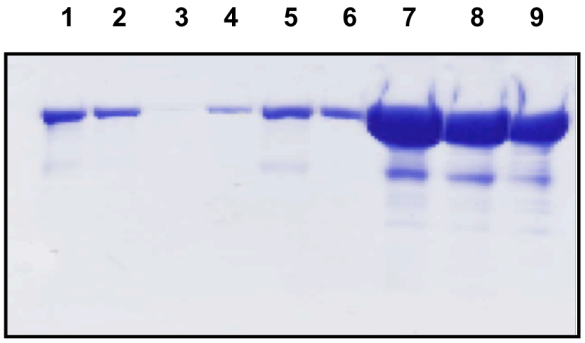

Figure 4-3 SDS-PAGE analysis of fractions from 10 mg of commercial hsTf purification by Fe^{3+}-affinity chromatography. Lane (1) is flow-through, (2-3) wash with binding buffer (BB), (4) 5 mM imidazole in BB, (5) 10 mM imidazole in BB, (6) 15 mM imidazole in BB, (7-8) elution with 0.05 M EDTA in BB, (9) supernatant from the beads incubated overnight in 0.05 mM EDTA in BB.

second wash with binding buffer (lanes 2-3). 5, 10, and 15 mM imidazole was included in the wash buffer to test the stability of hsTf-immobilized Fe^{3+} interaction. Imidazole competes with the imidazole side-chain of histidine residues in the protein that might coordinate to the metal ion immobilized by the chelator on the matrix and causes the release of the protein from the beads. For this reason, inclusion of low concentrations of imidazole in the wash buffer was necessary to evaluate if hsTf remains bound to Fe^{3+} immobilized on the matrix, during elimination of nonspecifically bound background proteins. 5 mM imidazole had little effect on the dissociation of Tf from the beads. 10 mM imidazole removed more Tf than 15 mM imidazole indicating that only a small amount of Tf was coordinated to immobilized Fe^{3+} with histidine residues. Attempts to elute Tf with a low pH buffer (pH 4.5) failed even in the presence of 5 mM EDTA. This was surprising because hsTf should release iron below pH 4.8 under normal

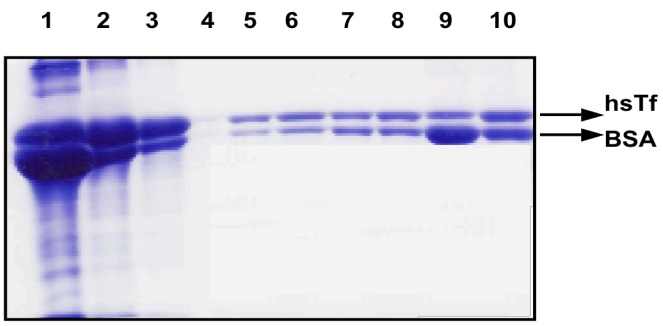

Figure 4-4 SDS-PAGE analysis of fractions from 1:1 mixture of commercial hsTf (10 mg) :and BSA (10 mg) purification by Fe^{3+}-affinity chromatography. Lane (1) is flow-through, (2-3) wash with binding buffer (BB), (4) 500 mM acetate buffer pH 4.5, (5) 5 mM imidazole in BB, (6) 10 mM imidazole in BB, (7) 15 mM imidazole in BB, (8) 20 mM imidazole in BB, (9-10) elution with 0.05 M EDTA in BB.

conditions. Elution of hsTf was only possible binding buffer containing 50 mM EDTA (figure 4.3, lanes 7-9). This experiment proved that IMAC with Fe^{3+} can be used for purification of hsTf. In addition, stability of the hsTf-Fe^{3+} interaction against imidazole renders this method potentially efficient for purification of hsTf from complex mixtures facilitating elimination of background proteins that may attach to Fe^{3+} with their imidazole side-chains.

In order to test the efficacy of immobilized Fe^{3+}-affinity chromatography for purification of hsTf from complex mixtures, a 1:1 mixture of hsTf (10 mg) and bovine serum albumin (BSA, 10 mg) was used. Figure 4.4 shows that Tf and BSA have similar affinities for the Fe^{3+}-NTA-agarose beads. A considerable amount of Tf and BSA was detected both in the flow-through and the fractions obtained from washing with binding buffer, indicating that the protein binding capacity of 0.75 mL Fe^{3+}-NTA-agarose media is less than 20 mg. A wash step

with 500 mM acetate buffer, pH 4.5, was included in hopes of removing BSA from the beads without affecting Tf. Although serum albumin is known to bind iron weakly and nonspecifically, it was not possible to eliminate BSA with either acetate buffer at pH 4.5 or imidazole-containing binding buffer. Lanes 9 and 10 (figure 4.4) demonstrate that a significant amount of BSA is bound to Fe^{3+} on the beads along with hsTf even after elution with 50 mM EDTA in binding buffer.

IMAC with Cu^{2+}

IMAC with Cu^{2+} was tested for possible separation of albumin from Tf based on the differential affinities of these proteins for Cu^{2+} ion.[75, 167] Unlike Fe^{3+}-affinity chromatography, loading the protein mixture at pH 7.4 did not cause any metal leaching from the chelator on the matrix. No protein bands were detected in either the flow through or the fraction from washing with 1 mM imidazole (figure 4.5). In order to determine the critical imidazole concentration to separate albumin from hsTf, a small imidazole gradient was used in the wash steps (1-20 mM imidazole). 2 mM imidazole started removing albumin (lane 3) while leaving hsTf unaffected up to 4 mM imidazole (lane 5), at which point most of the BSA was already removed. However, albumin and hsTf removal from the beads overlapped during the wash with 4-6 mM imidazole (lanes 5-7). In hopes of increasing the yield of pure hsTf by removing more BSA before hsTf is affected, beads loaded with sample were washed four times with 4 mM imidazole (Figure 4.6, lanes 2-5) followed by four times with 5 mM imidazole (lanes 6-9) and four times with 15 mM imidazole. Unfortunately, washing with a larger volume of 4 mM imidazole did not improve the yield of pure Tf.

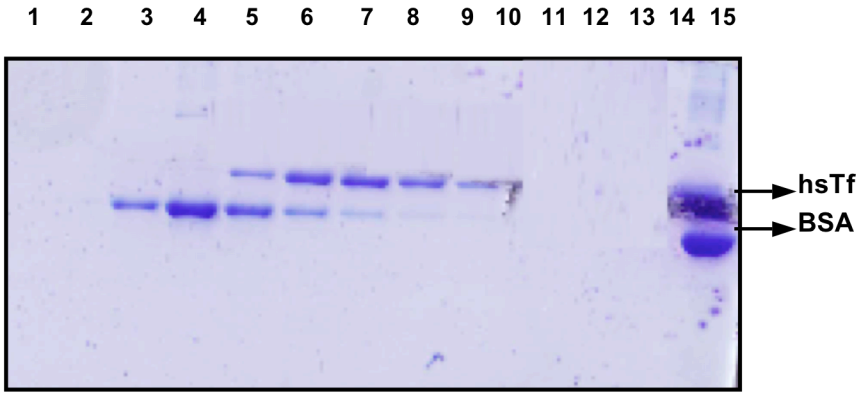

Figure 4-5 SDS-PAGE analysis of fractions from 1:1 mixture of commercial hsTf (10 mg) and BSA (10 mg) purification by Cu^{2+}-affinity chromatography. Lane (1) is flow-through, (2) wash with 1 mM imidazole in BB, (3) 2 mM imidazole in BB, (4) 3 mM imidazole in BB, (5) 4 mM imidazole in BB, (6) 5 mM imidazole in BB, (7) 6 mM imidazole in BB, (8) 7 mM imidazole in BB, (9) 8 mM imidazole in BB, (10) 9 mM imidazole in BB, (11) 10 mM imidazole in BB, (12) 12 mM imidazole in BB, (13) 15 mM imidazole in BB, (14) 20 mM imidazole in BB), (15) control, Tf/BSA mixture.

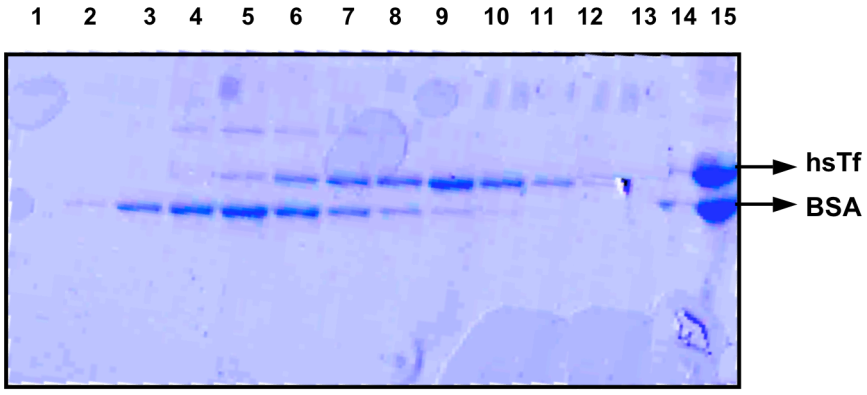

Figure 4-6 SDS-PAGE analysis of fractions from 1:1 mixture of commercial hsTf (10 mg) and BSA (10 mg) purification by Cu^{2+}-affinity chromatography. Lane (1) is flow-through, (2-5) wash with 4 mM imidazole in BB, (5-9) 5 mM imidazole in BB, (10-13) 15 mM imidazole in BB, (14) 50 mM EDTA in BB, (15) Control, Tf/BSA mixture.

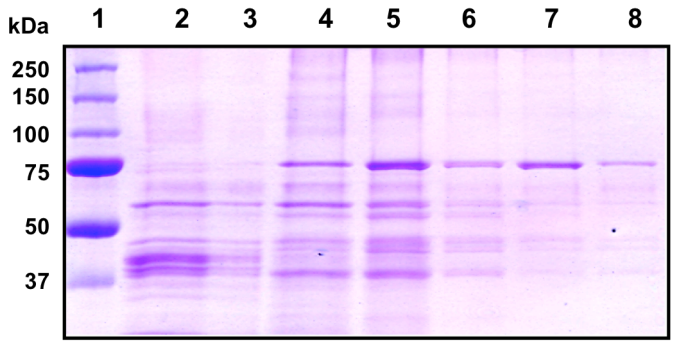

Figure 4-7 SDS-PAGE analysis of fractions from purification of recombinant hsTf (expressed in *P. pastoris*) by Cu^{2+}-affinity chromatography. Lane (1) is the molecular weight marker, (2) is the flow-through, (3) is the wash with BB, (4) is the wash with 40 mM imidazole in BB, (5) is the wash with 60 mM imidazole in BB, (6) is the wash with 100 mM imidazole in BB, (7) is the wash with 300 mM imidazole, (8) is the 50 mM EDTA in BB (after 1 hour incubation at 4 °C).

4.4.2 Application of IMAC with Fe^{3+} and Cu^{2+} to purification of full-length recombinant Tf produced in *P. pastoris*

IMAC with Fe^{3+}

Purification of recombinant hsTf was attempted using Fe^{3+}-charged agarose beads. However, the beads turned into black as soon as the sample in binding buffer was added. This suggests that a component (or components) of the protein expression medium (BMMY) interacts with Fe^{3+} on the beads to produce insoluble iron species, and NTA coupled to the beads is not a sufficiently strong chelator to prevent this event. This observation is consistent with the results given in chapter 3. SDS-PAGE analysis did not reveal any proteins in the fractions (data not shown) identifying this method impractical for purification of recombinant hsTf from the BMMY medium.

IMAC with Cu^{2+}

Since the Fe^{3+}-affinity chromatography purification failed, Cu^{2+}-affinity chromatography was tested for purification of recombinant hsTf from the expression medium. The colour of the beads changed only slightly to the colour of the media (yellow-brown) upon mixing the sample with the beads. Figure 4.7 displays the SDS-PAGE analysis of the fractions from the purification. As seen on lanes 2 and 3, no recombinant hsTf was found in the flow-through and the wash fraction with binding buffer, indicating that almost all of the protein is efficiently bound to the Cu^{2+}-charged beads. Lanes 4 and 5 show that wash steps with 40 mM imidazole in binding buffer started removing the recombinant hsTf (corresponding to the band at 75 kDa). Washing the beads with 100 mM and 300 mM imidazole in binding buffer removed most of the recombinant protein from the beads (lanes 6 and 7). Elution with 50 mM EDTA in binding buffer did not improve the yield (lane 8) suggesting that the recombinant hsTf can be eluted if a higher volume of 300 mM imidazole in binding buffer is used in the wash step without the need of EDTA.

4.4.3 Application of IMAC to purification of Tf from rabbit serum

IMAC with Fe^{3+}

IMAC with Fe^{3+} was also tested for its ability to purify Tf from serum. Although human serum was intended to be used initially, the experiments were limited to rabbit serum (rs) due to biosafety concerns. Since rsTf is similar to hsTf functionally and structurally,[168-171] it constitutes a model for hsTf for application of IMAC to purify Tf from serum. Figure 4.8 illustrates similar results

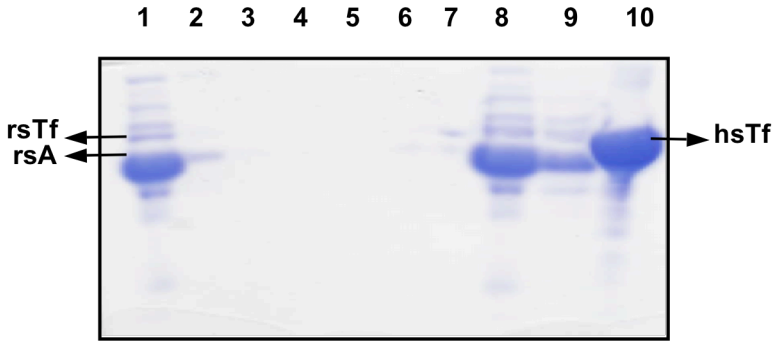

Figure 4-8 SDS-PAGE analysis of fractions from rabbit serum fractionation by Fe^{3+}-affinity chromatography. Lane (1) control (rabbit serum), (2) flow through, (3-4) wash with binding buffer (BB), (5) 10 mM imidazole in BB, (6) 15 mM imidazole in BB, (7) 20 mM imidazole in BB, (8-9) elution with 0.05 M EDTA in BB, (10) control (hsTf).

as obtained from Tf/BSA mixture purification. At pH 5.8 Tf and albumin appear to have similar affinities for immobilized Fe^{3+} and neither of them can be eluted with imidazole (lanes 4-7) suggesting that both proteins coordinate to immobilized Fe^{3+} with residues other than (or in addition to) histidine residues. Application of 50 mM EDTA eluted both proteins, as well as other serum proteins (lanes 8-9). These results suggest that IMAC with Fe^{3+} does not fractionate serum proteins efficiently.

IMAC with Cu^{2+}

Partial separation of BSA from hsTf by IMAC with Cu^{2+} suggested that this method could be optimized to purify Tf from serum. An imidazole gradient was used to determine if it is feasible to separate rsAlbumin from rsTf. Since albumin-binding to immobilized Cu^{2+} appeared to be weaker than Tf-binding, 1 mM imidazole was included in the binding buffer to reduce the amount of Cu^{2+}-bound

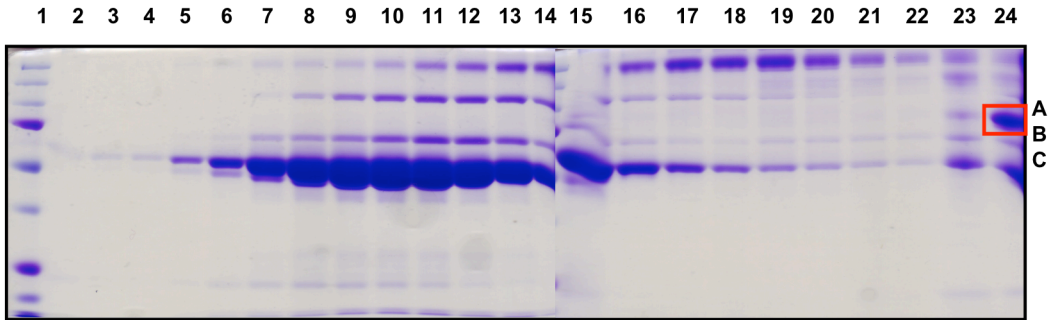

Figure 4-9 SDS-PAGE analysis of fractions from rabbit serum fractionation by Cu^{2+}-affinity chromatography at pH 7.4. Lane (1) protein molecular weight marker (2) flow through, (3-4) wash with binding buffer (BB), (5-6) 2 mM imidazole (7-8) 3 mM imidazole (9-10) 3.5 mM imidazole (11-12) 4 mM imidazole (13-14) 5 mM imidazole (15-16) 6 mM imidazole (17-18) 10 mM imidazole (19-20) 15 mM imidazole (21-22) 20 mM imidazole (23-24) elution with 0.05 M EDTA in BB. "A" is the histidine-rich glycoprotein, "B" is rsTf, and "C" is rsAlbumin.

albumin. As shown in figure 4.9, it was not possible to remove albumin even though it was released from the beads earlier than rsTf. The failure of the imidazole gradient to separate rsAlbumin from rsTf might be because of the much higher concentration of albumin in serum compared to that of Tf. For this reason, another experiment was devised to eliminate the protein with the low concentration (Tf) earlier than the one with much higher concentration (albumin). In order to disrupt the binding of rsTf and collect it in flow-through without affecting albumin-binding, the purification procedure was carried out at pH 5.8 since hsTf has been shown to release Cu^{2+} from its metal-binding sites below pH 6.0.[65, 172, 173] Figure 4.10 suggests that at pH 5.8, rsTf can still bind to the immobilized Cu^{2+} with a similar affinity as of albumin, and almost all serum proteins are eluted with binding buffer containing 20 mM imidazole at pH 5.8

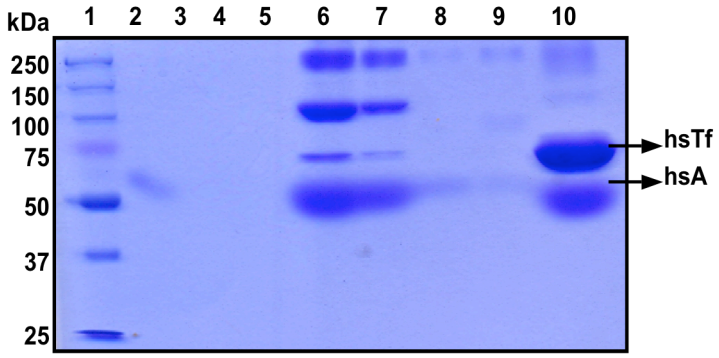

Figure 4-10 SDS-PAGE analysis of fractions from rabbit serum fractionation by Cu^{2+}-affinity chromatography at pH 5.8. Lane (1) protein marker (2-3) flow through, (4-5) wash with binding buffer (BB), (6-7) 20 mM imidazole in BB, (8-9) elution with 50 mM EDTA in BB, (10) control, hsTf/hsAlbum mixture.

without the need of EDTA. Binding of rsTf to immobilized Cu^{2+} at pH 5.8 can be attributed to non-specific binding with exposed imidazole groups on the surface of the protein to Cu^{2+} below pH 6.0.[172] As a result, purification at pH 5.8 did not separate rsTf from other rabbit serum proteins.

A rabbit serum protein, histidine-rich glycoprotein with approximately 95 kDa molecular weight was obtained in the elution fraction with 50 mM EDTA at pH 7.4 (figure 4.9, lane 24, marked as “A”). The identity of this protein was confirmed by LC/MS/MS protein sequencing analysis. To further investigate the efficiency of the Cu^{2+}-affinity chromatography to purify this protein, rabbit serum was applied to a Cu^{2+}-charged IDA-sepharose column. 5 mM imidazole was included in the binding buffer to prevent the binding of other serum proteins. Despite its very high concentration in serum, albumin was almost completely eliminated from the column with increasing concentrations of imidazole (figure

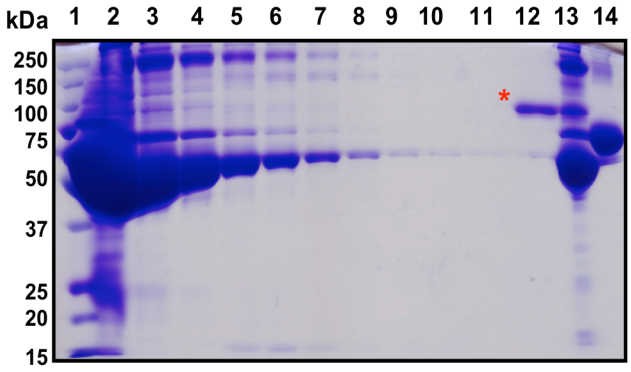

Figure 4-11 SDS-PAGE analysis of fractions from rabbit serum fractionation by Cu^{2+}-charged IDA-sepharose column at pH 7.4. Lane (1) protein marker (2) flow through, (3-4) wash with binding buffer (BB), (5-6) wash with 40 mM imidazole in BB, (7-8) wash with 60 mM imidazole, (9-10) wash with 100 mM imidazole, (11-12) elution with 50 mM EDTA in BB, (13) control, rabbit serum, (14) control, hsTf. * A serum protein, histidine-rich glycoprotein was obtained with very high purity in the second elution fraction (lane 12).

4.11, lanes 2-10), and the histidine rich glycoprotein was eluted with 50 mM EDTA almost as a single protein. To the best of our knowledge, this study has been the first to show that histidine-rich glycoprotein can be purified in one simple step from rabbit serum with > 95% purity using IMAC with Cu^{2+} at pH 7.4. Details of the studies on histidine rich glycoprotein are beyond the purpose of this thesis project and hence, will not be discussed here any further.

4.5 Discussion

Previous studies employed 6xHis-tag – Ni^{2+} - affinity chromatography[120] and anion-exchange chromatography[119] to purify the full-length recombinant hsTf expressed in mammalian cells. However, use of the 6xHis-tag on the recombinant hsTf is impractical for our studies because of the possibility of the

interference with Ru(III)-complex-binding experiments. Besides, purification by anion-exchange chromatography did not yield high-levels of pure recombinant hsTf expressed in *P. pastoris* (see chapter 3.4.3). Therefore development of an alternative method that is simple and cost-effective was necessary to eliminate the problems encountered with the common simple purification methods. Initially, it was hypothesized that IMAC with Fe^{3+} may be used efficiently to purify any member of the Tf family proteins, which function to bind Fe^{3+} specifically in their easily accessible iron-binding sites. Purification of recombinant hsTf from the expression medium (BMMY) using IMAC with Fe^{3+} was unsuccessful due to the formation of insoluble iron species in the presence of BMMY expression media. Thus, IMAC with another metal ion, Cu^{2+}, was employed to purification of recombinant hsTf. hsTf binds Cu^{2+} much more weakly than Fe^{3+} in its binding sites[65, 172-177] allowing the use of a neutral pH in the purification procedure unlike the low pH (5.8) of Fe^{3+}-affinity chromatography. In this study, it was shown that IMAC with Cu^{2+} can be used to purify the recombinant hsTf produced in *P. pastoris* from the expression media without the problems seen in the IMAC with Fe^{3+} purification. Although the yield of the pure recombinant hsTf obtained from IMAC with Cu^{2+} purification is similar to that of anion-exchange chromatography, this method eliminated the difficulties in the clarification of the viscous sample prior to loading onto the column. Since hsTf can also bind Cu^{2+} nonspecifically with its surface exposed His residues,[172, 176, 178] the interaction between the hsTf and the Cu^{2+} ions on the chelating chromatography media cannot be considered solely as a specific interaction. Therefore, IMAC with Cu^{2+} will also be useful in

the purification of the binding-site mutants of hsTf. In order to increase the yield of the pure protein, a two-step purification may be used. In the first step the recombinant hsTf may be isolated by IMAC media charged with Cu^{2+}, and following that, the fractions containing the impurities may be polished using anion-exchange chromatography.

The possible application of IMAC to purify Tf from serum was also evaluated using rabbit serum as a model. Although rsTf was shown to bind efficiently to the IMAC media charged with Fe^{3+} or Cu^{2+} (as demonstrated for commercial hsTf), it was not possible to completely remove the serum albumin in the wash steps and hence, the rsTf was eluted from the chromatography media along with albumin. Isolation of the serum proteins, including serum transferrin, has been reported to be a difficult process, which requires coupling of several sequential purification techniques.[156, 179-186] The results shown here are in agreement with the previous studies on the difficulty of one-step separation of Tf from other serum proteins, especially from albumin. Therefore it was concluded that although one-step purification of Tf from *P. pastoris* expression media is effective, isolation from serum using this process is not possible.

CHAPTER 5: CONCLUSION AND FUTURE DIRECTIONS

The aim of this thesis was to characterize the interactions of the three anti-cancer Ru(III)-complexes, KP1019, KP418, and NAMI-A with serum proteins, hsTf and hsA, as well as of the species they form in serum in order to better understand their anti-cancer activities. The research was divided into two main areas. The first aspect is covered in the chapter 2, which was the charecterization of the Ru(III)-complexes with respect to their interactions with serum proteins, and the species they form in serum. The second aspect was to develop a procedure for expression of full-length recombinant hsTf in *P. pastoris* for production of its site-directed mutants, as well as a protocol for easy purification of the recombinant protein from *P. pastoris* expression medium; are described in chapter 3 and 4 respectively.

The +3-oxidation state of the ruthenium-centre in NAMI-A was found to be highly unstable in buffer (pH 7.4) and the presence of hsTf did not prevent Ru(III)/Ru(II) reduction. KP1019 and KP418 were both stable in the +3-oxidation state in buffer as well as in solution with hsTf and in hsA. The EPR data suggested that KP1019 and KP418 bind to hsTf at a single site via ligand-exchange, whereas they bind to hsA at more than one site. Binding via hydrophobic interactions was also observed for hsA.

EPR studies of KP1019 and KP418 in serum showed that Ru(III)/Ru(II) reduction is not significant in serum at 37 °C over a period of 24 hours,

supporting the findings of other groups.[22, 33] The speciation of KP1019 in serum was determined to occur in three steps. In the first step the complex binds to a serum protein(s) as soon as it is introduced into serum through hydrophobic interactions. Since the same feature was observed when the complex was incubated in hsA, it was suggested that hsA is the most likely serum protein responsible for this hydrophobic interaction. In the following steps, binding to serum protein(s) via ligand exchange occurs. The speciation of KP418 in serum was found to be different from that of KP1019. The initial binding of KP418 to serum protein(s) through hydrophobic interactions was less significant. Instead, an almost complete ligand exchange took place as soon as the complex was mixed with serum, and the same structure persisted over 24 hours. Consistent with literture reports,[27] KP1019-binding to hsTf was (pH 7.4, 37 °C) faster than that of KP418, as demonstrated by UV-visible studies. It was proposed that the differences in the speciation of KP1019 and KP418 in serum, and faster binding of KP1019 to hsTf might partially account for their different anti-cancer activities.

The weak EPR signal obtained from KP1019 bound to the iron-binding site of the His249Ala mutant of the N-terminal half molecule of hsTf (N/hsTf) constituted evidence for the involvement of His249 residue in KP1019-binding. KP1019 binding to the His249Ala mutant of N/hsTf and to the diferric-hsTf was found to be intact, strongly indicating an interaction outside the iron-binding sites. However, the ruthenium centre of KP1019 was no longer in the +3-oxidation state when bound to hsTf outside the iron-binding sites. It was concluded that KP1019 is in the Ru(III)-state when it is bound to hsTf at the iron-binding site,

whereas binding outside the iron-binding site results in the reduction to Ru(II).

The recombinant full-length hsTf was expressed in *P. pastoris* successfully. However, high-level expression in this system for use in EPR studies was not feasible. The recombinant hsTf was easily isolated from the *P. pastoris* expression medium by a protocol developed using immobilized metal ion affinity chromatography charged with Cu^{2+}.

Future studies on the binding ability of KP1019 to diferric-hsTf, in which the histidyl imidazole groups outside the iron-binding sites are chemically modified, could address the importance of these residues in KP1019-binding. Parallel experiments with KP418 may identify differences between these two structurally similar anti-cancer agents.

The stability of the Ru(III)-oxidation state of KP1019 and KP418 in serum over 24 hours, as demonstrated in this study, is significant with respect to the "activation by reduction theory": that Ru(III) / Ru(II) reduction does not take place outside tumors. Keeping in mind that the tumor tissue is hypoxic, EPR studies of the complexes under hypoxic conditions should be included in future studies, which would provide strong evidence for the oxidation state of the ruthenium centre in the complexes in tumors.

Aquation of the metal-based complexes is an important factor in their anti-cancer activities. Future studies could also investigate whether aquation of KP1019 and KP418 takes place when they are bound to the serum proteins. Such studies could employ electron nuclear double resonance (ENDOR) spectroscopy, which has the ability to detect water coordination to the Ru(III)-

centre. This knowledge will contribute to the findings of the EPR and UV-visible spectroscopy studies presented here by clarifying the structure of KP1019 and KP418 species bound to the serum proteins.

Taken together, this thesis established the instability of the anti-metastatic agent NAMI-A in the Ru(III)-state even in the presence of hsTf, which distinguishes it from the anti-cancer agents KP1019 and KP418. Moreover, it was demonstrated that the differences in the speciation of KP1019 and KP418 in serum, as well as in the nature of their interactions with hsTf, might be responsible for their disparate anti-cancer activities. EPR analysis of KP1019-binding to His249Ala mutant of hsTf and to diferric-hsTf revealed a Ru(III)-state-stabilizing role of the iron-binding site of hsTf in KP1019 binding.

APPENDICES

Appendix A: DNA sequencing results

pPICZα-A/Tf-Kex2

CTCGAG : *Xho I* site

ATG……GCT : Codons encoding the hsTf native signal sequence

GAGAAAAGAGAG : Codons for Kex2 cleavage site

GTCCCT…… : Codons encoding the mature hsTf

TGGACTTTTTAACGACACTTGAGAAGACAAAAAACAACTAATTATTCGAAACGATGAGA
TTTCCTTCAATTTTTACTGCTGTTTTATTCGCAGCATCCTCCGCATTAGCTGCTCCAGT
CAACACTACAACAGAAGATGAAACGGCACAAATTCCGGCTGAAGCTGTCATCGGTTACT
CAGATTTAGAAGGGGATTTCGATGTTGCTGTTTTGCCATTTTCCAACAGCACAAATAAC
GGGTTATTGTTTATAAATACTACTATTGCCAGCATTGCTGCTAAAGAAGAAGGGGTATC
T**CTCGAG****ATGAGGCTCGCCGTGGGAGCCCTGCTGGTCTGCGCCGTCCTGGGGCTGTGTC**
TGGCTGAGAAAAGAGAG**GTCCCTGATAAAACTGTGAGATGGTGTGC**AGTGTCGGAGCAT
GAGGCCACTAAGTGCCAGAGTTTCCGCGACCATATGAAAAGCGTCATTCCATCCGATGG
TCCCAGTGTTGCTTGTGTGAAGAAAGCCTCCTACCTTGATTGCATCAGGGCCATTGCGG
CAAACGAAGCGGATGCTGTGACACTGGATGCAGGTTTGGTGTATGATGCTTACCTGGCT
CCCAATAACCTGAAGCCTGTGGTGGCAGAGTTCTATGGGTCAAAAGAGGATCCACAGAC
TTTCTATTATGCTGTTGCTGTGGTGAAGAAGGATAGTGGCTTCCAGATGAACCAGCTTC
GAGGCAAGAAGTCCTGCCACACGGGTCTAGGCAGGTCCGCTGGGTGGAACATCCCCATA
GGCTTACTTTACTGTGACTTACCTGAGCCACGTAAACCTCTTGAGAAAGCAGTGGCCAA
TTTCTTCTCGGGCAGCTGTGCCCCTTGTGCGGATGGGACGGACTTCCCCCAGCTGTGTC
AACTGTGTCCAGGGTGTGGCTGCTCCACCCTTACCAATACTTCGGCTACTCGGGAGCCT
TCAAGTGTCTGAAGGATGGTGCTGGGGATGTGGCCTTTGTCAAGCACTCGACTATATTT
GAGAACTTGCCAAACAAGGCTGACAGGGACCAGTATGAGCTGCTTTGCCTGGACAACAC
CCGGAAGCCGGTAGATGAATACAAGGACT

pPICZα-A/TfNS-Kex2

TATCT : Vector sequence

CTCGAG : *Xho I* site

GAGAAAAGAGAG : Codons for Kex2 cleavage site

GTCCCT…… : Codons encoding the mature hsTf

NNNNNNNNANTTTTACGACACTTGAGAAGANCAAAAAACAACTAATTATTCGAAACGAT
GAGATTTCCTTCAATTTTTACTGCTGTTTTATTCGCAGCATCCTCCGCATTAGCTGCTC
CAGTCAACACTACAACAGAAGATGAAACGGCACAAATTCCGGCTGAAGCTGTCATCGGT
TACTCAGATTTAGAAGGGGATTTCGATGTTGCTGTTTTGCCATTTTCCAACAGCACAAA
TAACGGGTTATTGTTTATAAATACTACTATTGCCAGCATTGCTGCTAAAGAAGAAGGGG
TATCTCTCGAGAAAAGAGAGGTCCCTGATAAAACTGTGAGATGGTGTGCAGTGTCGGAG
CATGAGGCCACTAAGTGCCAGAGTTTCCGCGACCATATGAAAAGCGTCATTCCATCCGA
TGGTCCCAGTGTTGCTTGTGTGAAGAAAGCCTCCTACCTTGATTGCATCAGGGCCATTG
CGGCAAACGAAGCGGATGCTGTGACACTGGATGCAGGTTTGGTGTATGATGCTTACCTG
GCTCCCAATAACCTGAAGCCTGTGGTGGCAGAGTTCTATGGGTCAAAAGAGGATCCACA
GACTTTCTATTATGCTGTTGCTGTGGTGAAGAAGGATAGTGGCTTCCAGATGAACCAGC
TTCGAGGCAAGAAGTCCTGCCACACGGGTCTAGGCAGGTCCGCTGGGTGGAACATCCCC
ATAGGCTTACTTTACTGTGACTTACCTGAGCCACGTAAACCTCTTGAGAAAGCAGTGGC
CAATTTCTTCTCGGGCAGCTGTGCCCCTTGTGCGGATGGGACGGACTTCCCCCAGCTGT
GTCAACTGTGTCCAGGGTGTGGCTGCTCCACCCTTAACCAATACTTCGGCTACTCGGGA
GCCTTCAAGTGTCTGAAGGATGGTGCTGGGGATGTGGCCTTTGTCAAGCACTCGACTAT
ATTTGAGAACTTGGCAAACAAGGCTGACAGGGACCAGTATGAGCTGCTTTGCCTGGNNA
CACCCGGAAGCCGGTANATGANACAGGACTGCCACTTGGCCCAGGTCCCTTCTCATACC
GTCGTGGCCCGAAGTATGGGCGGCAAGGAGGACTN

pPICZα-A/NGTf

*TFN611D-R and **TFN413D-R primer sites are given in bold, mutagenic codons are highlighted.

ATGATGATGATGATGATG : Hexa-His tag

TCTAGA : Xba I site

GC : Extra base pairs to enable in frame cloning with hexa-His tag

AGGTCTACGG…… : Codons encoding the C-terminal of hsTf (no stop codon)

GTTTTAATCTAGCAGACCGGTCTTCTCGTAAGTGCCCAACTTGAACTGAGGAACAGTCA
TGTCTAAGGCTACAAACTCAATGATGATGATGATGATGGTCGACGGCGCTATTCAGATC
CTCTTCTGAGATGAGTTTTTGTTCTAGAGCAGGTCTACGGAAAGTGCAGGCTTCCAGGA
GTGATGAGGTGGAGCATTTTCTCAGGTTACCAACAGCCTTGACATATTCTTCTCCTAAG
TATTTTTCATATGTGTTTCTGTCATGAAGTTTGGCCAAACATACTGTGTCATCTCTGAA
CAGAAGGTCCTTGGTTTCCGACCGGAACAAACAAAAGTTGCC*CGAGCAGTCAGTTACGT
CGCTTCCAAATAGGTGCTGCTGTTGACGTAATATCTTGTGGACGCAAGCTTCCTTGTGT
GGCGGAGCGACCCCAACGAGAGTCTCACTTCTGCTTCTGTGCTCTGACGAATACTGCTC
CATACGTTTACTGACATCATACTCGAATGATTTTTCCTAACCCCTACCATTCGATATTC
TTACACCTGGGATATAGGCTGATTCCGACCAAGCTCGGAGGAGACAGAACTGGAGTGAC
ACAAAAGATCCTATTCTCTTCACGTTACAACTCCTGAAAGCTCCTGTGTGAACCCTGCA
TCTCTCATGTGAAGTGGGGTTCACAGAGGTTTAGGCCTGAGCCCATACACAGCTTACAG
AGACTGGAGTCTTTCTTAGACCCAGGGGCACAACCTTCACTGAAAAATTCATCAAATCT
GCAGTGGTTGATCTTATTGTAGAGCAGGCCCATGGGGATGTTCCAGCCAGCGGTTCTGC
CAACTGCCGTATGGCAGGACTTCTTGCCTTTCAGATTGTCCCAGGTGAGGTCAGAAGCT
GATTTCTTCACCACTGCTACAGCAAAATACCCTGTCTCTGGTGTATCCT**CACAATTAT
CGCTCTTATCTAGTTTTCTGCCAAGACAGGCACCAAACCCACCTTGCCCGCTATGTAGA
CAAACCCTTCATCCAAGCTCATGGCATCAGCTTCTCCATACATGATCTTGGCGATGCAG
TCTTCGGGGTCTCTGCTGATACACACT

pPICZα-A/NGTf-Kex2

CTCGAG : *Xho I* site

ATG.....GCT : Codons encoding the hsTf native signal sequence

GAGAAAAGAGAG : Codons for Kex2 cleavage site

GTCCCT..... : Codons encoding the mature hsTf

(Mutated glycosylation sites are not given)

TGAACTTTTTACGACAACTTGAGAAGACAAAAAACAACTAATTATTCGAAACGATGAGA
TTTCCTTCAATTTTTACTGCTGTTTTATTCGCAGCATCCTCCGCATTAGCTGCTCCAGT
CAACACTACAACAGAAGATGAAACGGCACAAATTCCGGCTGAAGCTGTCATCGGTTACT
CAGATTTAGAAGGGGATTTCGATGTTGCTGTTTTGCCATTTTCCAACAGCACAAATAAC
GGGTTATTGTTTATAAATACTACTATTGCCAGCATTGCTGCTAAAGAAGAAGGGGTATC
TCTCGAGATGAGGCTCGCCGTGGGAGCCCTGCTGGTCTGCGCCGTCCTGGGGCTGTGTC
TGGCTGAGAAAAGAGAGGTCCCTGATAAAACTGTGAGATGGTGTGCAGTGTCGGAGCAT
GAGGCCACTAAGTGCCAGAGTTTCCGCGACCATATGAAAAGCGTCATTCCATCCGATGG
TCCCAGTGTTGCTTGTGTGAAGAAAGCCTCCTACCTTGATTGCATCAGGGCCATTGCGG
CAAACGAAGCGGATGCTGTGACACTGGATGCAGGTTTGGTGTATGATGCTTACCTGGCT
CCCAATAACCTGAAGCCTGTGGTGGCAGAGTTCTATGGGTCAAAAGAGGATCCACAGAC
TTTCTATTATGCTGTTGCTGTGGTGAAGAAGGATAGTGGCTTCCAGATGAACCAGCTTC

GAGGCAAGAAGTCCTGCCACACGGGTCTAGGCAGGTCCGCTGGGTGGAACATCCCCATA
GGCTTACTTTACTGTGACTTACCTGAGCCACGTAAACCTCTTGAGAAAGCAGTGGCCAA
TTTCTTCTCGGGCAGCTGTGCCCCTTGTGCGGATGGGACGGACTTCCCCCAGCTGTGTC
AACTGTGTCCAGGGTGTGGCTGCTCCACCCTTAACCAATACTTCGGCTACTCGGGAGCC
TTNCAGTGTCTGAAGGATGGTGCTGGGGATGTGGCCTTTGTCAAGCACTCGACTATATT
TGAGAACTTGGCAAACAAGGCTGACAGGGACCAGTATGAGCTGCTTTTGCTGGACAACA
CCCGGAAGCGGGTAAATGAATACAAGGACTGCCCCTGGGC

pPICZα-A/H249A-N-Lobe/Tf-Kex2

TCTAGA : *Xba I* site

TTA : Stop codon

TAC : Codon encoding the 318th residue of mature hsTf

GCCACGACGGTAGCAGAAGGGACCTGG : H249A primer site (mutagenic codon is highlighted)

NNNNNNNNNNNNNAGANCGGTCTTCTCGTAAGTGCCCAACTTGAACTGAGGAACAGTCA
TGTCTAAGGCTACAAACTCAATGATGATGATGATGATGGTCGACGGCGCTATTCAGATC
CTCTTCTGAGATGAGTTTTTGT**TCTAGA**TTATACTCATAGCCCAGGTACATCTTGGCAT
CCATCCTGGGGGGGACTTTTAAAAACCCGTGGGCAGAGTCCTTAAACAGCAGGTCCTTC
CCATGAGGAGAGCTGAATAGTTGGAATTCTTTTGATTTGTCTTTGCCAAAATGTTCCTG
GGCCTGGTTGAGAAGCTCCCAGATCAAGTCCTCCTTGCCGCCCATACTTCGG**GCCACGA**
CGGTAGCAGAAGGGACCTGGGCCAAGTGGCAGTCCTTGTATTCATCTACCGGCTTCCGG
GTGTTGTCCAGGCAAAGCAGCTCATACTGGTCCCTGTCAGCCTTGTTTGCCAAGTTCTC
AAATATAGTCGAGTGCTTGACAAAGGCCACATCCCCAGCACCATCCTTCAGACACTTGA
AGGCTCCCGAGTAGCCGAAGTATTGGTTAAGGGTGGAGCAGCCACACCCTGGACACAGT
TGACACAGCTGGGGGAAGTCCGTCCCATCCGCACAAGGGGCACAGCTGCCCGAGAAGAA
ATTGGCCACTGCTTTCTCAAGAGGTTTACGTGGCTCAGGTAAGTCACAGTAAAGTAAGC
CTATGGGGATGTTCCACCCAGCGGACCTGCCTAGACCCGTGTGGCAGGACTTCTTGCCT
CGAAGCTGGTTCATCTGGAAGCCACTATCCTTCTTCACCACAGCAACAGCATAATAGAA
AGTCTGTGGATCCTCTTTTGACCCATAGAACTCTGCCACCACAGGCTTCAGGTTATTGG
GAGCCAGGTAAGCATCATACACCAAACCTGCATCCAGTGTCACAGCATCCGCTTCGTTT
GCCGCAATGGCCCTGATGCAATCAAGGTAGGAGGCTTTCTTCACACAAGCAACACTGGG
ACCATCGGATGGAATGACGCTTTTCATATGGTCGCGGAAACTCTGGCACTTAGTN

REFERENCE LIST

(1) Galanski, M.; Arion, V. B.; Jakupec, M. A.; Keppler, B. K. Curr. Pharm. Des. 2003, 9, 2078-2089.

(2) Hartinger, C. G.; Zorbas-Seifried, S.; Jakupec, M. A.; Kynast, B.; Zorbas, H.; Keppler, B. K. J. Inorg. Biochem. 2006, 100, 891-904.

(3) Zhang, C. X.; Lippard, S. J. *Curr. Opin. Chem. Biol.* **2003**, *7*, 481-489.

(4) Barnes, K. R.; Lippard, S. J. *Met. Ions Biol. Syst.* **2004**, *42*, 143-177.

(5) Jakupec, M. A.; Galanski, M.; Arion, V. B.; Hartinger, C. G.; Keppler, B. K. *Dalton Trans.* **2008**, *(2)*, 183-194.

(6) Clarke, M. J.; Zhu, F.; Frasca, D. R. *Chem. Rev.* **1999**, *99*, 2511-2534.

(7) Alessio, E.; Mestroni, G.; Bergamo, A.; Sava, G. *Curr. Top. Med. Chem.* **2004**, *4*, 1525-1535.

(8) Kapitza, S.; Pongratz, M.; Jakupec, M. A.; Heffeter, P.; Berger, W.; Lackinger, L.; Keppler, B. K.; Marian, B. *J. Cancer Res. Clin. Oncol.* **2005**, *131*, 101-110.

(9) Kapitza, S.; Jakupec, M. A.; Uhl, M.; Keppler, B. K.; Marian, B. *Cancer Lett.* **2005**, *226*, 115-121.

(10) Bergamo, A.; Gava, B.; Alessio, E.; Mestroni, G.; Serli, B.; Cocchietto, M.; Zorzet, S.; Sava, G. *Int. J. Oncol.* **2002**, *21*, 1331-1338.

(11) Cebrian-Losantos, B.; Reisner, E.; Kowol, C. R.; Roller, A.; Shova, S.; Arion, V. B.; Keppler, B. K. *Inorg. Chem.* **2008**, *47*, 6513-6523.

(12) Kung, A.; Pieper, T.; Wissiack, R.; Rosenberg, E.; Keppler, B. K. *J. Biol. Inorg. Chem.* **2001**, *6*, 292-299.

(13) Pieper, T.; Peti, W.; Keppler, B. K. *Met. Based. Drugs* **2000**, *7*, 225-232.

(14) Groessl, M.; Reisner, E.; Hartinger, C. G.; Eichinger, R.; Semenova, O.; Timerbaev, A. R.; Jakupec, M. A.; Arion, V. B.; Keppler, B. K. *J. Med. Chem.* **2007**, *50*, 2185-2193.

(15) Bacac, M.; Hotze, A. C.; van der Schilden, K.; Haasnoot, J. G.; Pacor, S.; Alessio, E.; Sava, G.; Reedijk, J. *J. Inorg. Biochem.* **2004**, *98*, 402-412.

(16) Sava, G.; Bergamo, A.; Zorzet, S.; Gava, B.; Casarsa, C.; Cocchietto, M.; Furlani, A.; Scarcia, V.; Serli, B.; Iengo, E.; Alessio, E.; Mestroni, G. *Eur. J. Cancer* **2002**, *38*, 427-435.

(17) Reisner, E.; Arion, V. B.; Guedes da Silva, M. F.; Lichtenecker, R.; Eichinger, A.; Keppler, B. K.; Kukushkin, V. Y.; Pombeiro, A. J. *Inorg. Chem.* **2004**, *43*, 7083-7093.

(18) Jakupec, M. A.; Reisner, E.; Eichinger, A.; Pongratz, M.; Arion, V. B.; Galanski, M.; Hartinger, C. G.; Keppler, B. K. *J. Med. Chem.* **2005**, *48*, 2831-2837.

(19) Mura, P.; Piccioli, F.; Gabbiani, C.; Camalli, M.; Messori, L. *Inorg. Chem.* **2005**, *44*, 4897-4899.

(20) Ravera, M.; Baracco, S.; Cassino, C.; Zanello, P.; Osella, D. *Dalton Trans.* **2004**, *(15)*, 2347-2351.

(21) Hartinger, C. G.; Hann, S.; Koellensperger, G.; Sulyok, M.; Groessl, M.; Timerbaev, A. R.; Rudnev, A. V.; Stingeder, G.; Keppler, B. K. *Int. J. Clin. Pharmacol. Ther.* **2005**, *43*, 583-585.

(22) Piccioli, F.; Sabatini, S.; Messori, L.; Orioli, P.; Hartinger, C.; Keppler, B. K. *J. Inorg. Biochem.* **2004**, *98*, 1135-1142.

(23) Timerbaev, A. R.; Rudnev, A. V.; Semenova, O.; Hartinger, C. G.; Keppler, B. K. *Anal. Biochem.* **2005**, *341*, 326-333.

(24) Sulyok, M.; Hann, S.; Hartinger, C. G.; Keppler, B. K.; Stingeder, G.; Koellensperger, G. *J. Anal. At. Spectrom.* **2005**, *20*, 856-863.

(25) Trynda-Lemiesz, L.; Keppler, B. K.; Kozlowski, H. *J. Inorg. Biochem.* **1999**, *73*, 123-128.

(26) Trynda-Lemiesz, L.; Karaczyn, A.; Keppler, B. K.; Kozlowski, H. *J. Inorg. Biochem.* **2000**, *78*, 341-346.

(27) Kratz, F.; Hartmann, M.; Keppler, B.; Messori, L. *J. Biol. Chem.* **1994**, *269*, 2581-2588.

(28) Brindell, M.; Stawoska, I.; Supel, J.; Skoczowski, A.; Stochel, G.; van Eldik, R. *J. Biol. Inorg. Chem.* **2008**, *13*, 909-918.

(29) Bergamo, A.; Messori, L.; Piccioli, F.; Cocchietto, M.; Sava, G. *Invest. New Drugs* **2003**, *21*, 401-411.

(30) Malina, J.; Novakova, O.; Keppler, B. K.; Alessio, E.; Brabec, V. *J. Biol. Inorg. Chem.* **2001**, *6*, 435-445.

(31) Kung, A.; Pieper, T.; Keppler, B. K. *J. Chromatogr. B Biomed. Sci. Appl.* **2001**, *759*, 81-89.

(32) Egger, A.; Arion, V. B.; Reisner, E.; Cebrian-Losantos, B.; Shova, S.; Trettenhahn, G.; Keppler, B. K. *Inorg. Chem.* **2005**, *44*, 122-132.

(33) Schluga, P.; Hartinger, C. G.; Egger, A.; Reisner, E.; Galanski, M.; Jakupec, M. A.; Keppler, B. K. *Dalton Trans.* **2006**, *(14)*, 1796-1802.

(34) Tan, C.; Liu, J.; Li, H.; Zheng, W.; Shi, S.; Chen, L.; Ji, L. *J. Inorg. Biochem.* **2008**, *102*, 347-358.

(35) Groessl, M.; Hartinger, C. G.; Dyson, P. J.; Keppler, B. K. *J. Inorg. Biochem.* **2008**, *102*, 1060-1065.

(36) Pluim, D.; van Waardenburg, R. C.; Beijnen, J. H.; Schellens, J. H. *Cancer Chemother. Pharmacol.* **2004**, *54*, 71-78.

(37) Wang, F.; Habtemariam, A.; van der Geer, E. P.; Fernandez, R.; Melchart, M.; Deeth, R. J.; Aird, R.; Guichard, S.; Fabbiani, F. P.; Lozano-Casal, P.; Oswald, I. D.; Jodrell, D. I.; Parsons, S.; Sadler, P. J. *Proc. Natl. Acad. Sci. U. S. A.* **2005**, *102*, 18269-18274.

(38) Wang, D.; Lippard, S. J. *Nat. Rev. Drug Discov.* **2005**, *4*, 307-320.

(39) Clarke, M. J. *Coordination Chemistry Reviews* **2002**, *232*, 69-93.

(40) Berger, M. R.; Garzon, F. T.; Keppler, B. K.; Schmahl, D. *Anticancer Res.* **1989**, *9*, 761-765.

(41) Seelig, M. H.; Berger, M. R.; Keppler, B. K. *J. Cancer Res. Clin. Oncol.* **1992**, *118*, 195-200.

(42) Pongratz, M.; Schluga, P.; Jakupec, M. A.; Arion, V. B.; Hartinger, C. G.; Allmaier, G.; Keppler, B. K. *J. Anal. At. Spectrom.* **2004**, *19*, 46-51.

(43) Frasca, D.; Ciampa, J.; Emerson, J.; Umans, R. S.; Clarke, M. J. *Met. Based. Drugs* **1996**, *3*, 197-209.

(44) Sava, G.; Gagliardi, R.; Bergamo, A.; Alessio, E.; Mestroni, G. *Anticancer Res.* **1999**, *19*, 969-972.

(45) Bergamo, A.; Gagliardi, R.; Scarcia, V.; Furlani, A.; Alessio, E.; Mestroni, G.; Sava, G. *J. Pharmacol. Exp. Ther.* **1999**, *289*, 559-564.

(46) Sava, G.; Zorzet, S.; Turrin, C.; Vita, F.; Soranzo, M.; Zabucchi, G.; Cocchietto, M.; Bergamo, A.; DiGiovine, S.; Pezzoni, G.; Sartor, L.; Garbisa, S. *Clin. Cancer Res.* **2003**, *9*, 1898-1905.

(47) Sava, G.; Clerici, K.; Capozzi, I.; Cocchietto, M.; Gagliardi, R.; Alessio, E.; Mestroni, G.; Perbellini, A. *Anticancer Drugs* **1999**, *10*, 129-138.

(48) Vacca, A.; Bruno, M.; Boccarelli, A.; Coluccia, M.; Ribatti, D.; Bergamo, A.; Garbisa, S.; Sartor, L.; Sava, G. *Br. J. Cancer* **2002**, *86*, 993-998.

(49) Morbidelli, L.; Donnini, S.; Filippi, S.; Messori, L.; Piccioli, F.; Orioli, P.; Sava, G.; Ziche, M. *Br. J. Cancer* **2003**, *88*, 1484-1491.

(50) Sava, G.; Frausin, F.; Cocchietto, M.; Vita, F.; Podda, E.; Spessotto, P.; Furlani, A.; Scarcia, V.; Zabucchi, G. *Eur. J. Cancer* **2004**, *40*, 1383-1396.

(51) Sanna, B.; Debidda, M.; Pintus, G.; Tadolini, B.; Posadino, A. M.; Bennardini, F.; Sava, G.; Ventura, C. *Arch. Biochem. Biophys.* **2002**, *403*, 209-218.

(52) Cocchietto, M.; Zorzet, S.; Sorc, A.; Sava, G. *Invest. New Drugs* **2003**, *21*, 55-62.

(53) Groessl, M.; Hartinger, C. G.; Polec-Pawlak, K.; Jarosz, M.; Keppler, B. K. *Electrophoresis* **2008**, *29*, 2224-2232.

(54) Keppler, B. K.; Rupp, W. *J. Cancer Res. Clin. Oncol.* **1986**, *111*, 166-168.

(55) Messori, L.; Vilchez, F. G.; Vilaplana, R.; Piccioli, F.; Alessio, E.; Keppler, B. *Met. Based. Drugs* **2000**, *7*, 335-342.

(56) Polec-Pawlak, K.; Abramski, J. K.; Ferenc, J.; Foteeva, L. S.; Timerbaev, A. R.; Keppler, B. K.; Jarosz, M. *J. Chromatogr. A* **2008**, *1192*, 323-326.

(57) Polec-Pawlak, K.; Abramski, J. K.; Semenova, O.; Hartinger, C. G.; Timerbaev, A. R.; Keppler, B. K.; Jarosz, M. *Electrophoresis* **2006**, *27*, 1128-1135.

(58) DeLano, W. L. **2002**, .

(59) Wally, J.; Halbrooks, P. J.; Vonrhein, C.; Rould, M. A.; Everse, S. J.; Mason, A. B.; Buchanan, S. K. *J. Biol. Chem.* **2006**, *281*, 24934-24944.

(60) MacGillivray, R. T.; Moore, S. A.; Chen, J.; Anderson, B. F.; Baker, H.; Luo, Y.; Bewley, M.; Smith, C. A.; Murphy, M. E.; Wang, Y.; Mason, A. B.; Woodworth, R. C.; Brayer, G. D.; Baker, E. N. *Biochemistry* **1998**, *37*, 7919-7928.

(61) Sargent, P. J.; Farnaud, S.; Evans, R. W. *Curr. Med. Chem.* **2005**, *12*, 2683-2693.

(62) MacGillivray, R. T. A. In *Transferrins;* Templeton, D. M., Ed.; Molecular and cellular iron transport; Marcel Dekker, Inc.: New York, NY, 2002; pp 41-69.

(63) Princiotto, J. V.; Zapolski, E. J. *Nature* **1975**, *255*, 87-88.

(64) Princiotto, J. V.; Zapolski, E. J. *Biochim. Biophys. Acta* **1976**, *428*, 766-771.

(65) Sun, H.; Li, H.; Sadler, P. J. *Chem. Rev.* **1999**, *99*, 2817-2842.

(66) Harris, W. R. In *Iron chemistry;* Templeton, D. M., Ed.; Molecular and cellular iron transport; Marcel Dekker, Inc.: New York, NY, 2002; pp 1-40.

(67) Anderson, G. J.; Darshan, D.; Wilkins, S. J.; Frazer, D. M. *Biometals* **2007**, *20*, 665-674.

(68) Richardson, D. R.; Ponka, P. *Biochim. Biophys. Acta* **1997**, *1331*, 1-40.

(69) Wessling-Resnick, M. *Crit. Rev. Biochem. Mol. Biol.* **1999**, *34*, 285-314.

(70) Chung, J.; Wessling-Resnick, M. *Crit. Rev. Clin. Lab. Sci.* **2003**, *40*, 151-182.

(71) Kostova, I. *Curr. Med. Chem.* **2006**, *13*, 1085-1107.

(72) He, X. M.; Carter, D. C. *Nature* **1992**, *358*, 209-215.

(73) Curry, S.; Mandelkow, H.; Brick, P.; Franks, N. *Nat. Struct. Biol.* **1998**, *5*, 827-835.

(74) Carter, D. C.; He, X. M.; Munson, S. H.; Twigg, P. D.; Gernert, K. M.; Broom, M. B.; Miller, T. Y. *Science* **1989**, *244*, 1195-1198.

(75) Quinlan, G. J.; Martin, G. S.; Evans, T. W. *Hepatology* **2005**, *41*, 1211-1219.

(76) Sudlow, G.; Birkett, D. J.; Wade, D. N. *Mol. Pharmacol.* **1975**, *11*, 824-832.

(77) Sudlow, G.; Birkett, D. J.; Wade, D. N. *Mol. Pharmacol.* **1976**, *12*, 1052-1061.

(78) Fischer, M. J.; Bos, O. J.; van der Linden, R. F.; Wilting, J.; Janssen, L. H. *Biochem. Pharmacol.* **1993**, *45*, 2411-2416.

(79) Bhattacharya, A. A.; Grune, T.; Curry, S. *J. Mol. Biol.* **2000**, *303*, 721-732.

(80) Zunszain, P. A.; Ghuman, J.; Komatsu, T.; Tsuchida, E.; Curry, S. *BMC Struct. Biol.* **2003**, *3*, 6.

(81) Wardell, M.; Wang, Z.; Ho, J. X.; Robert, J.; Ruker, F.; Ruble, J.; Carter, D. C. *Biochem. Biophys. Res. Commun.* **2002**, *291*, 813-819.

(82) Peters, T.,Jr *Adv. Protein Chem.* **1985**, *37*, 161-245.

(83) Pedersen, S. M. *Biochem. Pharmacol.* **1987**, *36*, 2661-2666.

(84) Dixon, J. W.; Sarkar, B. *J. Biol. Chem.* **1974**, *249*, 5872-5877.

(85) Kratz, F.; Keppler, B. K.; Hartmann, M.; Messori, L.; Berger, M. R. *Met. Based. Drugs* **1996**, *3*, 15-23.

(86) Kratz, F.; Keppler, B. K.; Messori, L.; Smith, C.; Baker, E. N. *Met. Based. Drugs* **1994**, *1*, 169-173.

(87) Frasca, D. R.; Gehrig, L. E.; Clarke, M. J. *J. Inorg. Biochem.* **2001**, *83*, 139-149.

(88) Lipponer, K. G.; Vogel, E.; Keppler, B. K. *Met. Based. Drugs* **1996**, *3*, 243-260.

(89) Keppler, B. K.; Wehe, D.; Endres, H.; Rupp, W. *Inorg. Chem.* **1987**, *26*, 844-846.

(90) Alessio, E.; Balducci, G.; Lutman, A.; Mestroni, G.; Calligaris, M.; Attia, W. M. *Inorganica Chimica Acta,* **1993**, *203*, 205-217.

(91) Mason, A. B.; Halbrooks, P. J.; James, N. G.; Connolly, S. A.; Larouche, J. R.; Smith, V. C.; MacGillivray, R. T. A.; Chasteen, N. D. *Biochemistry* **2005**, *44*, 8013-8021.

(92) Harlow, E. and Lane, D. In *Antibodies: A Laboratory Manual;* Cold Spring Harbor Laboratory Press: Cold Spring Harbor, New York, 1988; .

(93) James, N. G.; Mason, A. B. *Anal. Biochem.* **2008**, *378*, 202-207.

(94) Ni Dhubhghaill, O. M.; Hagen, W. R.; Keppler, B. K.; Lipponer, K. G.; Sadler, P. J. *J. Chem. Soc. Dalton Trans.* **1994**, , 3305-3311.

(95) Steinlein, L. M.; Graf, T. N.; Ikeda, R. A. *Protein Expr. Purif.* **1995**, *6*, 619-624.

(96) Mason, A. B.; Woodworth, R. C.; Oliver, R. W.; Green, B. N.; Lin, L. N.; Brandts, J. F.; Tam, B. M.; Maxwell, A.; MacGillivray, R. T. *Protein Expr. Purif.* **1996**, *8*, 119-125.

(97) Steinlein, L. M.; Ligman, C. M.; Kessler, S.; Ikeda, R. A. *Biochemistry* **1998**, *37*, 13696-13703.

(98) Bouma, M.; Nuijen, B.; Jansen, M. T.; Sava, G.; Flaibani, A.; Bult, A.; Beijnen, J. H. *Int. J. Pharm.* **2002**, *248*, 239-246.

(99) Sato, M.; Kon, H.; Kumaki, K.; Nebert, D. W. *Biochim. Biophys. Acta* **1977**, *498*, 403-421.

(100) Asakura, T.; Leigh, J. S.,Jr; Drott, H. R.; Yonetani, T.; Chance, B. *Proc. Natl. Acad. Sci. U. S. A.* **1971**, *68*, 861-865.

(101) Fasano, M.; Mattu, M.; Coletta, M.; Ascenzi, P. *J. Inorg. Biochem.* **2002**, *91*, 487-490.

(102) Baker, E. N.; Baker, H. M.; Kidd, R. D. *Biochem. Cell Biol.* **2002**, *80*, 27-34.

(103) Hoefkens, P.; de Smit, M. H.; de Jeu-Jaspars, N. M.; Huijskes-Heins, M. I.; de Jong, G.; van Eijk, H. G. *Int. J. Biochem. Cell Biol.* **1996**, *28*, 975-982.

(104) Ward, P. P.; Cunningham, G. A.; Conneely, O. M. *Biotechnol. Genet. Eng. Rev.* **1997**, *14*, 303-319.

(105) Sun, X. L.; Baker, H. M.; Shewry, S. C.; Jameson, G. B.; Baker, E. N. *Acta Crystallogr. D Biol. Crystallogr.* **1999**, *55*, 403-407.

(106) Hershberger, C. L.; Larson, J. L.; Arnold, B.; Rosteck, P. R.,Jr; Williams, P.; DeHoff, B.; Dunn, P.; O'Neal, K. L.; Riemen, M. W.; Tice, P. A. *Ann. N. Y. Acad. Sci.* **1991**, *646*, 140-154.

(107) Ikeda, R. A.; Bowman, B. H.; Yang, F.; Lokey, L. K. *Gene* **1992**, *117*, 265-269.

(108) Steinlein, L. M.; Ikeda, R. A. *Enzyme Microb. Technol.* **1993**, *15*, 193-199.

(109) de Smit, M. H.; Hoefkens, P.; de Jong, G.; van Duin, J.; van Knippenberg, P. H.; van Eijk, H. G. *Int. J. Biochem. Cell Biol.* **1995**, *27*, 839-850.

(110) Wang, S.; Yang, T.; Lin, S.; Tsai, M.; Wu, S.; Mao, S. J. T. *Protein Expr. Purif.* **2002**, *25*, 41-49.

(111) Paramasivam, M.; Saravanan, K.; Uma, K.; Sharma, S.; Singh, T. P.; Srinivasan, A. *Protein Expression and Purification* **2002**, *26*, 28-34.

(112) Chen, G. H.; Yin, L. J.; Chiang, I. H.; Jiang, S. T. *J. Food Sci.* **2007**, *72*, M67-71.

(113) Mizutani, K.; Okamoto, I.; Fujita, K.; Yamamoto, K.; Hirose, M. *Biosci. Biotechnol. Biochem.* **2004**, *68*, 376-383.

(114) Ward, P. P.; May, G. S.; Headon, D. R.; Conneely, O. M. *Gene* **1992**, *122*, 219-223.

(115) Ward, P. P.; Lo, J. Y.; Duke, M.; May, G. S.; Headon, D. R.; Conneely, O. M. *Biotechnology* **1992**, *10*, 784-789.

(116) Ward, P. P.; Piddington, C. S.; Cunningham, G. A.; Zhou, X.; Wyatt, R. D.; Conneely, O. M. *Biotechnology (N. Y)* **1995**, *13*, 498-503.

(117) Ali, S. A.; Joao, H. C.; Csonga, R.; Hammerschmid, F.; Steinkasserer, A. *Biochem. J.* **1996**, *319 (Pt 1)*, 191-195.

(118) Salmon, V.; Legrand, D.; Georges, B.; Slomianny, M. C.; Coddeville, B.; Spik, G. *Protein Expr. Purif.* **1997**, *9*, 203-210.

(119) Mason, A. B.; Miller, M. K.; Funk, W. D.; Banfield, D. K.; Savage, K. J.; Oliver, R. W.; Green, B. N.; MacGillivray, R. T.; Woodworth, R. C. *Biochemistry* **1993**, *32*, 5472-5479.

(120) Mason, A. B.; He, Q. Y.; Adams, T. E.; Gumerov, D. R.; Kaltashov, I. A.; Nguyen, V.; MacGillivray, R. T. *Protein Expr. Purif.* **2001**, *23*, 142-150.

(121) Mason, A. B.; Halbrooks, P. J.; Larouche, J. R.; Briggs, S. K.; Moffett, M. L.; Ramsey, J. E.; Connolly, S. A.; Smith, V. C.; MacGillivray, R. T. *Protein Expr. Purif.* **2004**, *36*, 318-326.

(122) Mason, A. B.; Funk, W. D.; MacGillivray, R. T. A.; Woodworth, R. C. *Protein Expr. Purif.* **1991**, *2*, 214-220.

(123) Mason, A. B.; Woodworth, R. C.; Oliver, R. W.; Green, B. N.; Lin, L. N.; Brandts, J. F.; Savage, K. J.; Tam, B. M.; MacGillivray, R. T. *Biochem. J.* **1996**, *319 (Pt 2)*, 361-368.

(124) Ward, P. P.; Chu, H.; Zhou, X.; Conneely, O. M. *Gene* **1997**, *204*, 171-176.

(125) Zhang, J.; Li, L.; Cai, Y.; Xu, X.; Chen, J.; Wu, Y.; Yu, H.; Yu, G.; Liu, S.; Zhang, A.; Chen, J.; Cheng, G. *Protein Expr. Purif.* **2008**, *57*, 127-135.

(126) Chen, H. L.; Lai, Y. W.; Yen, C. C.; Lin, Y. Y.; Lu, C. Y.; Yang, S. H.; Tsai, T. C.; Lin, Y. J.; Lin, C. W.; Chen, C. M. *J. Mol. Microbiol. Biotechnol.* **2004**, *8*, 141-149.

(127) Guarna, M. M.; Lesnicki, G. J.; Tam, B. M.; Robinson, J.; Radziminski, C. Z.; Hasenwinkle, D.; Boraston, A.; Jervis, E.; Macgillivray, R. T.; Turner, R. F.; Kilburn, D. G. *Biotechnol. Bioeng.* **1997**, *56*, 279-286.

(128) Cregg, J. M. *Methods Mol. Biol.* **2007**, *389*, 1-10.

(129) Cregg, J. M.; Vedvick, T. S.; Raschke, W. C. *Biotechnology (N. Y)* **1993**, *11*, 905-910.

(130) Niebauer, R.T. and Robinson A.S. In *Saccharomyces cerevisiae protein expression: from protein production to protein engineering;* Baneyx, F., Ed.; Protein expression technologies; Horizon Bioscience: Norfolk, U.K., 2004; pp 253.

(131) Smith, R. A.; Duncan, M. J.; Moir, D. T. *Science* **1985**, *229*, 1219-1224.

(132) Coughlan, C. M.; Walker, J. L.; Cochran, J. C.; Wittrup, K. D.; Brodsky, J. L. *J. Biol. Chem.* **2004**, *279*, 15289-15297.

(133) Cereghino, G. P.; Cregg, J. M. *Curr. Opin. Biotechnol.* **1999**, *10*, 422-427.

(134) Cereghino, J. L.; Cregg, J. M. *FEMS Microbiol. Rev.* **2000**, *24*, 45-66.

(135) Cregg, J. M.; Cereghino, J. L.; Shi, J.; Higgins, D. R. *Mol. Biotechnol.* **2000**, *16*, 23-52.

(136) Brake, A. J.; Merryweather, J. P.; Coit, D. G.; Heberlein, U. A.; Masiarz, F. R.; Mullenbach, G. T.; Urdea, M. S.; Valenzuela, P.; Barr, P. J. *Proc. Natl. Acad. Sci. U. S. A.* **1984**, *81*, 4642-4646.

(137) Cleveland, D. W.; Fischer, S. G.; Kirschner, M. W.; Laemmli, U. K. *J. Biol. Chem.* **1977**, *252*, 1102-1106.

(138) Zamost, B. L.; Lesnicki, G. J.; Jain, S. In *Production of recombinant proteins using the methylotropic yeast Pichia pastoris and Pichia Methanolica;* Baneyx, F., Ed.; Protein expression technologies; horizon bioscience: Norfolk, U.K., 2004; pp 297-344.

(139) Gatignol, A.; Durand, H.; Tiraby, G. *FEBS Lett.* **1988**, *230*, 171-175.

(140) Higgins, D. R.; Busser, K.; Comiskey, J.; Whittier, P. S.; Purcell, T. J.; Hoeffler, J. P. *Methods Mol. Biol.* **1998**, *103*, 41-53.

(141) Kjeldsen, T.; Pettersson, A. F.; Hach, M. *J. Biotechnol.* **1999**, *75*, 195-208.

(142) Kjeldsen, T.; Pettersson, A. F.; Hach, M. *Biotechnol. Appl. Biochem.* **1999**, *29 (Pt 1)*, 79-86.

(143) Kobayashi, K.; Kuwae, S.; Ohya, T.; Ohda, T.; Ohyama, M.; Ohi, H.; Tomomitsu, K.; Ohmura, T. *J. Biosci. Bioeng.* **2000**, *89*, 55-61.

(144) Barr, K. A.; Hopkins, s. A.; and Sreekrishna, K. *Pharm Eng.* **1992**, *12*, 48-51.

(145) Xiong, R.; Chen, J.; Chen, J. *Biotechnol. Appl. Biochem.* **2008**, *51*, 129-134.

(146) Sargent, P. J.; Farnaud, S.; Cammack, R.; Zoller, H. M.; Evans, R. W. *Biometals* **2006**, *19*, 513-519.

(147) Boehm, J.; Ulrich, H. D.; Ossig, R.; Schmitt, H. D. *EMBO J.* **1994**, *13*, 3696-3710.

(148) Ngsee, J. K.; Hansen, W.; Walter, P.; Smith, M. *Mol. Cell. Biol.* **1989**, *9*, 3400-3410.

(149) Allison, D. S.; Young, E. T. *Mol. Cell. Biol.* **1989**, *9*, 4977-4985.

(150) Ardon, O.; Kaplan, J.; and Martin, B. D. In *Iron uptake in yeast;* Templeton, D. M., Ed.; Molecular and cellular iron transport; Marcel Dekker, Inc.: New York, NY, 2002; pp 375-393.

(151) Stintzi, A.; and Raymond, K. N. In *Siderophore chemistry;* Templeton, D., Ed.; Molecular and cellular iron transport; Marcel Dekker, Inc.: New York, NY, 2002; pp 273-319.

(152) Porath, J.; Carlsson, J.; Olsson, I.; Belfrage, G. *Nature* **1975**, *258*, 598-599.

(153) Hearon, J. Z.; Burk, D.; Schade, A. L. *J. Natl. Cancer Inst.* **1949**, *9*, 337-377.

(154) Sulkowski, E. *Bioessays* **1989**, *10*, 170-175.

(155) Porath, J.; Olin, B. *Biochemistry* **1983**, *22*, 1621-1630.

(156) Jiang, W.; Graham, B.; Spiccia, L.; Hearn, M. T. *Anal. Biochem.* **1998**, *255*, 47-58.

(157) Kronina, V. V.; Wirth, H. J.; Hearn, M. T. *J. Chromatogr. A* **1999**, *852*, 261-272.

(158) Zachariou, M.; Hearn, M. T. *J. Protein Chem.* **1995**, *14*, 419-430.

(159) Zachariou, M.; Hearn, M. T. *Biochemistry* **1996**, *35*, 202-211.

(160) Andersson, L.; Porath, J. *Anal. Biochem.* **1986**, *154*, 250-254.

(161) Andersson, L.; Sulkowski, E.; Porath, J. *Bioseparation* **1991**, *2*, 15-22.

(162) Muszynska, G.; Andersson, L.; Porath, J. *Biochemistry* **1986**, *25*, 6850-6853.

(163) Muszynska, G.; Dobrowolska, G.; Medin, A.; Ekman, P.; Porath, J. O. *J. Chromatogr.* **1992**, *604*, 19-28.

(164) Zachariou, M.; Hearn, M. T. *J. Chromatogr. A* **2000**, *890*, 95-116.

(165) Zachariou, M.; Traverso, I.; Hearn, M. T. *J. Chromatogr.* **1993**, *646*, 107-120.

(166) Evans, R. W.; Williams, J. *Biochem. J.* **1978**, *173*, 543-552.

(167) Lovstad, R. A. *Biometals* **2004**, *17*, 111-113.

(168) Welch, S.; Skinner, A. *Comp. Biochem. Physiol. B.* **1989**, *93*, 417-424.

(169) Gorinsky, B.; Horsburgh, C.; Lindley, P. F.; Moss, D. S.; Parkar, M.; Watson, J. L. *Nature* **1979**, *281*, 157-158.

(170) Zak, O.; Aisen, P. *Biochim. Biophys. Acta* **1990**, *1052*, 24-28.

(171) Hadden, J. M.; Bloemendal, M.; Haris, P. I.; Srai, S. K.; Chapman, D. *Biochim. Biophys. Acta* **1994**, *1205*, 59-67.

(172) Messori, L.; Poggetto, G. D.; Monnanni, R.; Hirose, J. *Biometals* **1997**, *10*, 303-313.

(173) Spears, D. R.; Vincent, J. B. *Biotechnol. Bioeng.* **1997**, *53*, 1-9.

(174) Li, H.; Sadler, P. J.; Sun, H. *Eur. J. Biochem.* **1996**, *242*, 387-393.

(175) Aisen, P.; Leibman, A.; Zweier, J. *J. Biol. Chem.* **1978**, *253*, 1930-1937.

(176) Zweier, J. L.; Aisen, P. *J. Biol. Chem.* **1977**, *252*, 6090-6096.

(177) Zweier, J.; Aisen, P.; Peisach, J.; Mims, W. B. *J. Biol. Chem.* **1979**, *254*, 3512-3515.

(178) Smith, C. A.; Anderson, B. F.; Baker, H. M.; Baker, E. N. *Acta Crystallogr. D Biol. Crystallogr.* **1994**, *50*, 302-316.

(179) Porath, J. *J. Chromatogr.* **1988**, *443*, 3-11.

(180) de la Calle Guntinas,M.B.; Bordin, G.; Rodriguez, A. R. *Anal. Bioanal Chem.* **2002**, *374*, 369-378.

(181) Guerrier, L.; Lomas, L.; Boschetti, E. *J. Chromatogr. A* **2007**, *1156*, 188-195.

(182) McCann, K. B.; Hughes, B.; Wu, J.; Bertolini, J.; Gomme, P. T. *Biotechnol. Appl. Biochem.* **2005**, *42*, 211-217.

(183) Pabst, T. M.; Antos, D.; Carta, G.; Ramasubramanyan, N.; Hunter, A. K. *J. Chromatogr. A* **2008**, *1181*, 83-94.

(184) van Gelder, W.; Huijskes-Heins, M. I.; Hukshorn, C. J.; de Jeu-Jaspars, C. M.; van Noort, W. L.; van Eijk, H. G. *Comp. Biochem. Physiol. B. Biochem. Mol. Biol.* **1995**, *111*, 171-179.

(185) Wu, L.; Wu, J.; Zhang, J.; Zhou, Y.; Ren, G.; Hu, Y. *J. Chromatogr. B. Analyt Technol. Biomed. Life. Sci.* **2008**, *867*, 62-68.

(186) Al-Mashikhi, S. A.; Nakai, S. *J. Dairy Sci.* **1988**, *71*, 1756-1763.